République Algérienne Démocratique et Populaire
Ministère de l'Enseignement Supérieur et de la Recherche Scientifique

Université de Batna 2 – Mostefa Ben Boulaïd
Faculté de Technologie
Département d'Electronique

Thèse

Présentée pour l'obtention du titre de :
Docteur LMD 3ème Cycle en Electronique
Option : Hyperfréquence et traitement du signal

Sous le Thème :

Analysis by the full wave approach of patch resonators embedded in multilayered medium containing isotropic dielectrics, anisotropic substances and chiral materials

Présentée par :

Youssouf BENTRCIA

Devant le jury composé de :

Mr. MAHAMDI Ramdane	Prof.	Université de Batna	Président
Mr. FORTAKI Tarek	Prof.	Université de Batna	Rapporteur
Mr. BENATIA Djamel	Prof.	Université de Batna	Examinateur
Mr. CHAABI Abdelhafid	Prof.	Université Frères Mentouri Constantine	Examinateur
Mr. BEDRA Sami	MCA	Université de Khenchela	Examinateur

Juillet 2018

Abstract

This thesis presents a full wave analysis of microstrip patch embedded in a multilayered medium containing isotropic or anisotropic dielectrics and chiral substances. The analysis is based on the derivation of the dyadic Green's function in the spectral domain. Then the electric field integral equation is formulated, and solved by the method of moments. The resonant frequency and the bandwidth of the antenna are computed by finding the complex roots of the determinant of the impedance matrix. Stationary phase theorem is used to compute the far-field and thus determining the antenna radiation pattern. A parametric study is achieved to investigate the influence of the patch dimensions and the substrate characteristics, including the effect of anisotropy, on the resonance and the radiation characteristics of the microstrip antenna. The mathematical details of the formulation are presented. The basic theory involved in the modeling of the electromagnetic field with chiral media is provided, and the different approaches proposed in the literature are mentioned. The influence of chirality on the resonant frequency, bandwidth and the far field is shown. Finally, an introduction into the modeling of the different feeding techniques and the effects of two feeding techniques on the antenna performance is presented.

Résumé

Cette thèse présente une analyse rigoureuse d'un résonateur patch noyé dans un milieu multicouche qui contient des matériaux isotropes, ou anisotropes et des substances chiraux. L'analyse est basée sur le calcul de la fonction dyadique de Green formulée dans le domaine spectral. Ensuite, l'équation intégrale du champ électrique est formulée. La méthode des moments est utilisée pour résoudre l'équation intégrale. La fréquence de résonance et la bande passante sont calculées en cherchant les racines complexes du déterminant de la matrice d'impédance. Le théorème de phase stationnaire est exploité afin de déterminer le champ électrique lointain, ce qui permet la détermination du diagramme de rayonnement. Les effets des différents paramètres de la structure sur les caractéristiques de résonance et rayonnement de l'antenne microbande, ont été analysés, notamment les dimensions du patch et les caractéristiques de substrat en plus de l'effet de l'anisotropie. Les détails mathématiques de la modélisation ont été présentés. La théorie qui décrit l'interaction du champ électromagnétique avec les milieux chiraux, est présentée. En plus, les approches proposées dans la littérature pour modéliser ce genre des milieux, ont été mentionnées. L'influence de chiralité sur la fréquence de résonnance, la bande passante et le champ rayonné est présentée. Finalement, une introduction est présentée sur la modélisation des différentes méthodes d'excitation et l'influences de deux techniques sur la performance de l'antenne microbande.

ملخص

هذه الأطروحة تقدم دراسة مبنية على نموذج شامل لدراسة الهوائيات المطبوعة ضمن بنية مادة عازلة متعددة الطبقات حيث أن خصائصها الفيزيائية يمكن أن توصف بثوابت على شكل أعداد سلمية أو مصفوفات، كما يمكن أن تحوي البنية مواد من نوع كيرال. دراسة هذه البنية مبنية على استخراج دالة غرين في المجال الطيفي، ثم كتابة المعادلة التكاملية للحقل الكهربائي، و بعد ذلك يتم استخدام طريقة عددية وهي طريقة العزوم لأجل حل هذه المعادلة. تردد الرنين و عرض النطاق تم حسابهما عن طريق إيجاد الجذور المركبة لمميز مصفوفة الممانعة. بينما تم استخدام نظرية الطور المستقر لحساب الحقل الكهربائي و استخراج مخطط الإشعاع الخاص بالهوائي. تم دراسة مختلف العوامل و أثرها على الخصائص الوظيفية للهوائي، هذه العوامل تتمثل بشكل أساسي في خصائص الشريط المطبوع وكذلك خصائص المادة العازلة المستخدمة. كما تم عرض الجوانب الرياضية للنموذج المتبع. المبادئ الأساسية التي تصف تفاعل الحقل الكهرومغناطيسي مع المواد من نوع كيرال تم عرضها، كما تم ذكر النماذج المختلفة المقترحة لدراسة هذا النوع من المواد بالإضافة إلى تبين أثر الخاصية المميزة لهذا النوع من المواد على الخصائص الوظيفية للهوائي. و في الأخير، تم إعطاء مقدمة عن نمذجة مختلف التقنيات المستعملة لتغذية الهوائيات المطبوعة، وكذا دراسة تأثير نوعين من هذه التقنيات على أداء هذه الهوائيات.

Acknowledgment

I would like thank my advisor Pr. Tarek Fortaki, for his guidance, advices and support during the time required to prepare this thesis. I would like thank also the friends, the colleagues and the people how have aided and encouraged me to accomplish this work.

Table of contents

Introduction 9

1. Computational electromagnetics
   1.1. Introduction 14
   1.2. Analytical models 15
      1.2.1. Transmission line model 15
      1.2.2. Cavity model 18
      1.2.3. Multiport connection method 19
   1.3. Numerical methods 20
      1.3.1. Differential equation methods 24
      a. Finite element method 24
      b. Finite difference methods 28
      c. Transmission line matrix method 33
      1.3.2. Integral equation methods 36
      a. Finite integration technique 36
      b. Partial element equivalent circuit method 38
      c. Method of moments 39
   1.4. Green's functions 41
   1.5. Conclusion 46
2. Full wave analysis of microstrip patch embedded in a multilayered medium containing isotropic or anisotropic materials
   2.1. Introduction 48
   2.2. Theory 50
      2.2.1. Derivation of dyadic Green's function 51
      2.2.2. Formulation of integral equation 57
      2.2.3. Solving the integral equation 57
   2.3. Results and discussions 59
      2.3.1. Effect of dielectric parameters 59
      a. Effect of thickness 59
      b. Effect of permittivity 62
      c. Effect of permeability 65
      d. Effect of anisotropy 68
      2.3.2. Effect of patch dimensions 72
   2.4. Conclusion 78
3. Full wave analysis of microstrip patch embedded in a multilayered medium containing chiral materials
   3.1. Introduction 81

3.2. Theory 83
3.3. Results and discussions 89
3.4. Conclusion 93
4. Feeding techniques
4.1. Introduction 96
4.2. Theory 98
4.2.1. Microstrip line feed 98
4.2.2. Coaxial probe feed 101
4.2.3. Proximity coupling feed 104
4.2.4. Aperture coupling feed 106
4.3. Results and discussions 111
4.3.1. Microstrip line feed 111
4.3.2. Coaxial probe feed 115
4.4. Conclusion 118

Conclusion 120

References 123

Introduction

Introduction

The first microstrip patch antennas have been fabricated on single layer isotropic substrates. The emerging trend toward multilayered configurations was imposed by many practical needs. For instance, in wireless applications, cover layers have been used for protection against environmental effects. Also in microwave circuit applications where microstrip antennas are integrated with feed networks and active devices, multilayered substrates are used extensively [1] – [3]. The inherent narrow bandwidth of microstrip antennas requires modeling methods capable of accurately predicting the resonant frequency and examining the possible effects of different parameters on the antenna performance. The available methods for such task are based on full wave approach and they are implemented using numerical methods. These methods account rigorously for all radiation, coupling and loss mechanisms. Furthermore, they are powerful tools for modeling arbitrarily shaped radiating elements, arrays and different feeding techniques [4], [5].

Early substrates used for microstrip antenna technology, were isotropic. However, it was proven that even the dielectrics considered isotropic, posses some amount of anisotropy. In addition to the fact that, some artificial anisotropic materials are intentionally used to achieve certain operational characteristics. Therefore, an accurate characterization of the effect of anisotropy on the antenna performance is needed [6] – [8]. Chiral materials gained a significant interest in electromagnetics community, where a great amount of research has been accomplished on the theory of electromagnetic wave propagation in chiral media. The research on chiral media, which is a bi-isotropic media, has been accomplished in the course of the greater context of bi-anisotropic materials [9] – [12]. This thesis presents an efficient algorithm, based on the use of spectral dyadic Green's function and the method moments, for the analysis of microstrip patch embedded in a multilayered medium containing isotropic, anisotropic and chiral materials.

The thesis is organized in the following manner:

The first chapter presents an overview on two broad categories of methods developed for modeling RF and microwave devices. These categories are, simplified or reduced analysis based methods, and full wave or rigorous analysis based methods. Reduced-analysis approaches are based on the use of simple physical models, where simplicity and physical insight are granted at the expense of accuracy. These methods are generally, of a limited scope. In this chapter, transmission line, cavity and multiport connection models are described and their features are presented. Then, a comparison is made between these models in terms of different criteria. Full wave approaches are based on the use of numerical methods; these methods sacrifice simplicity and physical insight at the expense of accuracy. These methods are the core algorithms of almost all CAD commercial microwave packages. The Numerical methods presented in this chapter, are classified according to the kind of equations usually, these methods are applied to. Thus, we will have two categories:

Differential equation methods and integral equation methods, finite element method, finite difference and transmission line matrix methods are treated under differential equation methods. Whereas, the method of moments, the finite integration technique and partial element equivalent circuit methods, are treated under integral equation methods. At the end of this chapter, the most popular methods are compared in terms of their performance and features. Since the method of moments requires the formulation of the appropriate

Green's function, a section is added on the mathematical concept, the types and the methods used to derive Green's functions.

In chapter 2, an efficient algorithm based on the use of spectral dyadic Green's function and the method moments, is provided. This model is used to characterize a microstrip patch embedded in a multilayered medium, where the dielectric can be isotropic or anisotropic. The resonant frequency and the bandwidth are computed by seeking the complex roots of the determinant of the impedance matrix. The radiated field is calculated using the stationary phase theorem. The mathematical features of the present formulation, makes it an efficient tool for analyzing stratified media. The use of the concept of transfer matrix to represent the layered medium is of a great importance for two main reasons; it allows the formulation of the Green's function easily, furthermore, the characteristics of each layer are easily included. A parametric study on the influence of the patch dimensions, the permittivity, permeability and the thickness of the substrate, is provided. Also the effect of electric and magnetic anisotropy is investigated.

Chapter 3 provides a survey on the theoretical models proposed for the study of electromagnetic wave propagation in a chiral media, and the refection and scattering from achiral-chiral interface. A comprehensive formulation describing the process yielding the derivation of dyadic Green's function in the Fourier transform domain. The process starts from the constitutive relations of a chiral media, and proceeds until the transverse components of the electric and magnetic fields are written, in spectral domain, in terms of longitudinal components of right- and left-circularly polarized waves. Enforcing boundary conditions yields the derivation of the corresponding Green's function. The effect of chirality on resonant frequency, bandwidth and the far field, is shown.

In the last chapter, an overview is presented on the characteristics and the mathematical formulation of popular feeding techniques, namely microstrip line, coaxial probe, proximity coupling and aperture coupling feeding techniques. The influence of the parameters of two feeding techniques is presented. Finally, summary and discussion results are listed in the conclusion.

Chapter 1:

Computational

Electromagnetics

1.1. Introduction

Electromagnetic analysis treats the interaction of the electromagnetic fields with objects and the surrounding environment. The analysis approaches can be divided into two broad categories, reduced or simplified analysis and full wave analysis. In the reduced-analysis, some approximations are made in the description of the problem; these simplifying assumptions allow the use of simple physical models where the analysis results are close to those of the original problem. Simplified analysis usually employs analytical methods, and these methods maintain simplicity at the expense of accuracy or versatility. On the other hand, full wave analysis involves the use of numerical methods. These methods maintain rigor and accuracy at the expense of computational simplicity.

The applied methods in the modeling of the electromagnetic fields and devices can be classified as [13], [14]:

- Analytical methods: where closed-form solutions are obtained through the use of analytical formulas.
- Semi-analytical methods: which provide explicit solutions requiring final numerical evaluation (such as complicated integrals, infinite series …)
- Numerical methods: these methods transform the integral or differential equations of Maxwell (or an equation derived from them), into an approximate discrete formulation (matrix equation) solved directly (by matrix inversion) or iteratively.

We will start by describing the popular analytical models as applied for microstrip antenna structures. These models can be classified into three main models: transmission line model, cavity model and multiport network model.

1.2. Analytical models

1.2.1. Transmission line model

The transmission line model is the first technique employed to analyze a rectangular microstrip antenna by Munson in 1974 [14]. In this model, the microstrip patch antenna is assimilated to a section of a transmission line of length *L* where its characteristic impedance and the propagation constant are determined by the patch size and the substrate parameters. The edges of the patch are classified into radiating and non-radiating edges such as the radiating edges are associated with slow (uniform) field variations along their lengths, whereas non-radiating edges have an integral multiple of half-wave length variations along each edge which results in almost complete cancellation of the radiated power at these edges [14]. Usually, the radiating edges are considered as two narrow apertures (slots), each of width *W*, height *d* (representing the substrate thickness) separated by a distance *L* **Fig.1**. Each of the two slots is represented by a parallel equivalent admittance *Y* with a conductance *G* and a susceptance *B* **Fig.2**.

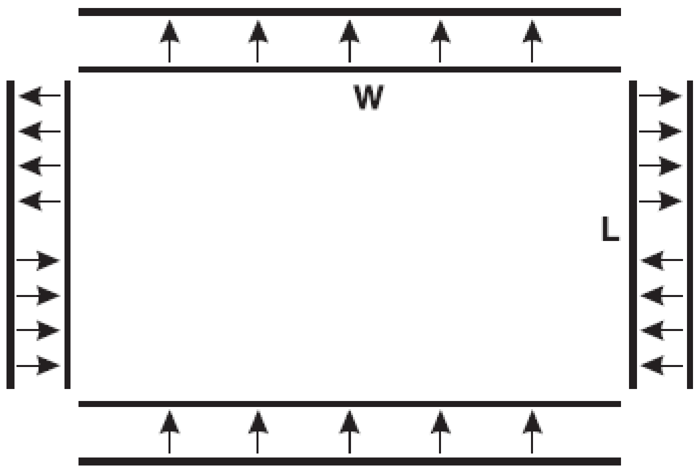

Fig. 1 Radiating and non-radiating edges of the patch

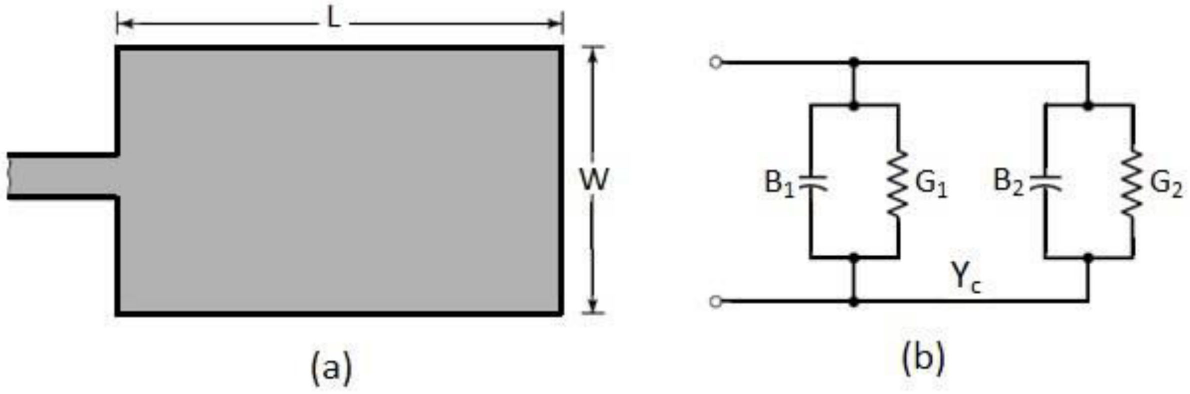

Fig. 2 ***(a)*** Rectangular patch, ***(b)*** Transmission line equivalent

Where Y_c is the characteristic admittance (it is related to the characteristic impedance Z_c by $Y_c = 1/Z_c$). The conductance *G* is associated with the radiated power, and the susceptance *B* is related to the stored energy in the fringing field near the edge [5], [14]. The resonant frequency is function of the ratio *L/d*. The determination of the resonant frequency requires the computation of the effective length of the patch which is a result of the fringing, and the effective dielectric constant which accounts for the Quasi-TEM nature of the wave in the microstrip antenna structure. This model is conceptually simple, however, it is very approximate and the model is applicable only for a rectangular patch, besides, the effects of substrate on radiation and input impedance, are not considered.

Further improvement is achieved on this model by including mutual coupling between the radiating edges through a mutual admittance Y_m connected between the two ends of the transmission line [15], as depicted in **Fig. 3**. In **Fig. 3**, y_0 is the characteristic admittance, y_s is the shunt load admittance and ϒ is the complex propagation constant having the form $ϒ = \alpha + j\beta$ where α accounts for the dielectric and conductor losses of the antenna.

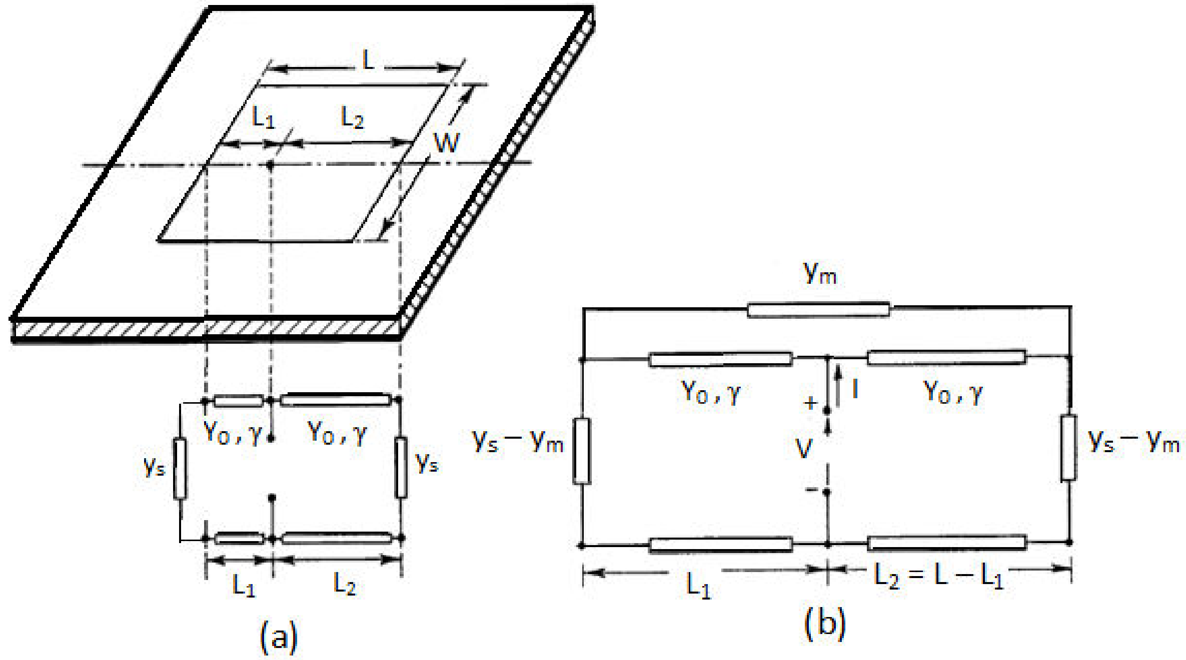

Fig. 3 Transmission line equivalent circuit ***(a)*** simple model ***(b)*** including mutual coupling

The improved transmission line model can be applied on rectangular and square microstrip patches only. Furthermore, only microstrip and coaxial feeds are supported. Proximity-coupled and aperture-coupled fed microstrip antennas cannot be analyzed.

More elaborate model called the generalized transmission line model GTLM [16]-[18] has been proposed. In this model, transmission line sections, which may be non-uniform, on either sides of the current source (which represents the feed), are converted into π-network equivalent circuit. This equivalent circuit is then simplified using the star-delta and delta-star transformations to obtain the voltage across the current source [19]. GTLM can be applied to any separable geometry of the microstrip antenna including rectangular, circular and annular ring patches, with linear or circular polarization. However, the application GTLM to an arbitrary patch shape is not possible. Also, some of the feeding techniques such as Proximity- coupled and aperture-coupled microstrip feeds cannot be modeled.

1.2.2. Cavity model

Microstrip antennas are narrow-band resonant antennas, so they resemble dielectric-loaded cavities. But unlike cavities, microstrip patch antennas are radiating elements; therefore they must be treated as lossy cavities. Cavity model was advanced by Lo et al [20]-[22], where the microstrip antenna is modeled as a cavity bounded by electric walls on the top and the bottom, and magnetic walls along the periphery. We should point out that, in this model, the substrate is assumed truncated and it does not extend beyond the edges of the patch. The patch antenna is represented by four slots, only two (the radiating slots) account for most of the radiation, the fields radiated by the two (non-radiating slots) cancel along the principle planes as shown in **Fig. 4**.

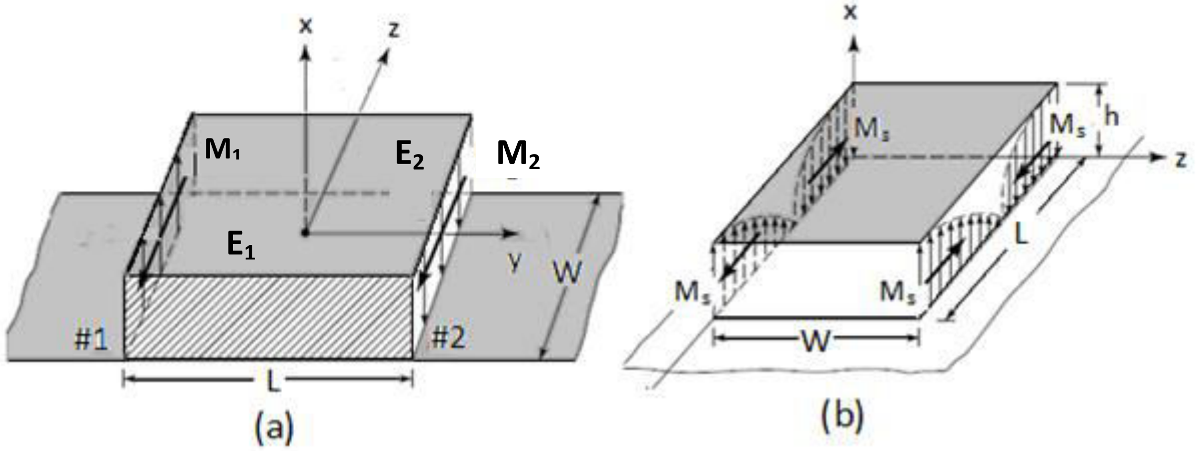

Fig. 4 Electric field in ***(a)*** radiating slots and ***(b)*** non-radiating slots of microstrip patch

Various types of losses (such as dielectric, conductor and radiation loss) are characterized in the cavity model by an effective tangent loss δ_{eff} which is related to the quality factor Q by $\delta_{eff} = 1/Q$. The resonant frequency of the antenna is defined to be the resonant frequency of the cavity for a given mode. Different patch shapes with linear or circular polarization and even stacked patches antennas have been treated by the cavity model. Also, the mutual coupling between the apertures is included implicitly, however, the cavity model does not estimate the ratio of aperture fields correctly in microstrip antennas with more than one aperture therefore cavity model is not suitable for array applications [14].

The cavity model also has been generalized to analyze non-separable geometries [23], [24], where Green's functions have been used. In this model, the analysis of a given geometry proceeds as the following:

- First, the given geometry is converted into an equivalent geometry with magnetic walls at the peripheries.
- Then, the geometry with the magnetic walls is segmented into regular geometries for which Eigen-functions are available.
- The planar circuit approach [25] is applied to determine the electric fields under the patch.
- Next, the quality factor of the patch cavity is calculated using the procedure given in the cavity model.
- Finally, the input impedance can be obtained from the ratio of the voltage and the current at the feed point.

This approach has been used to analyze a rectangular ring, cross-shaped and H-shaped patches.

1.2.3. Multiport Connection Method

Multiport connection method (MNM) model [26] can be considered an extension of the cavity model in which the impedance boundary condition at the periphery is enforced explicitly. This model takes into account the mutual coupling between various edges. The

MNM use the planar circuit approach [25], where the field in the interior region is modeled as a multiport planar circuit with ports located all along the periphery. The field in the exterior region, which includes the fringing fields, the radiation fields and the surface wave fields, are represented by load admittances. Unlike transmission line model, all the edges, radiating and non-radiating are represented as load admittances in the MNM. **Table 1** provides a comparison between the different analytical models that have been presented in the literature for the analysis of microstrip patch antennas.

1.3. Numerical methods

Finding a solution for practical problems is a complex task. It requires simplifying assumptions and/or numerical approximations [27]. Analytical models, as we have seen, are based on analytical formulas which are exact, however, the made simplifying assumptions make them applicable to only a limited set of problems [28]. In the other hand, the approaches relaying on numerical methods, although their results are also approximate, but they generally offer results with good accuracy. Besides, they are applicable on wide range of problems which makes them the preferred choice for solving most of engineering problems. Eventually, even numerical methods based approaches make some simplifying assumptions such as infinite dielectric and ground plane, zero thickness strips or patches… etc [27]. Solving electromagnetic field problems is known as computational electromagnetics CEM [27], or also numerical electromagnetics [13]. Full-wave analysis uses CEM methods as powerful tools to account rigorously for electromagnetic waves propagation in the structure under study.

Table 1 comparison of various analytical models [14].

Application	Model					
	Transmission line model	GTLM	Lossy trans. line	Cavity model	Generalized cavity.model	MNM
Patch shapes	Rectangular only	Separable geometries	Arbitrary shapes	Regular shapes	Separable geometries	Separable geometries
Substrate thickness	Thin	Thin	Thin	Thick	Thin	Thin
Feed type used	Microstrip edge feed, probe feed	Microstrip edge feed, probe feed	Possibly all types	Microstrip edge, probe and aperture feed	Microstrip edge feed, probe feed	Microstrip edge, probe feed and proximity coupling
Circular polarization	No	Yes	No	Yes	Yes	Yes
Stacked patches	No	No	Yes	Yes	No	No
Mutual coupling between edges	Explicitly included	Explicitly included	implicitly included	implicitly included	implicitly included	Explicitly included
Application to arrays	Yes	Yes	No	No	No	Yes

The purpose of all numerical methods used in electromagnetics is to find approximate solutions to Maxwell’s equations (or of equations derived from them) that satisfy boundary conditions [13]. That is why such kind of problems is referred to as boundary value problems [29], [30]. Almost all numerical methods in electromagnetics share the idea of discretizing some unknown electromagnetic property, that is , the unknown function (the solution) is expanded in terms of expansion functions with unknown coefficients [13], [27]. Nevertheless, numerical techniques have differences in their mathematical foundation which makes one technique more suitable for a specific class of problems compared to the other [28].

The classification of computational electromagnetics techniques can be made according to different criteria such as:

- The quantity being discretized or solution variable (circuit or field variables) [27], [28]
- Domain of the solution (space and time or frequency)
- Number of dimensions (1D, 2D, 2.5D, 3D) [13], [27].
- The form of the equation(s) being treated by the method (differential or integral form) [31].

We note that, in general, the above classifications are not rigid, that is, labeling a method to as a time domain method does not mean that it cannot be applied in frequency domain, but rather it means that the method is usually applied in time domain. For instance, the methods usually applied in time domain include finite difference time domain (FDTD) and Transmission line matrix (TLM), where the methods usually applied in frequency domain include Finite element method (FEM) and the method of moments (MoM).

In this thesis, the numerical methods applied for the electromagnetic field problems, are classified on the basis of the form of the equations usually treated by these methods, and hence, they will be classified into differential equation methods (usually applied on partial differential equation or PDE), and integral equation (IE) methods, as shown in **Fig. 5**.

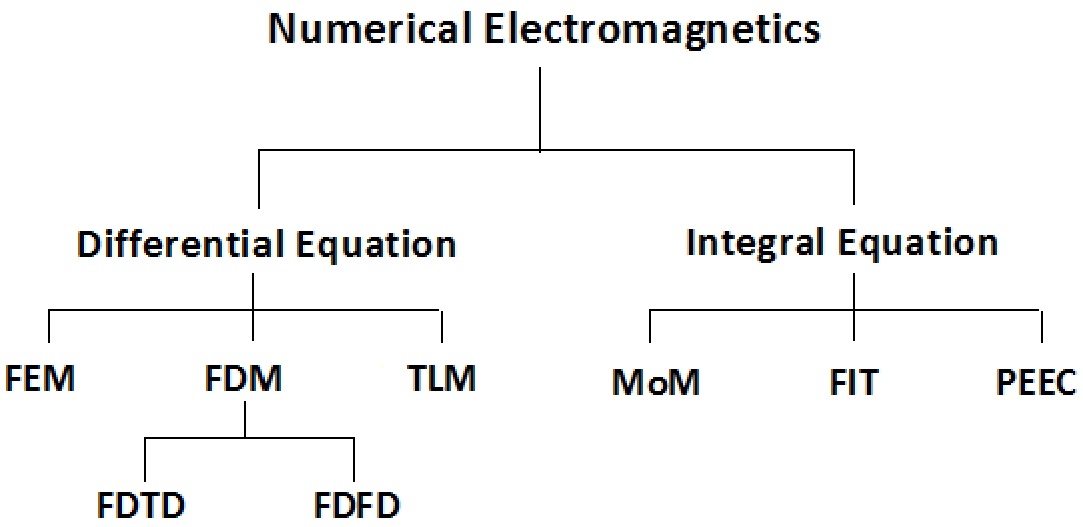

Fig. 5 Differential equation and Integral equation CEM methods

For a given application, some methods are more suitable than the others. For example [28]:

- Electrical interconnect packaging (EIP) analysis (PEEC, MoM)
- Printed circuit board (PCB) simulations (mixed circuit and EM problems) (PEEC)
- Coupling mechanism characterization (MoM, PEEC)
- Electromagnetic field strength and pattern characterization (MoM)
- Antenna design (MoM)
- Scattering problems (FEM, FDM)

The differences between the methods illustrated in **Fig. 5**, arise in two main points [28]:

- Discretization of the structure: For the differential formulation, the complete structure including the air needs to be discretized. Whereas, in integral formulation, only the materials need to be discretized.
- Solution variables: Differential equation based techniques deliver the solution in field variables i.e. electric and magnetic field. Post-processing of the field

variables is needed to obtain the currents and the voltages of the structure. For the integral equation based techniques, the solution is expressed in terms of circuit variables, i.e. currents and voltages. To convert the system current and voltages to EM field components, post-processing is needed.

In the following section, the concept and the main features of each of the methods illustrated in **Fig. 5** will be presented.

1.3.1. Differential equation methods

a- Finite Element Method (FEM)

The laws of physics for space- and time-dependent problems are usually expressed in terms of partial differential equations (PDEs). For the majority of geometries and problems, these PDEs cannot be solved analytically. Instead, they are solved approximately, typically using different types of discretization [32]. Finite element method (FEM) is used to convert the PDEs describing a boundary value problem into a system of equations (matrix equation). FEM is powerful technique for handling problems involving complex geometries and heterogeneous media, and it is applicable in both time and frequency domain [28]. The procedure of FEM analysis can be summarized as the following [33]:

- Discretizing the solution domain into a finite number of sub-domains or elements.
- Deriving the governing equations (elemental equation) for a typical element.
- Assembling all the elements in the solution domain to form matrix equation.
- Solving the system of the obtained equations.

The first step consists of subdividing the domain of the problem into smaller parts called finite elements, this process is called meshing. The shape of these elements depends on the domain of the given problem. The advantages of the subdivision of the whole domain into smaller parts are [34]:

- Accurate representation of complex geometry
- Inclusion of dissimilar material properties
- Easy representation of the total solution
- Capture of local effects

The element equations derived in the second step, are simple equations that locally approximate the original complex equation to be studied. Next, a global system of equations is generated from the element equations through a transformation of coordinates from the sub-domain local nodes to the domain global nodes. After that, the system of equations is solved by a direct or iterative method. Post-processing provides an estimate of the error in terms of the quantity of interest. When the error is larger than the acceptable value, the discretization level (i.e. meshing) has to be changed manually or by an automated adaptive process (adaptive meshing).

Generally, three approaches are being used when formulating an FEM problem [35]:

- Direct approach
- Variational approach
- Weighted residual method

Direct approach: This approach was applied initially in structural analysis, and it is the easiest to understand because it involves the application of the concept of FEM it its simplest form. This approach consists of two steps: first, the system under consideration is replaced by an equivalent idealized system consisting of individual elements. These elements are assumed to be connected to each other at specified points called nodes. When the elements are defined, the direct physical reasoning can be used to establish the element equations in terms of pertinent variables. In the second step, the individual element equations are combined to form the equations for the complete system, and then the system of equations is solved for the unknown nodal variables. This approach can be used only for simple problems.

Variational approach: this approach relies on some variational principle such as the principle of minimizing the energy of a functional, where the energy can be obtained by integrating the (unknown) fields over the structure volume [36]. The variational approach is widely used whenever classical variational statement is available for the given problem. Such statement may not be available for some physical problems such as nonlinear problems.

Weighted residual methods: It is a generic class that is developed to obtain approximate solution to differential equations of the form:

$$\mathcal{L}\,(\phi) + f = 0 \quad \text{In the domain D} \tag{1}$$

Where, $\phi\ (x)$ is an unknown function (a dependent variable) of the variable x such as x ϵ D

$f(x)$ Is a known function, and $\mathcal{L}$ is a differential operator involving spatial derivatives of ϕ

Weighted residual method involves two main steps. In the first step, an approximate solution $\psi(x)$ which satisfies the boundary conditions is assumed. The approximate solution is expressed in terms of a sum that consists of (chosen) trial functions multiplied by unknown fitting coefficients. This approximate solution is substituted in the differential equation. Since the approximate solution will not satisfy the differential equation that is, $\mathcal{L}\,(\psi) + f \neq$

0 producing an error which measures the difference between the exact and the approximate solution, this error is called a residual R defined as

$$\mathcal{L}(\psi) + f = R \tag{2}$$

The residual is then made to vanish in some average sense over the entire solution domain to produce a system of algebraic equations. Mathematically, this is accomplished by multiplying eq. (2) by weighting functions w(x) and integrating over the domain D to obtain

$$\int w(x)[\mathcal{L}(\psi) + f]\, dD = \int w(x)R(x)\, dD \tag{3}$$

Then, the weighted residual integral is forced to vanish over the solution domain, that is

$$\int w(x)R(x)\, dD = 0 \tag{4}$$

The second step is to solve the resulting system of equations to find the sought approximate solution by defining the fitting coefficients. Galerkin procedure, in which trial functions are equal to weighting functions, is among the weighted residual methods. FEM in general, has the following features:

- Meshing of the entire domain is required (object + background)
- Great flexibility in modeling complicated and irregular geometries.
- Good handling of inhomogeneous media, 2-D and 3-D linear and nonlinear problems
- Solution domain has to be terminated by ''numerical'' absorbing boundaries ABC or perfectly matched layers PML.
- Widely used in frequency domain
- FEM produces large sparse matrices

b- Finite Difference Methods (FDM)

Finite difference methods (FDMs) are numerical methods for solving differential equations by approximating them with difference equations. The domain is partitioned in space and time (**Fig. 6**) and an approximation of the solution is computed at space and time points [37]. The error between the numerical solution and the exact solution is produced when going from differential operator to difference operator, and this error is called discretization or truncation error [37]. The main concept behind any finite difference scheme is related to the definition of the derivative of a smooth function f in the neighborhood of a point x ϵ R: $f'(x) = \lim_{h\to 0}\frac{f(x+h)-f(x)}{h} \cong \frac{f(x+h)-f(x)}{h}$ for sufficiently small h. near the point of interest (i.e. point x), $f'(x)$ can be approximated by Taylor series.

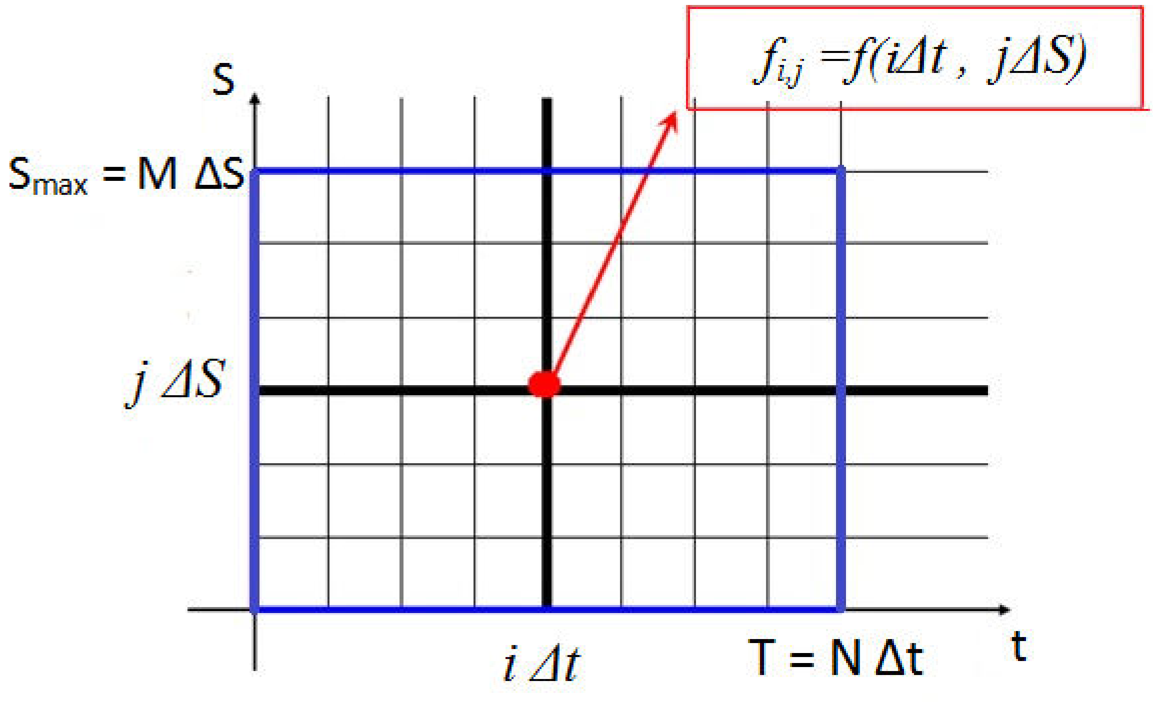

Fig. 6 Discretization of the domain in space and time [38]

For the 1st derivative, we can distinguish forward-, backward- and central- difference approximations such as:

- Forward difference: $\frac{\partial f}{\partial t} \cong \frac{f_{i+1,j} - f_{i,j}}{\Delta t}$, $\frac{\partial f}{\partial s} \cong \frac{f_{i,j+1} - f_{i,j}}{\Delta s}$
- Backward difference: $\frac{\partial f}{\partial t} \cong \frac{f_{i,j} - f_{i-1,j}}{\Delta t}$, $\frac{\partial f}{\partial s} \cong \frac{f_{i,j} - f_{i,j-1}}{\Delta s}$
- Central difference: $\frac{\partial f}{\partial t} \cong \frac{f_{i+1,j} - f_{i-1,j}}{2\Delta t}$, $\frac{\partial f}{\partial s} \cong \frac{f_{i,j+1} - f_{i,j-1}}{2\Delta s}$

For the second derivative, we have: $\frac{\partial^2 f}{\partial s^2} \cong \frac{f_{i,j+1} - 2f_{i,j} + f_{i,j-1}}{(\Delta s)^2}$

Finite Difference Time Domain (FDTD)

Finite difference time domain (FDTD) belongs to finite difference methods. The first FDTD algorithm was established by Yee in 1966. FDTD is a numerical technique for finding approximate solutions for the associated system of differential equations, where time- and space- derivatives are approximated using finite difference expressions [36]. This method is widely used within electromagnetic modeling, mainly, due to its simplicity, where Maxwell's equations (in differential form), are discretized using central difference approximations to the space and time partial derivatives [31], [39]. In FDTD, the whole domain must be divided (discretized) into volume elements (cells), often, these elements are cubes (called voxels) [27]. For these elements, Maxwell's equations are approximated by finite difference equations. The volume elements sizes are determined by considering two main factors [36]:

- Frequency: the cell size should not exceed λ/10, where λ corresponds to the maximum frequency in the excitation
- Structure: the cell size must allow discretization of thin structures. The time step is limited by courant's condition [33]:

$$\Delta t \le \frac{1}{\sqrt{\left(1/\Delta x\right)^2 + \left(1/\Delta y\right)^2 + \left(1/\Delta z\right)^2}}$$

The three-dimensional space of the problem is truncated by absorbing boundaries. The most popular absorbing boundary is the perfectly matched layer (PML) [31]. The unknown function to be computed for FDTD method is field variables i.e. electric and magnetic fields which are alternatively calculated at every half time step and at all locations of the discretized domain [33]. When Maxwell's equations are examined, it can be seen that the change in the E-field in time (the time derivative) is dependent in the H-field across space (the curl). This is the basic idea behind FDTD time-stepping relation that is, at any point in space, the updated value of the E-field in time is dependent on the stored value of the E-field and the numerical curl of the local distribution of the H-field in space. The H-field is time-stepped in a similar manner. At any point in space, the updated value of the H-field in time is dependent on the stored value of the H-field and the numerical curl of the local distribution of the E-field in space. This process known as loop-frog procedure, its algorithm is illustrated in **Fig. 7** [31].

The FDTD method has the following advantages:

- Simple implementation and easy to understand.
- No matrix inversion involved.
- Easy modeling of complex material configuration
- Since FDTD is a time domain technique, the response of the system over a wide frequency range can be obtained with a single simulation.
- FDTD calculate the electric and magnetic fields everywhere in the computational domain as they evolve in time, which provides animated displays of the electromagnetic field movement through the model.

- FDTD computes the electric and magnetic fields directly which is more convenient to EMC/EMI modeling.
- A wide variety of linear and nonlinear dielectric and magnetic materials can be naturally and easily modeled.
- Ability to perform both transient and steady state analysis.

However, FDTD have some weaknesses such as:

- Since the entire domain have to be discretized and the resulting elements must be sufficiently fine to resolve both the smallest wavelengths and the smallest geometrical feature of the model which results a large computational domain resulting a long simulation time.
- The need of absorbing boundaries ABC (PML) to truncate unbounded problem domain
- Difficulties with curve structures.

Finite Difference Frequency Domain (FDFD)

Finite Difference Frequency domain (FDFD) method is conceptually a simple method to solve time-dependent differential equations for steady state solutions. FDFD method transforms Maxwell's equations (or other PDE for fields and source), into a matrix equation of the form

- ***A x = b*** where ***A*** is a matrix derived from the wave equation operator, the column vector operator ***x*** contains (the unknown) field components and the column vector ***b*** describes the source.

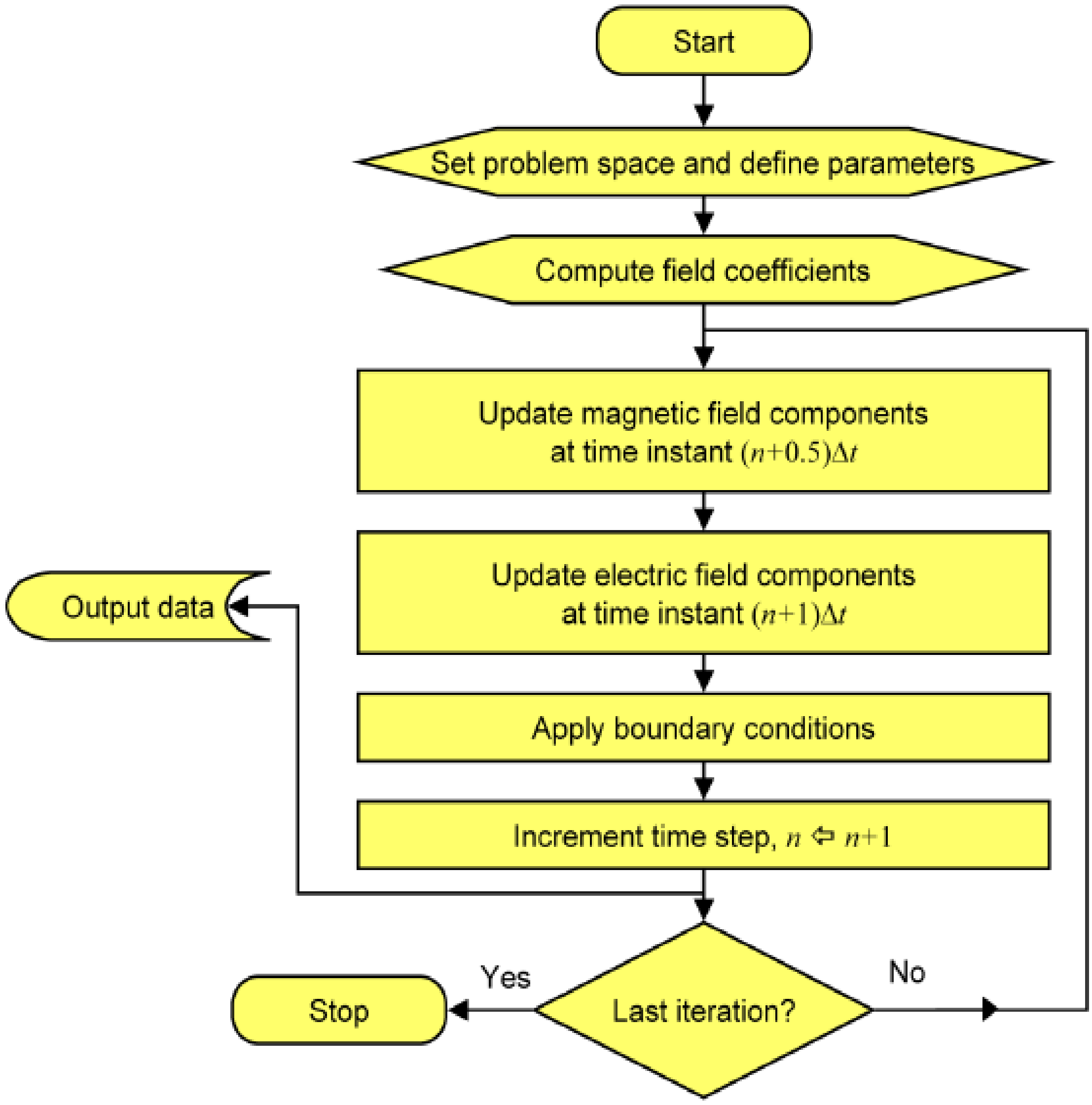

Fig. 7 Leap-frog algorithm

FDFD and FDTD share many common features. Beside the fact that FDFD is implemented in frequency domain, they are different in some points:

- There no time step to be computed in FDFD
- FDFD solves a large sparse matrix (FDFD in this point is similar to FEM).

c- Transmission Line Matrix (TLM) method

Transmission line matrix (TLM) is a space and time discretization method for the computation of the electromagnetic fields. TLM is based on Huygens principle **Fig. 8** in which Huygens states that: ′′ All points on a wave front serve as point sources of spherical secondary wavelets. After a time *t* the new position of the wave front will be the surface of tangency to these secondary wavelets ′′. This principle can be explained as the following:

At time 0 the central point scatters a wave. At time t_1 all the points in the wave front are acting as point sources, and the wave front at any time later, is the wave front from these secondary point sources.

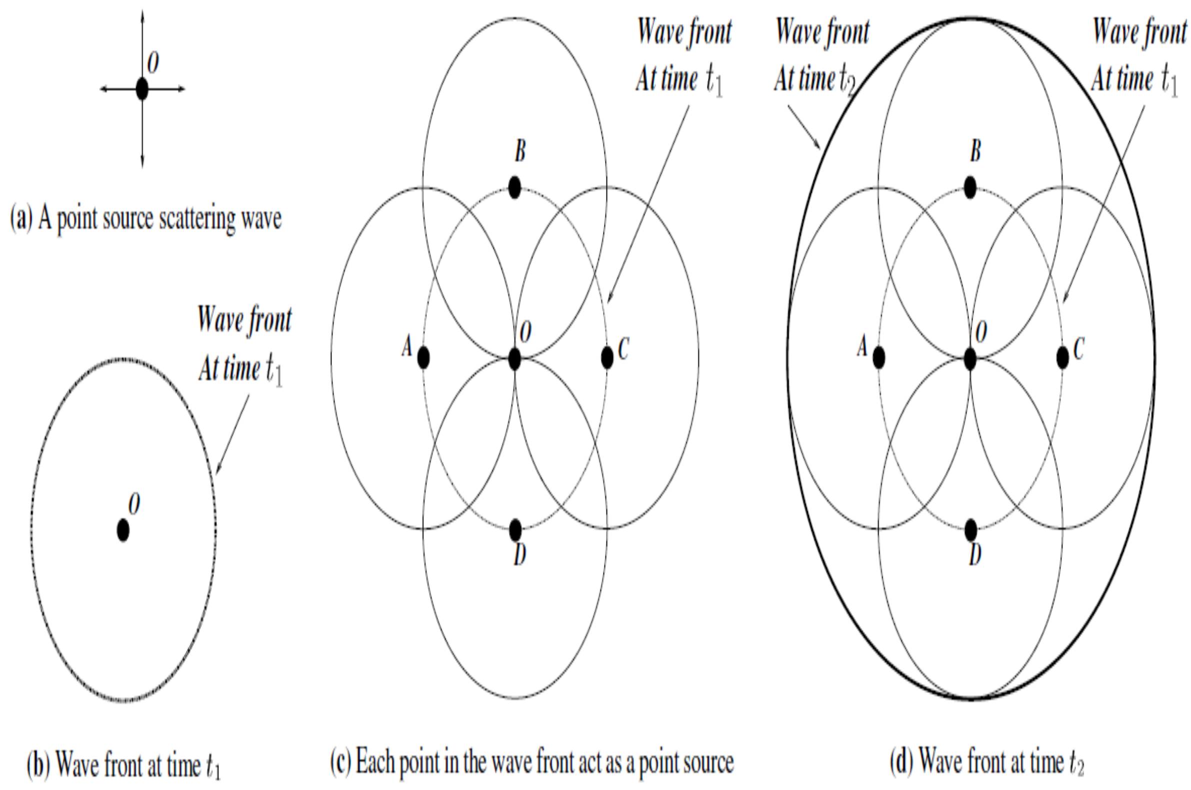

Fig. 8 Huygens principle

Johns [40] modeled Huygens principle by sampling time and the space and representing it with a mesh of passive transmission line components. He modeled the wave propagation as voltage and current travelling in this mesh. The relationship between time sample Δt and space sample Δl is given by: $\Delta l = c\Delta t$ where **c** is the free space light speed.

To understand the concept of TLM method, let us consider the TLM grid illustrated in **Fig. 9**. Assuming that at a time zero, an impulse is incident to the middle node, this node will scatter the wave to its 4 neighboring nodes. The scattered wave reaches these nodes at the instant Δt. Now these four nodes will scatter waves to their neighboring nodes at time equal to $2\Delta t$. At each time step, each node receives an incident wave from the adjacent nodes and scatters it to the other adjacent nodes. By repeating the above process for each node, the wave distribution in the medium can be calculated. The choice of two- or three-dimensional TLM modeling depends on the complexity of the problem under study. In two-dimensional TLM model represented in **Fig. 9**, each node is surrounded by 4 nodes (**Fig. 10**), while in three dimensional TLM model (**Fig. 11**); each node is surrounded by 6 nodes (**Fig. 12**).

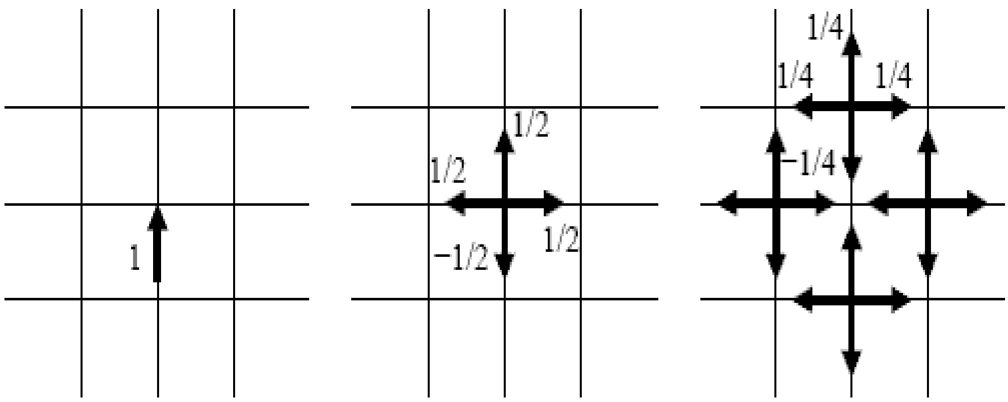

Fig. 9 Wave propagation in two-dimensional TLM mesh

TLM method uses the concept of scattering matrix where (for 2D TLM model) the voltages V_n^s representing the scattering waves, are related to the voltages V_n^i representing the incident waves by

$$\begin{bmatrix} V_1 \\ V_2 \\ V_3 \\ V_4 \end{bmatrix}_{K+1}^{S} = \frac{1}{2}\begin{bmatrix} -1 & 1 & 1 & 1 \\ 1 & -1 & 1 & 1 \\ 1 & 1 & -1 & 1 \\ 1 & 1 & 1 & -1 \end{bmatrix}\begin{bmatrix} V_1 \\ V_2 \\ V_3 \\ V_4 \end{bmatrix}_{K}^{I} \tag{5}$$

Where

S, I: Scattered and Incident waves respectively

K, K+1: arbitrary consecutive time steps

Based on the above equation, if the magnitude of the wave (voltage in the TLM modeling) is known at any instant *KΔt*, then the magnitude of the wave could be found at the instant *(K+1) Δt*. By repeating this for each time step, wave propagation could be modeled. Similarly, for three-dimensional TLM model, the eq. (5) could be rewritten as:

$$\begin{bmatrix} V_1 \\ V_2 \\ V_3 \\ V_4 \\ V_5 \\ V_6 \end{bmatrix}_{K+1}^{S} = \frac{1}{3}\begin{bmatrix} -2 & 1 & 1 & 1 & 1 & 1 \\ 1 & -2 & 1 & 1 & 1 & 1 \\ 1 & 1 & -2 & 1 & 1 & 1 \\ 1 & 1 & 1 & -2 & 1 & 1 \\ 1 & 1 & 1 & 1 & -2 & 1 \\ 1 & 1 & 1 & 1 & 1 & -2 \end{bmatrix}\begin{bmatrix} V_1 \\ V_2 \\ V_3 \\ V_4 \\ V_5 \\ V_6 \end{bmatrix}_{K}^{I} \tag{6}$$

TLM method can model homogeneous and non-homogeneous, lossless and lossy structures, each one requires different mesh model. TLM and FDTD are considered the most powerful time domain methods.

1.3.2. Integral equation methods

a- Finite integration technique (FIT)

Finite integration technique (FIT) proposed in 1977 by Thomas Weiland, is a discretization method which is similar to FDTD method, however, FIT discretizes Maxwell's equations in their integral form. Maxwell's equations are transformed into a system of linear equations. This method is flexible in geometrical modeling and it handles curved boundaries and complex shapes with more accuracy. To explain the concept of the FIT, we consider Maxwell's equations for a linear and lossy medium [41]:

$$\frac{\partial}{\partial t}\iint \varepsilon(r)E(r,t)dA = \oint H(r,t)dr - \iint \sigma(r)E(r,t)dA \tag{7}$$

$$\frac{\partial}{\partial t}\iint \mu(r)H(r,t)dA^{*} = -\oint E(r,t)dr - \iint \sigma^{*}(r)H(r,t)dA^{*} \tag{8}$$

Where $E(r,t)$ and $H(r,t)$ represent the electric and magnetic fields respectively, and the media parameters are described by the permittivity $\varepsilon(r)$, the permeability $\mu(r)$, and the electric and magnetic conductivity $\sigma(r)$ and $\sigma^{*}(r)$. Equations (7) and (8) are approximated by the finite difference equations:

$$\frac{E_h^{n+1} - E_h^{n}}{\Delta t}\iint \varepsilon(r)dA = \oint H_h^{n+0.5}(r)dr - E_h^{n+1}\iint \sigma(r)dA \tag{9}$$

$$\frac{H_h^{n+0.5} - E_h^{n-0.5}}{\Delta t}\iint \mu(r)dA^{*} = -\oint E_h^{n}(r)dr - H_h^{n+0.5}\iint \sigma^{*}(r)dA^{*} \tag{10}$$

Where Δt is the time step, E_h^{n} and $H_h^{n+0.5}$ are dielectric and magnetic field vector approximated at time points nΔt and (n+0.5)Δt for n=0,1,…

Then, FIT proceeds in a similar manner as FDTD. Both methods share advantages such as simple implementation and efficient parallel computing. They share disadvantages such those encountered when Yee Cartesian grid is used. To overcome such shortcoming, adaptive mesh, and sub-gridding, non-orthogonal FIT (NFIT), have been proposed [41].

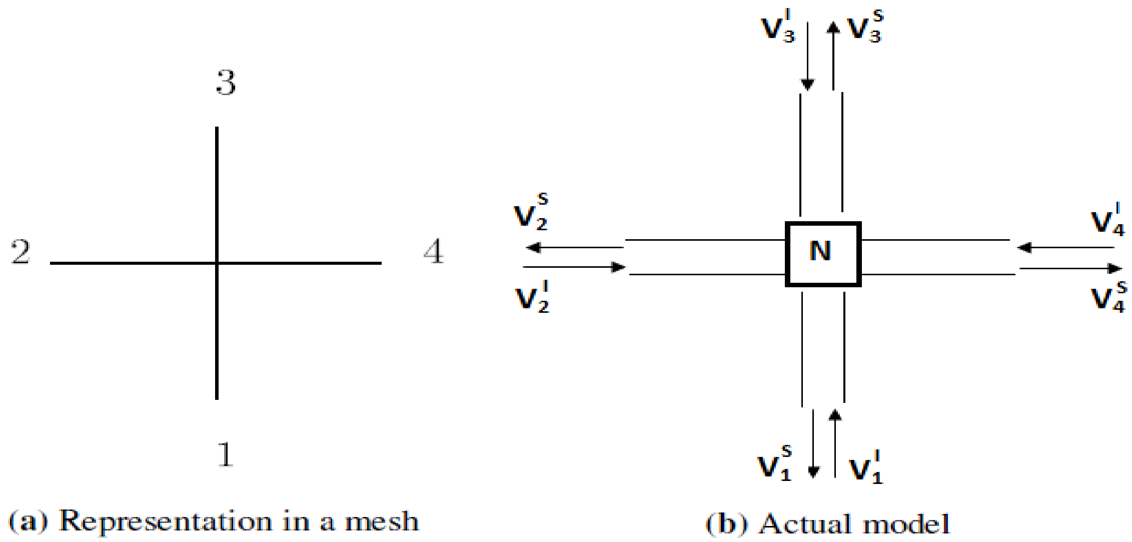

Fig. 10 Model for a node in TLM mesh

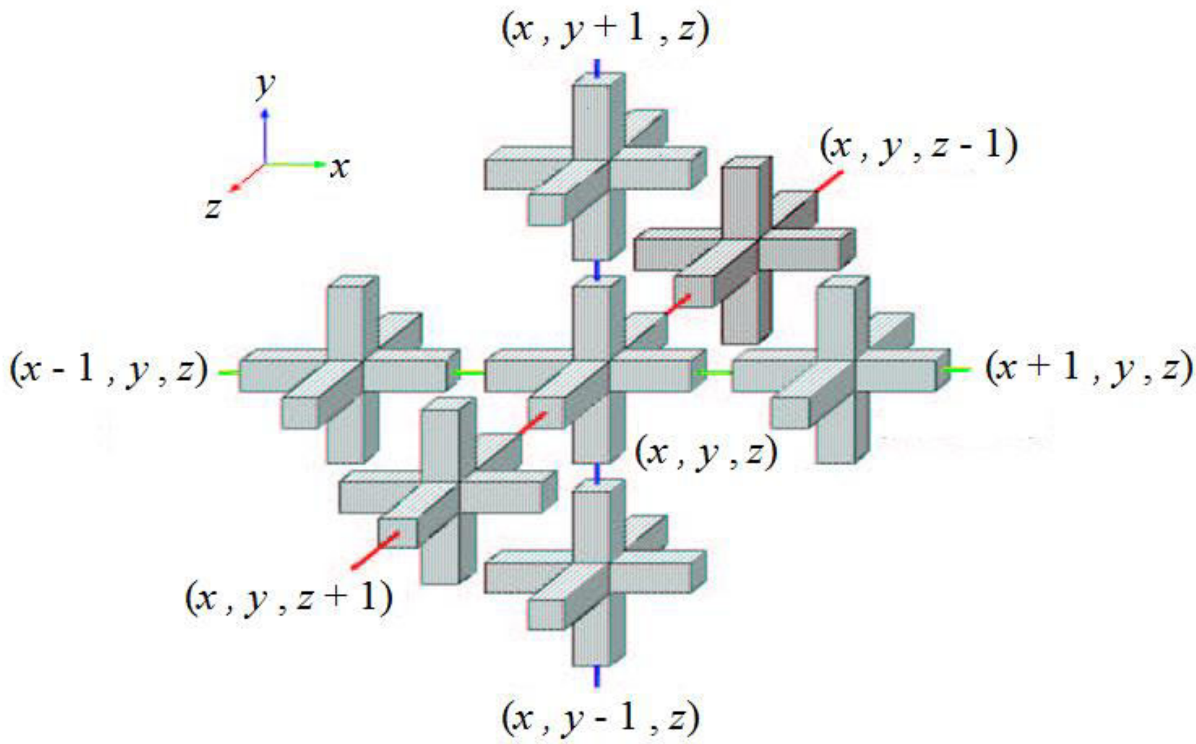

Fig. 11 Three-dimensional TLM mesh

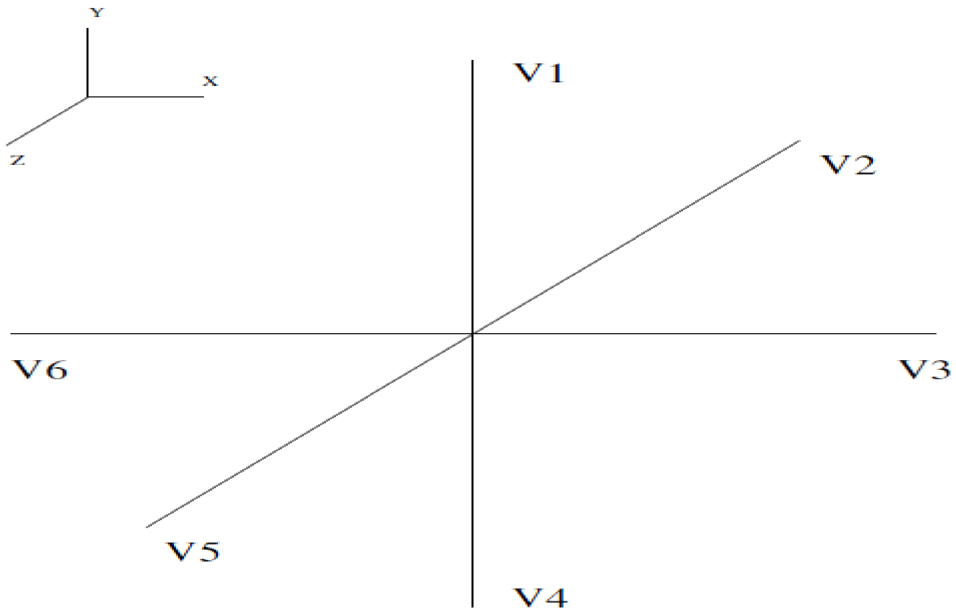

Fig. 12 Node model of three-dimensional TLM mesh

b- Partial element equivalent circuit (PEEC)

Partial element equivalent circuit (PEEC) introduced by Albert Ruehli in 1972, is a three dimensional full-wave method suitable for combined electromagnetic and circuit analysis. The main feature of the PEEC method is that the combined circuit and EM solution is performed with the same equivalent circuit in time or frequency domain [28]. PEEC method is applied to an integral equation like the method of moments. But, unlike MoM, PEEC is a full spectrum method that is valid from DC to the maximum frequency determined by the meshing. In the PEEC method, the integral equation is interpreted as the Kirchhoff's voltage applied to a basic PEEC cell which results in a complete circuit solution for three-dimensional geometries [36].

PEEC method is applied to mixed potential integral equation (MPIE), in which the current- and charge-densities are discretized. The resulting integral equation for the PEEC formulation is interpreted as an equivalent circuit. Then, the equivalent circuit is analyzed using circuit theory [28]. To obtain field variables, post-processing of circuit variables is necessary.

c- Method of moments

Method of moments (MoM) known also as boundary element method (BEM), is a numerical method for solving integral equations by transforming them into a matrix equation. The MoM owes its name to the process of taking moments by multiplying with appropriate weighting functions and integrating. In MoM, only conducting surfaces have to be discretized. The method of moments is applied to equations of the form

$$L \,.\, f = g \tag{11}$$

Where L is a linear operator (an integral operator), f the unknown function (current density) and g is a known excitation function (a voltage in radiation problems, and an incident electric field in scattering problems). The unknown current density is approximated in term of a finite number of chosen basis (expansion) functions f_i multiplied by unknown weighting coefficients α_i to be computed, that is

$$f \cong \sum_{i=1}^{N} \alpha_i \, f_i \tag{12}$$

The approximation of current density is substituted back in the integral equation (11) which now will have the form

$$L \;\; \sum_{i=1}^{N} \alpha_i f_i = g \tag{13}$$

The eq. (13) consists of N unknown to be determined. To solve eq. (13), we use M weighting (or testing) functions which are multiplied by each term in eq. (13) and integrating over the domain of the current densities to transform eq. (13) into a matrix equation of the form

$$[Z][I] = [V] \tag{14}$$

Where the vectors $[I]$ and $[V]$ represent the unknown current coefficient and the excitation, respectively. Whereas, the matrix $[Z]$, known as the impedance matrix, represents the interaction between the conducting object (e.g. an antenna) and the excitation voltage or the incident electric field. MoM is applicable to problems for which Green's function can be calculated. MoM discretization results in large dense matrix. Fast algorithms such as Multi-level fast multi-pole method (ML-FMM), Conjugate Gradient Fast Fourier Transform (CG-FFT) and Adaptive integral method (AIM) are proposed to reduce the memory storage and accelerate matrix –vector multiplication.

In **Table 2**, a comparison between the most popular computational electromagnetic techniques is provided [27]. In **Table 2**, TD and FD stand for time and frequency domains respectively.

Table 2 Comparison between FEM, FDTD and MoM

	MoM	FEM	FDTD
Descritization	Only wires or surfaces	Entire domain (tetrahedron)	Entire domain (cube)
Solution method	FD, linear equations Full matrix	FD, linear equations Sparse matrix	TD, iterations
Boundary conditions	No need for special BC	Absorbing Boundary conditions	Absorbing Boundary conditions
Numerical effort	~ N^3	~ N^2	~ N
Well suited for	Wire and surface Antennas, coupling Arbitrary shaped Surfaces, single or Few frequencies	Arbitrary shapes And metals, single Or few frequencies	Arbitrary materials Orthogonal Planar boundaries Broadband Investigations
Not well suited for	Electrically very Large structures, Broadband Investigations	Electrically large Structures, coupling Between distant Elements, Broadband Investigations	Coupling between Distant elements High-Q Structures

The dyadic Green's function is often found as a kernel in integral-equation technique, in combination with the method of moments, to solve the boundary value problem of the microstrip antennas [42]. The next section contains an overview on the concept, the types and the methods used to derive the Green's functions.

1.4. Green's functions

When a physical system is subject to some external disturbance, non-homogeneity arises in the mathematical formulation of the problem, that is, if the system is described by a differential equation, the external disturbance makes the differential equation non-homogeneous. Methods such as the method of undetermined coefficients or the variation of parameter technique could be used for solve non-homogeneous differential equation. However such methods do not have any special physical significance. Green's functions also could be used for such task. Green's functions have an advantage over the other methods, since every Green's function has a special physical significance. The Green's function measures the response of a system due to a point source somewhere in the fundamental domain [36]. To understand the concept of the Green's function, let us consider the following inhomogeneous differential equation:

$$L\,y = f \tag{15}$$

Where

L: is a differential operator

y: the unknown response function

f: the known excitation function (the source)

When the source function is an impulse located somewhere in the space δ (r, r'), the response function will be the Green's function G (r, r') such as

$$L\,G(r, r') = \delta(r, r') \tag{16}$$

The solution of the original equation can be found by integrating the product of the Green's function and the in-homogeneity f over the volume of the source such as [43]

$$y = \int G\,f\,ds \tag{17}$$

The process yielding to eq. (17) is described in [43], [44]. Thus, we can notice that the Green's function is the analogy of the impulse response of a linear system. The major advantage of the Green's function is that when the Green's function is derived for a particular problem, for a given set of boundary conditions, solving the same problem for a different source constrained by the same boundary conditions, is simple and straightforward [44]. However, there are cases when the Green's function does not exist, depending on the boundaries. In electrostatics, the Green's function G (r, r') is the potential due to a stimulus applied at a particular point in space [36]. Where r is the observation point and r' is the source (stimulus) point. G (r, r') is translational-invariant if it depends solely on the difference (r-r') rather than the separate values of r, r' [44]. The Green's function is often singular at r=r' and an infinitesimal exclusion volume surrounding r=r' has to be included [43]. In electromagnetics, most of the problems are of a vector nature; therefore it is necessary to extend the above one-dimensional scalar Green's function to multi-dimensional Green's function. Such type is often referred to as dyadic Green's function [44]. In electromagnetic computation, it is common to use two methods for determining the Green's function; these methods are the eigenfunction expansion method and the method of images [36].

There are many types of Green's functions, they are classified according to

- The quantity being treated: potentials or fields.
- The domain: spatial or spectral.

In terms of the potentials, we can distinguish two related types of Green's functions, scalar and vector potentials Green's functions i.e. G_V , G_A respectively. They are related to scalar- *V* and vector *A* potentials by the formulas [43]

$$A(r) = \int \bar{G}_A(r,r')J(r')\,ds' \tag{18}$$

$$\mathrm{V} = \int G_V(r,r')q(r')\,ds' \tag{19}$$

Where

J (r'): the surface current density

q (r'): the surface charge density

S: the surface of the PEC current surface.

In terms of fields, we can distinguish electric type Green's function and magnetic type Green's function. Eventually, there are many types of Green's functions according to whether the electric and magnetic field is generated by an electric or magnetic current [45]-[46]. When only the electric current density is considered, the electric and the magnetic fields are related to the electric type and the magnetic type Green's functions $\bar{G}_e, \bar{G}_m$ respectively, by the expressions [47]

$$E(r) = \iiint \bar{G}_e(r, r')J(r')dv' \tag{20}$$

$$H(r) = \iiint \bar{G}_m(r, r')J(r')dv' \tag{21}$$

The Green's functions presented so far depend only on spatial coordinates therefore they are referred to as spatial domain Green's functions. The counterpart of this type, are the spectral domain Green's functions.

It is common to express the space domain Green's function in term of Sommerfeld's Integral

$$G = \frac{1}{4\pi} \int_{SIP} H_0^{(2)}(k_\rho \rho)\tilde{\bar{G}}(k_\rho)k_\rho dk_\rho \tag{22}$$

Where

$\tilde{\bar{G}}(k_\rho)$ The dyadic Green's function in spectral domain

$H_0^{(2)}$ The Hankel's function of the second kind

SIP stands for Sommerfeld integration path

Evaluating Sommerfeld's integral is numerically time-consuming process. Therefore, fast techniques were dedicated to this task, which yields the determination of dyadic Green's function. Among these techniques, discrete complex images method (DCIM), Modified fast Hankel transform and window Function method [48]. For example, DCIM approximates the spectral domain Green's function in terms of complex exponentials using either the Generalized Pencil of function (GPOF) or the Prony's method. Then, these exponentials are transformed analytically into a set of complex images in space domain using the Sommerfeld's identity [48]. The Green's function in spectral domain is related to the spatial Green's function by the Fourier transform, or Hankel transform [47]. The main advantage of spectral green's function is that it can be written analytically i.e. in a closed-form. For instance, the electric field $\tilde{E}$ and the electric current density $\tilde{J}$ in the spectral domain are related as

$$\tilde{E} = \tilde{\bar{\bar{G}}}\,\tilde{J} \tag{23}$$

This formula is valid in both Fourier transform domain (FTD) and Hankel transform domain (HTD). Similarly to spatial domain Green's function, several methods have been suggested to derive the spectral dyadic Green's function, especially for multilayered medium. These methods include vector wave eigenfunction expansion technique (VWEET), wave iterative technique (WIT) [48] and full-wave equivalent circuit method [42]. Green's function in spectral domain has singularities i.e. points were the Green's function is not defined. These points represent surface wave poles. Since spectral Green's function is written in a closed-form, these singularities can be located [49]. Different approaches have been proposed to handle this problem such as extracting these singularities using the residue theory. Other approaches are based on changing the path of integration in the complex plane to avoid these singularities [50] – [51].

1.5. Conclusion

An overview on different analytical and numerical methods is presented. We have shown that each analytical model is actionably a set of sub-models, where each sub-model is an enhancement of the previous one. It is also shown the analytical methods differ in their capabilities and their range of applications. The best method, for a given problem, is the simplest method providing a result with the required accuracy. Full wave methods also introduce some assumptions on the problem description, however, since they offer good accuracy compared to analytical methods, they are more suitable for complex problems. The classification of numerical methods used in computational electromagnetics, is done according to different criteria such as the quantity being discretized, solution domain, the type of equation being treated … etc. In this chapter, different numerical methods have been presented, and their concept and features are explained. It was shown that for some applications, some methods are more suitable than the others. To give an idea how such decision is made, a comparison between three popular numerical electromagnetics methods is accomplished on the basis of different criteria. A section on Green's function is introduced due to its importance in the method of moment formulation adopted in this thesis. The concept behind the Green's function, in addition to its different types, are introduced. In this thesis, spectral domain Green's function in conjunction with the method of moments, are employed to model microstrip patch in a multilayered dielectric.

Chapter 2

Full-Wave Analysis of Microstrip Patch Embedded in a Multilayered Medium Containing Isotropic or Anisotropic Materials

2.1. Introduction

In This Chapter we present a mathematical formulation of multilayered microstrip antenna structure where the dielectric can be isotropic or anisotropic. Papers treating such structures have not been published until late 90s, such as the paper of Chunfei et al [52] for rectangular patch and the papers of Losada et al [3], [53] for circular patch antenna. The early works on microstrip antenna analysis and design have considered the simplest form which consists of a single rectangular or circular disc patch printed on a single layer isotropic substrate. The early studies date back to mid 70s [54] followed by [55]-[57] for circular patch, and [58], [59] and later [60]-[62] for rectangular patch structure. The influence of patch dimensions and substrate parameters on radiation and resonance characteristics of the antenna were studied, either incidentally in the context of presenting an analytical or numerical method, or deliberately as in the case of experimental studies [60], [62], in addition to their purpose of checking the validity of theoretical results.

The theory presented in this chapter has been applied on single layer and bi-layered structures; one example of bi-layered structure is the microstrip patch in a substrate-superstrate configuration, Bahl et al [1] was among the firsts who have published a paper in the early 80s, in which the effect of cover layer on the resonant frequency of the antenna is described. Two years later, Alexopoulos and Jackson [2] have published a paper containing a design study, in which they have defined the criteria of choosing the cover layer parameters to enhance the antenna radiation efficiency. Row and Wong [63] and later Losada et al [3] have presented numerical studies on such a structure, where Fortaki et al [64] have investigated the effect of cover layer properties on the antenna's radiation characteristics.

Most of the works published on the theory and the experiments of microstrip antennas have considered isotropic dielectrics, however, it was found that even the dielectrics that were considered isotropic possess a certain amount of anisotropy [6]. In addition to that some anisotropic dielectrics are intentionally used to achieve certain practical characteristics in microwave devices [6]. All this imply the developing of an appropriate formulation to characterize such materials. One of the first papers in this regard, was published by Pozar [6] who presented a theory based on the method of moments and investigated the effect of anisotropy on the resonant frequency and surface wave excitation. Wong et al [7] have presented a study on the influence of positive and negative anisotropy on the resonant frequency. Similar studies were published by [8] for single patch and [65] for stacked patches structures. We note that the anisotropy mentioned in the above references is the dielectric anisotropy that is the anisotropy related to the permittivity. Magnetic anisotropy (that is related to permeability) has not been studied before [3], [47], [66], until magneto-dielectric substrates have been used in microstrip antenna structures [67]-[70]. This new trend toward magneto-dielectric substrates allowed the characterization of the effect of permeability on the antenna characteristics. But the main motivation was antenna miniaturization offered by the use of magneto-dielectric materials. A good reference on this subject is [69].

2.2. Theory

The present formulation is for a multilayered structure of N layer, where the dielectric is characterized by permittivity and permeability tensors. The patch is placed on the layer P where P<N. The XY plane is the plane of the patch, therefore, x and y components represent the tangential (or transversal) components, and z component represents the normal (or longitudinal) component. The structure under study is illustrated in **Fig. 1**

As detailed in chapter 1, the general process to compute the resonant frequency and the bandwidth in addition to the radiation pattern of the microstrip antenna, can be summarized as the following:

1/ the derivation of the dyadic Green's function in the spectral domain

2/ the computation of the impedance matrix

3/Finding the root of the impedance matrix determinant, which corresponds to the complex resonant frequency, defines the antenna resonant frequency and bandwidth.

4/the eigenvector that corresponds to the smallest eigenvalue of the impedance matrix defines the weighting coefficients, and thus allowing the determination of the approximate formula of the current density on the patch. Then the stationary phase theorem is used to determine the radiation pattern of the antenna.

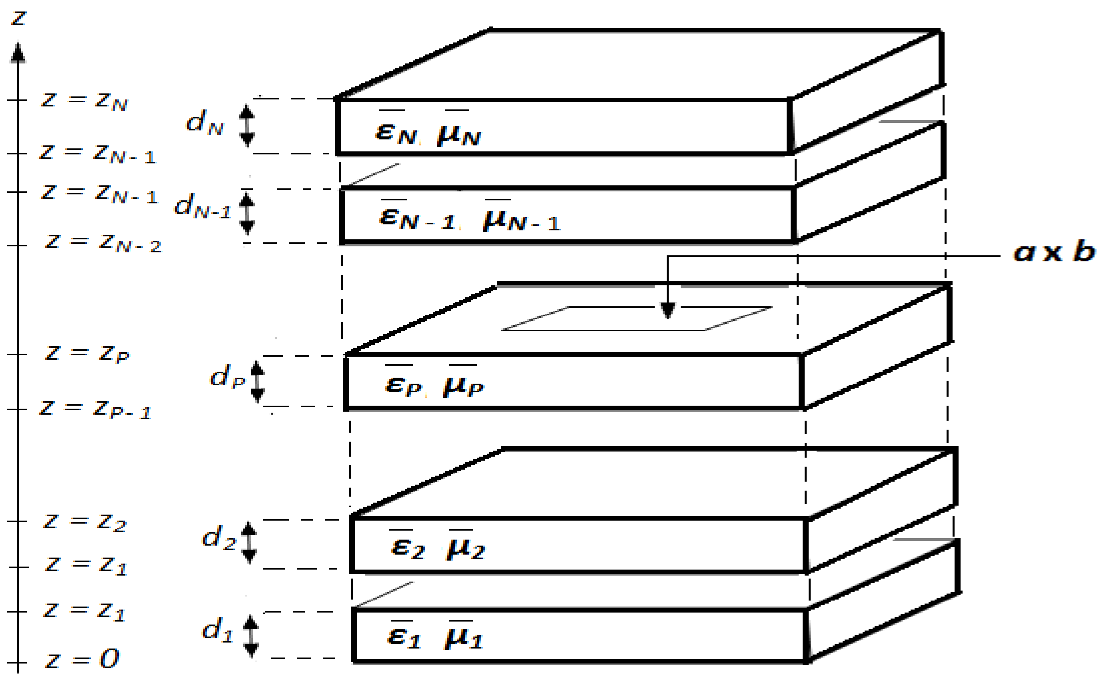

Fig. 1 multilayered microstrip antenna structure

2.2.1. Derivation of Dyadic Green's function

The dielectric is considered anisotropic medium characterized by a permittivity and permeability, tensors having the form:

$$\bar{\varepsilon} = \varepsilon_0 \begin{bmatrix} \varepsilon_x & 0 & 0 \\ 0 & \varepsilon_x & 0 \\ 0 & 0 & \varepsilon_z \end{bmatrix} \tag{1}$$

$$\bar{\mu} = \mu_0 \begin{bmatrix} \mu_x & 0 & 0 \\ 0 & \mu_x & 0 \\ 0 & 0 & \mu_z \end{bmatrix} \tag{2}$$

By assuming time dependence of $e^{j\omega t}$, and for a source free medium Maxwell's equations can written as:

$$\nabla \times \boldsymbol{E} = -j\omega \bar{\mu} \boldsymbol{H} \tag{3-a}$$

$$\nabla \times \boldsymbol{H} = j\omega\, \bar{\varepsilon}\boldsymbol{E} \tag{3-b}$$

$$\nabla . \boldsymbol{E} = 0 \tag{3-c}$$

$$\nabla . \boldsymbol{H} = 0 \tag{3-d}$$

The corresponding wave equations for E_z and H_z have the form

$$\frac{\partial^2 E_z}{\partial x^2} + \frac{\partial^2 E_z}{\partial y^2} + \frac{\varepsilon_z}{\varepsilon_x}\frac{\partial^2 E_z}{\partial z^2} + \mu_x\, \varepsilon_z\, k_0^2\, E_z = 0 \tag{4-a}$$

$$\frac{\partial^2 H_z}{\partial x^2} + \frac{\partial^2 H_z}{\partial y^2} + \frac{\mu_z}{\mu_x}\frac{\partial^2 H_z}{\partial z^2} + \mu_z\, \varepsilon_x\, k_0^2\, H_z = 0 \tag{4-b}$$

Where $k_0 = \omega\sqrt{\mu_0 \varepsilon_0}$ is the free space wavenumber.

We can rewrite the eq. (4-a), (4-b) in spectral domain by applying Fourier transform to obtain:

$$\frac{\partial^2 \tilde{E}_z}{\partial z^2} + \left(\mu_x \varepsilon_x k_0^2 + \frac{\varepsilon_x}{\varepsilon_z}\, k_s^2\right) \tilde{E}_z = 0 \tag{5-a}$$

$$\frac{\partial^2 \tilde{H}_z}{\partial z^2} + \left(\mu_x \varepsilon_x k_0^2 + \frac{\mu_x}{\mu_z}\, k_s^2\right) \tilde{H}_z = 0 \tag{5-b}$$

Where $k_s^2 = k_x^2 + k_y^2$

The general solutions for $\tilde{E}_z$ and $\tilde{H}_z$ have the form:

$$\tilde{E}_z = A_e\, e^{-ik_z^e z} + B_e\, e^{ik_z^e z} \tag{6-a}$$

$$\tilde{H}_z = A_h\, e^{-ik_z^h z} + B_h\, e^{ik_z^h z} \tag{6-b}$$

Where the coefficients A_e , B_e , A_h and B_h are functions of k_s , k_z^e and k_z^h are expressed as:

$$k_z^e = \left(\mu_x \varepsilon_x k_0^2 + \frac{\varepsilon_x}{\varepsilon_z}\, k_s^2\right)^{1/2} \tag{7-a}$$

$$k_z^h = \left(\mu_x \varepsilon_x k_0^2 + \frac{\mu_x}{\mu_z}\, k_s^2\right)^{1/2} \tag{7-b}$$

We can notice that in the case of an anisotropic medium, the electric and the magnetic fields have different wavenumbers.

By a simple mathematical manipulation, each of the components E_x , E_y , H_x and H_y can be written in terms of E_z and H_z , in spectral domain, the tangential components of the electric and magnetic fields can be expressed as:

$$\tilde{E}_x = \frac{ik_x}{k_s^2}\,\frac{\varepsilon_z}{\varepsilon_x}\,\frac{\partial \tilde{E}_z}{\partial z} + \omega\mu_0\mu_z\,\frac{k_y}{k_s^2}\,\tilde{H}_z \tag{8-a}$$

$$\tilde{E}_y = \frac{ik_y}{k_s^2}\,\frac{\varepsilon_z}{\varepsilon_x}\,\frac{\partial \tilde{E}_z}{\partial z} - \omega\mu_0\mu_z\,\frac{k_x}{k_s^2}\,\tilde{H}_z \tag{8-b}$$

$$\tilde{H}_x = \frac{ik_x}{k_s^2}\,\frac{\mu_z}{\mu_x}\,\frac{\partial \tilde{H}_z}{\partial z} - \omega\varepsilon_0\varepsilon_z\,\frac{k_y}{k_s^2}\,\tilde{E}_z \tag{8-c}$$

$$\tilde{H}_y = \frac{ik_y}{k_s^2}\,\frac{\mu_z}{\mu_x}\,\frac{\partial \tilde{H}_z}{\partial z} + \omega\varepsilon_0\varepsilon_z\,\frac{k_x}{k_s^2}\,\tilde{E}_z \tag{8-d}$$

The next step is to write each of the tangential components of the electric and magnetic fields as a superposition of TM and TE waves as:

$$\begin{bmatrix} \tilde{E}_x \\ \tilde{E}_y \end{bmatrix} = \bar{F}(k_s)\begin{bmatrix} e_e \\ e_h \end{bmatrix} \tag{9}$$

$$\begin{bmatrix} \tilde{H}_y \\ -\tilde{H}_x \end{bmatrix} = \bar{F}(k_s)\begin{bmatrix} h_e \\ h_h \end{bmatrix} \tag{10}$$

Where

$$\bar{F}(k_s) = {}^{1}\!/_{k_s}\begin{bmatrix} k_x & k_y \\ k_y & -k_x \end{bmatrix} = \bar{F}^{-1}(k_s) \tag{11}$$

$$e_e = \frac{i}{k_s}\frac{\varepsilon_z}{\varepsilon_x}\frac{\partial \tilde{E}_z}{\partial z} \tag{12-a}$$

$$e_h = \frac{\omega\mu_0\mu_z}{k_s}\tilde{H}_z \tag{12-b}$$

$$h_e = \frac{\omega\varepsilon_0\varepsilon_z}{k_s}\tilde{E}_z \tag{12-c}$$

$$h_h = \frac{i}{k_s}\frac{\mu_z}{\mu_x}\frac{\partial \tilde{H}_z}{\partial z} \tag{12-d}$$

The indexes *e* and *h* represent the TM and TE waves respectively.

We can put: $$\boldsymbol{e}(k_s, z) = \begin{bmatrix} e_e \\ e_h \end{bmatrix} \tag{13}$$

$$\boldsymbol{h}(k_s, z) = \begin{bmatrix} h_e \\ h_h \end{bmatrix} \tag{14}$$

e, ***h*** are the electric and magnetic fields in the (TM, TE) representation.

In a multilayered dielectric, let j be an arbitrary layer characterized by a permittivity $\bar{\varepsilon}_j$, permeability $\bar{\mu}_j$ and a thickness d_j . The layer j is located between the planes $z=z_{j-1}$ and $z=z_j$

The electric and the magnetic fields on the lower (at $z=z_{j-1}$) and the upper (at $z=z_j$) boundaries of the layer j can be related by transfer matrix $\bar{T}_j$ by the expression:

$$\begin{bmatrix} \boldsymbol{e}(k_s, z_j^-) \\ \boldsymbol{h}(k_s, z_j^-) \end{bmatrix} = \bar{T}_j \begin{bmatrix} \boldsymbol{e}(k_s, z_{j-1}^+) \\ \boldsymbol{h}(k_s, z_{j-1}^+) \end{bmatrix} \tag{15}$$

Where

$$\bar{T}_j = \begin{bmatrix} \bar{T}_j^{11} & \bar{T}_j^{12} \\ \bar{T}_j^{21} & \bar{T}_j^{22} \end{bmatrix} = \begin{bmatrix} cos\bar{\theta}_j & -i\,\bar{g}_j^{-1}sin\bar{\theta}_j \\ -i\,\bar{g}_j sin\bar{\theta}_j & cos\bar{\theta}_j \end{bmatrix} \tag{16}$$

With

$$\bar{\theta}_j = d_j \begin{bmatrix} k_{zj}^e & 0 \\ 0 & k_{zj}^h \end{bmatrix} \tag{17}$$

$$\bar{g}_j = \begin{bmatrix} \frac{\omega\varepsilon_0\varepsilon_x}{k_{zj}^e} & 0 \\ 0 & \frac{k_{zj}^h}{\omega\mu_0\mu_x} \end{bmatrix} \tag{18}$$

By applying the boundary conditions, we can relate the fields across the interface between the adjacent layers. The boundary conditions for the tangential components are defined as:

$$\widetilde{\boldsymbol{E}}\left(k_s, z_j^-\right) = \widetilde{\boldsymbol{E}}\left(k_s, z_j^+\right) \text{ , j=1, 2, … , N} \tag{19}$$

$$\widetilde{\boldsymbol{H}}\left(k_s, z_j^-\right) - \widetilde{\boldsymbol{H}}\left(k_s, z_j^+\right) = \delta_{jP}\tilde{\boldsymbol{J}}(k_s) = \delta_{jP} \begin{bmatrix} \tilde{J}_x(k_s) \\ \tilde{J}_y(k_s) \end{bmatrix} \tag{20}$$

Where $\tilde{J}_x$ and $\tilde{J}_y$ are the Fourier transforms of the x- and y- polarized current densities on the patch J_x , J_y respectively. δ_{jP} Is the symbol of Kronecker, and it is defined as

$$\delta_{jP} = \begin{cases} 1 & \text{if } \ j = P \\ 0 & \text{if } \ j \neq P \end{cases}$$

Similarly, for the fields in the (TM, TE) representation, the eq. (19), (20) can be rewritten as:

$$\boldsymbol{e}\left(k_s, z_j^-\right) = \boldsymbol{e}\left(k_s, z_j^+\right) \text{ , j=1, 2, … , N} \tag{21}$$

$$\boldsymbol{h}\left(k_s, z_j^-\right) - \boldsymbol{h}\left(k_s, z_j^+\right) = \delta_{jP}\boldsymbol{j}(k_s) = \delta_{jP} \begin{bmatrix} j_e(k_s) \\ j_h(k_s) \end{bmatrix} \tag{22}$$

Where

$$\begin{bmatrix} j_e(k_s) \\ j_h(k_s) \end{bmatrix} = \bar{F}(k_s)\,\tilde{\boldsymbol{J}}(k_s) \tag{23}$$

Using the eq. (15), (21) and (22), the fields on the plane z=0 can be related to the fields at the plane $z = z_p^-$ by the expression

$$\begin{bmatrix} \boldsymbol{e}(k_s, z_P^-) \\ \boldsymbol{h}(k_s, z_P^-) \end{bmatrix} = \bar{\Gamma}_< \begin{bmatrix} \boldsymbol{e}(k_s, 0) \\ \boldsymbol{h}(k_s, 0) \end{bmatrix} \tag{24}$$

And the fields on the plane $z = z_p^+$ can be related to the fields at the plane $z = z_N^+$ by the expression

$$\begin{bmatrix} \boldsymbol{e}(k_s, z_N^+) \\ \boldsymbol{h}(k_s, z_N^+) \end{bmatrix} = \bar{\Gamma}_> \begin{bmatrix} \boldsymbol{e}(k_s, z_P^+) \\ \boldsymbol{h}(k_s, z_P^+) \end{bmatrix} \tag{25}$$

With

$$\bar{\Gamma}_< = \begin{bmatrix} \bar{\Gamma}_<^{11} & \bar{\Gamma}_<^{12} \\ \bar{\Gamma}_<^{21} & \bar{\Gamma}_<^{22} \end{bmatrix} = \prod_{j=P}^{1} \bar{T}_j \quad , \bar{\Gamma}_> = \begin{bmatrix} \bar{\Gamma}_>^{11} & \bar{\Gamma}_>^{12} \\ \bar{\Gamma}_>^{21} & \bar{\Gamma}_>^{22} \end{bmatrix} = \prod_{j=N}^{P+1} \bar{T}_j \tag{26}$$

The purpose of these equations is to write the electric field in term of the current density on the patch by a formula having the form:

$$\boldsymbol{e}\big(k_s, z_p\big) = \bar{Q}(k_s)\boldsymbol{j}(k_s) \tag{27}$$

Where $\bar{Q}(k_s)$ the spectral dyadic Green's function in the (TM, TE) representation, and it is defined as

$$\bar{Q}(k_s) = \left[\bar{\Gamma}_<^{\mathbf{22}}\left(\bar{\Gamma}_<^{12}\right)^{\mathbf{-1}} + \left(\bar{g}_0\bar{\Gamma}_>^{12} - \bar{\Gamma}_>^{22}\right)^{\mathbf{-1}}\left(\bar{g}_0\bar{\Gamma}_>^{11} - \bar{\Gamma}_>^{21}\right)\right]^{\mathbf{-1}} \tag{28}$$

With

$$\bar{g}_0 = \begin{bmatrix} \frac{\omega\varepsilon_0}{k_{z0}} & 0 \\ 0 & \frac{k_{z0}}{\omega\mu_0} \end{bmatrix} \tag{29}$$

$$k_{z0} = (k_0^2 - k_s^2)^{1/2} \tag{30}$$

The dyadic spectral Green's function is given by the following expression

$$\bar{G}(k_s) = \bar{F}(k_s)\bar{Q}(k_s)\bar{F}(k_s) \tag{31}$$

We note that $\bar{G}(k_s)$ has the form

$$\bar{G}(k_s) = \begin{bmatrix} G_{xx} & G_{xy} \\ G_{yx} & G_{yy} \end{bmatrix} \tag{32}$$

The dyadic spectral Green's function relates the tangential electric field with current density on the patch in the spectral domain by the expression

$$\widetilde{\boldsymbol{E}}(k_s, z_p) = \bar{G}(k_s)\,\widetilde{\boldsymbol{J}}(k_s) \tag{33}$$

2.2.2. The formulation of the integral equation

The tangential electric field in eq. (33) is expressed in spectral domain, to derive its expression in space domain; we apply inverse Fourier transform on eq. (33) to obtain:

$$E(x, y, z) = \frac{1}{4\pi^2}\int_{-\infty}^{+\infty}\int_{-\infty}^{+\infty}\bar{G}(k_s)\,\widetilde{\boldsymbol{J}}(k_s)\,e^{i(k_x x + k_y y)}dk_x dk_y \tag{34}$$

Because the tangential electric field vanishes on the perfectly conducting patch, the eq. (34) becomes:

$$\frac{1}{4\pi^2}\int_{-\infty}^{+\infty}\int_{-\infty}^{+\infty}\bar{G}(k_s)\,\widetilde{\boldsymbol{J}}(k_s)\,e^{i(k_x x + k_y y)}dk_x dk_y = 0 \tag{35}$$

The equation above is called ''the electric field integral equation'' (EFIE).

2.2.3. Solving the integral equation

The eq. (35) cannot be solved directly because the current density on the patch is unknown. The method of moments (MoM) is used to solve this problem. The basic idea is to approximate the current density on the patch using a limited number of chosen basis functions weighted by unknown coefficients to be computed. In this work, entire domain basis functions are used, where the current density in the patch is expressed in terms of x- and y- polarized basis functions as:

$$J(x,y) = \sum_{k=1}^{K} a_k \begin{bmatrix} J_{xk}(x,y) \\ 0 \end{bmatrix} + \sum_{m=1}^{M} b_m \begin{bmatrix} 0 \\ J_{ym}(x,y) \end{bmatrix} \tag{36}$$

Where

J_{xk}, J_{ym} are the basis functions, and a_k , b_m are the weighting coefficients.

In this thesis, the Galerkin method applies the method of moments where the basis functions are chosen to be the same as testing functions. The method of moments converts the integral equation described in eq. (35) into a matrix equation of the form:

$$\begin{bmatrix} (\bar{Z}_{11})_{K \times K} & (\bar{Z}_{12})_{K \times M} \\ (\bar{Z}_{21})_{M \times K} & (\bar{Z}_{22})_{M \times M} \end{bmatrix} \begin{bmatrix} (a)_{K \times 1} \\ (b)_{M \times 1} \end{bmatrix} = 0 \tag{37}$$

Where

$$(\bar{Z}_{11})_{qk} = \int_{-\infty}^{+\infty} \int_{-\infty}^{+\infty} G_{xx} \tilde{J}_{xq}(-k_s) \tilde{J}_{xk}(k_s)\, dk_x dk_y \tag{38-a}$$

$$(\bar{Z}_{12})_{qm} = \int_{-\infty}^{+\infty} \int_{-\infty}^{+\infty} G_{xy} \tilde{J}_{xq}(-k_s) \tilde{J}_{ym}(k_s)\, dk_x dk_y \tag{38-b}$$

$$(\bar{Z}_{21})_{lk} = \int_{-\infty}^{+\infty} \int_{-\infty}^{+\infty} G_{yx} \tilde{J}_{yl}(-k_s) \tilde{J}_{xk}(k_s)\, dk_x dk_y \tag{38-c}$$

$$(\bar{Z}_{22})_{lm} = \int_{-\infty}^{+\infty} \int_{-\infty}^{+\infty} G_{yy} \tilde{J}_{yl}(-k_s) \tilde{J}_{ym}(k_s)\, dk_x dk_y \tag{38-d}$$

The matrix containing the elements Z_{mn} is called the impedance matrix. The value that cancels the determinant of the impedance matrix is the complex resonant frequency having the form $f = f_r + if_i$ where f_r is the resonant frequency and ${2f_i}/{f_r}$ is the fractional bandwidth. Once the resonant frequency is computed, the eigenvector that correspond the smallest eigenvalue of the impedance matrix determines the current weighting coefficients.

2.3. Results and Discussions

2.3.1. Effect of dielectric parameters

In this part, we shall investigate the effect of the dielectric parameters such as the thickness, the permittivity and the permeability as well as the influence of the dielectric and magnetic anisotropy on the resonance and radiation characteristics of the microstrip antenna. All the structures studied in this part and in the subsequent parts, will have the same dielectric thickness.

a- Effect of thickness

In this section we explore the effect of thickness on the resonant frequencies and the bandwidths of three different structures, a single layer structure, two layers substrate and substrate - superstrate configurations. For all the three structures, the dielectric is considered homogenous, its thickness is varied from 0.4-2.4 mm and the results are presented for three different values of permittivity. The effect of the thickness of the cover layer on the resonant frequency **Fig. 2** and the bandwidth **Fig. 3**, the case of superstrate configuration is also shown. Also the effect thickness variation on the radiation pattern is shown in **Fig. 4.** We note that the radiation pattern presented in **Fig. 4** and the subsequent figures is expressed in terms of the normalized radiated electric field as a function of the angle Ɵ. The radiation patterns are taken for the plane perpendicular to the patch i.e. at the angle $\phi = \pi/2$ rad. The TM_{01} resonant mode is considered unless otherwise specified.

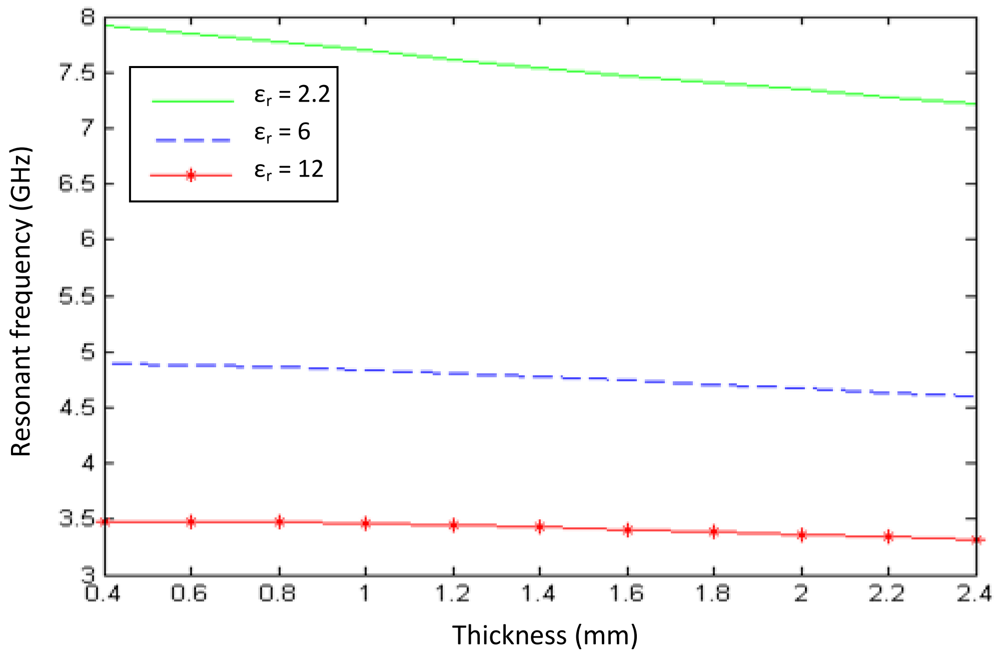

(a) Single layer substrate

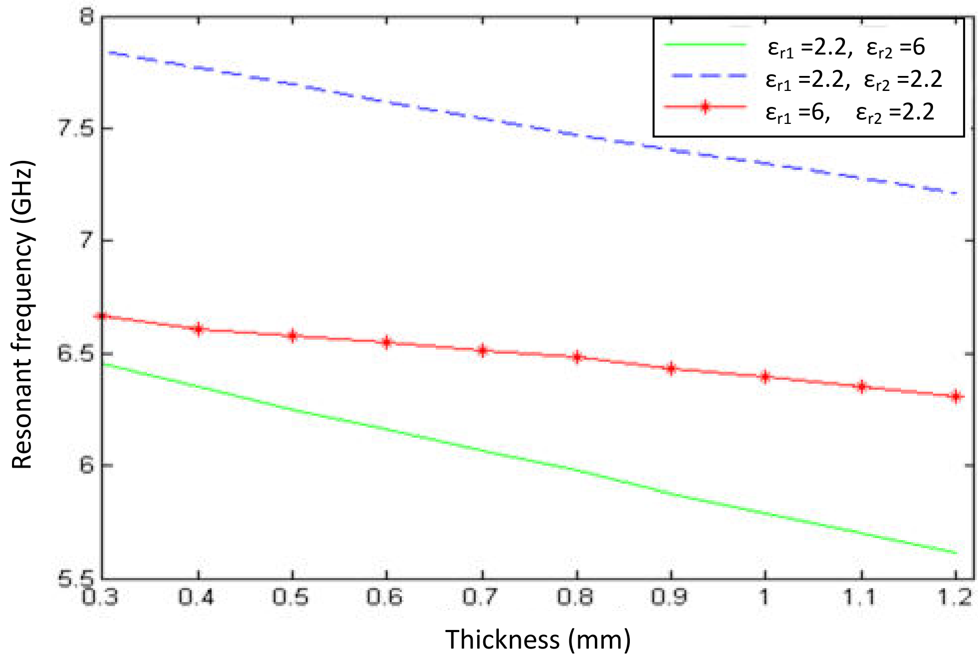

(b) Two-layer substrate

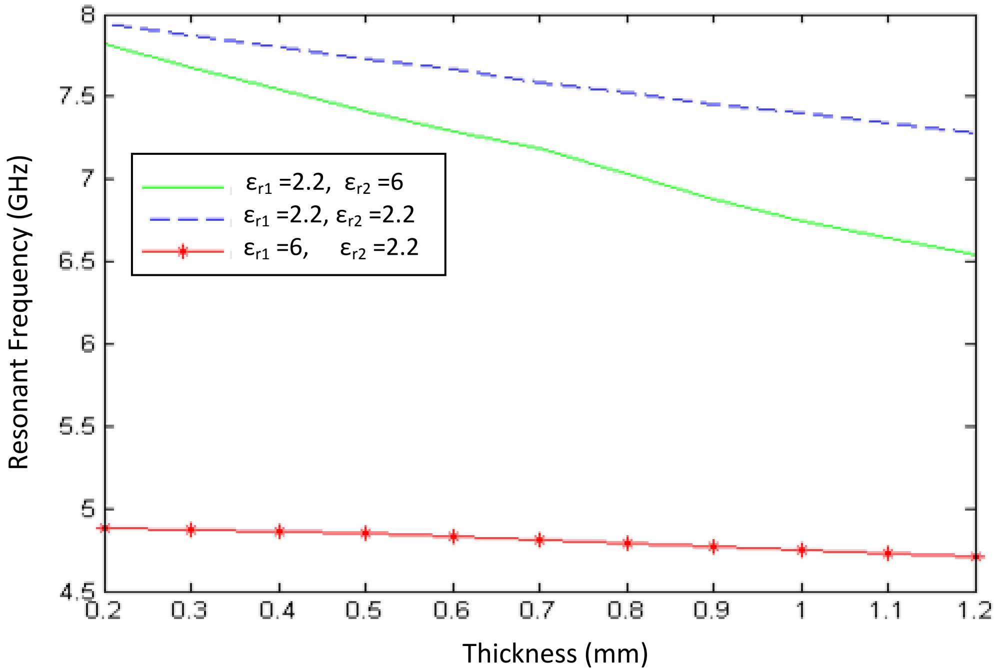

(c) Substrate-superstrate configuration

Fig. 2 Effect of thickness on resonant frequency of three structures for *a*=1 cm, *b*=1.25 cm

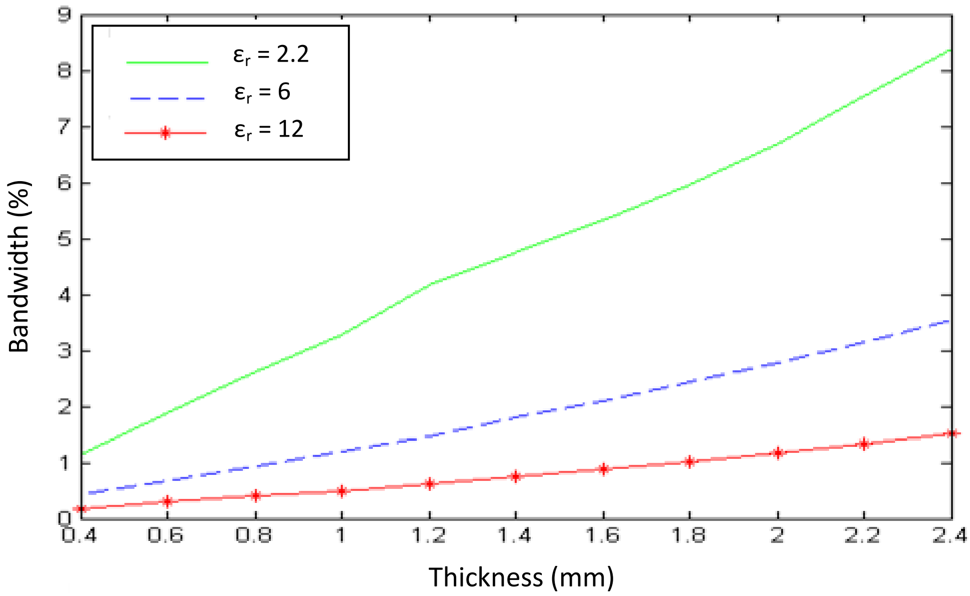

Fig. 3 Bandwidth of a single layer structure as a function of thickness for *a*=1 cm, *b*=1.25 cm

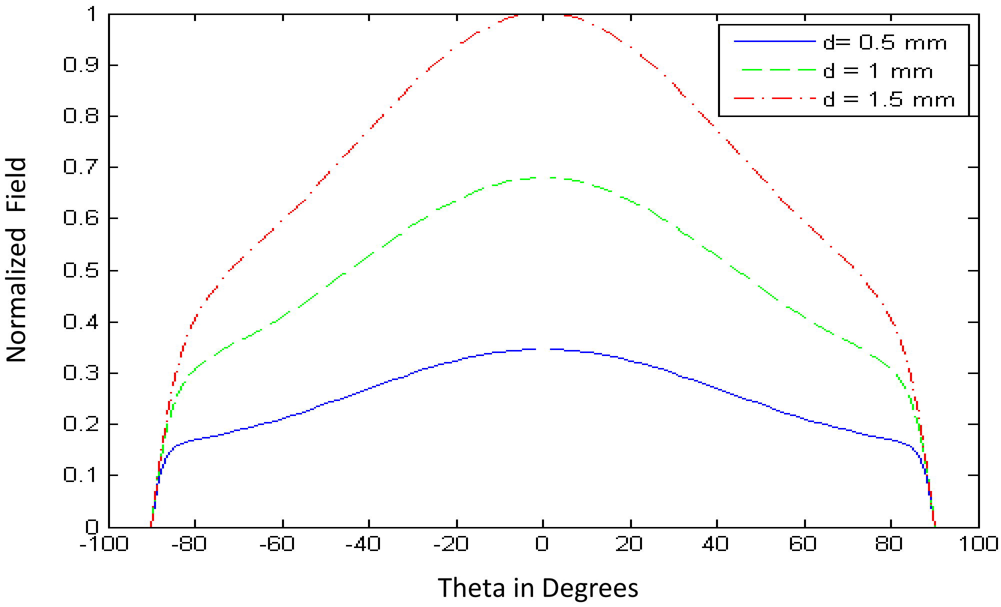

Fig. 4 Effect of thickness on the radiation pattern of for *a*=1 cm, *b*=1.25 cm, ε_r = 2.2

We can observe form the **Fig. 2(a)-(c)** that the resonant frequency is inversely proportional to the substrate thickness regardless of its permittivity or its homogeneity. From **Fig. 3**, we notice that the bandwidth is directly proportional to the substrate thickness, this is observed for both two-layer structures. Also we can observe that the radiated field strength is directly proportional to the substrate thickness.

b- Effect of permittivity

We can compare the effect of relative permittivity for both two-layers substrate and superstrate structures by considering an homogenous dielectric with the same thickness mm), and varying the relative permittivity from 2 to 12, and the patch size is *a*=1 cm, *b*=1.25 cm. The resonant frequency and the bandwidth variations are presented in **Fig. 5.** Furthermore, the influence of the dielectric permittivity on the radiation pattern is also illustrated in **Fig. 6**. We can notice that both the resonant frequency and bandwidth are inversely proportional to the relative permittivity. When we compare the effect of the thickness to the effect of the permittivity by comparing the maximum to the minimum resonant frequency ratio in both cases, we find that impact of the permittivity is larger than the effect of the thickness. In addition, the cover layer (superstrate) exhibit a similar behavior as mentioned above concerning the influence of the thickness and the permittivity on the resonant frequency as it is shown in **Fig. 7.** The permittivity as depicted by **Fig. 6** is inversely proportional with the radiated field.

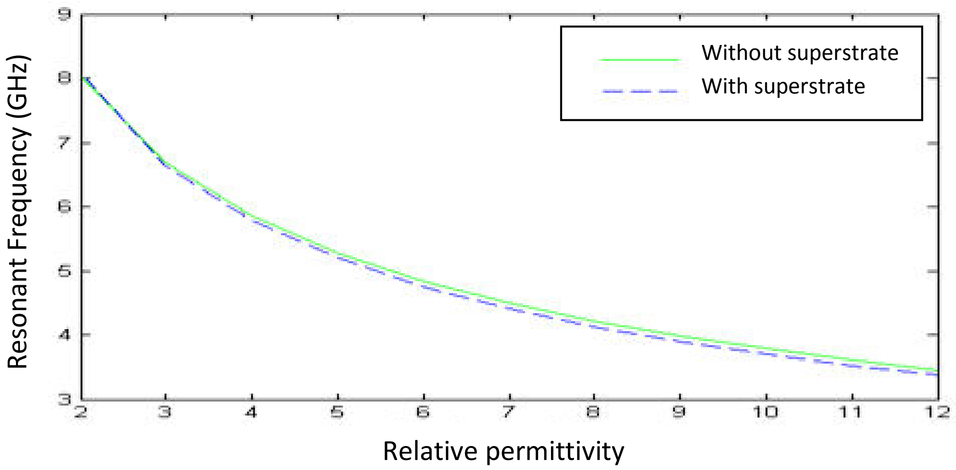

(a)

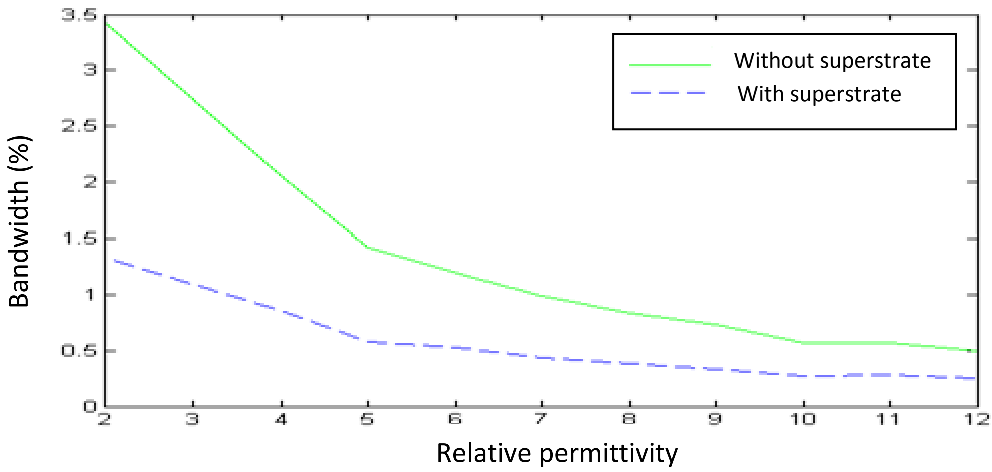

(b)

Fig. 5 Influence of permittivity on **(a)** resonant frequency **(b)** bandwidth (d_1 = d_2 = 0.5 mm)

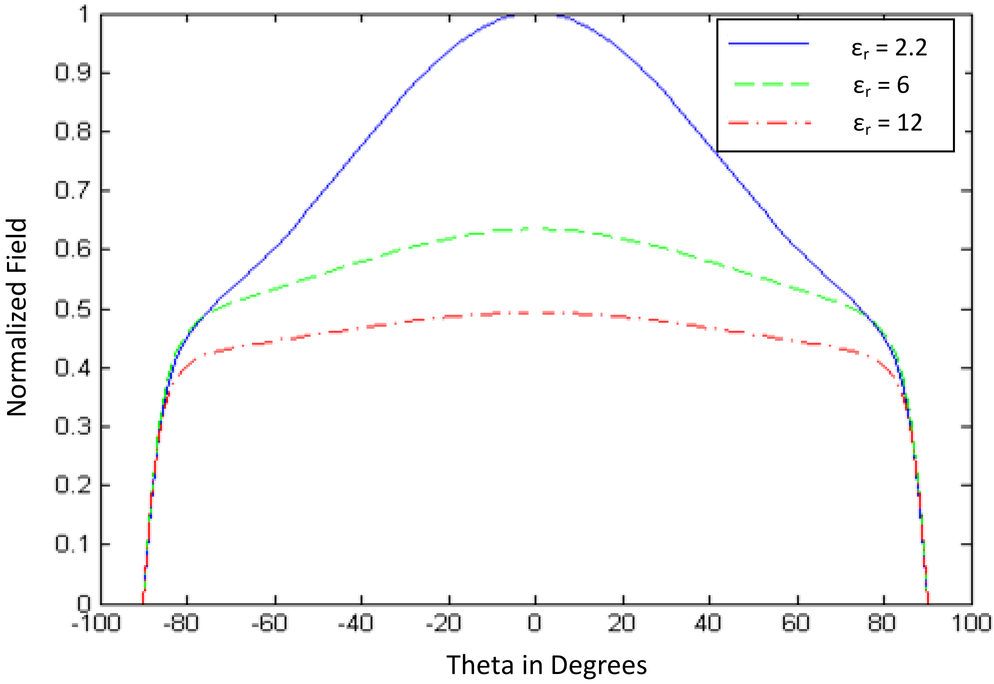

Fig. 6 Influence of permittivity on the radiation pattern for d = 1 mm

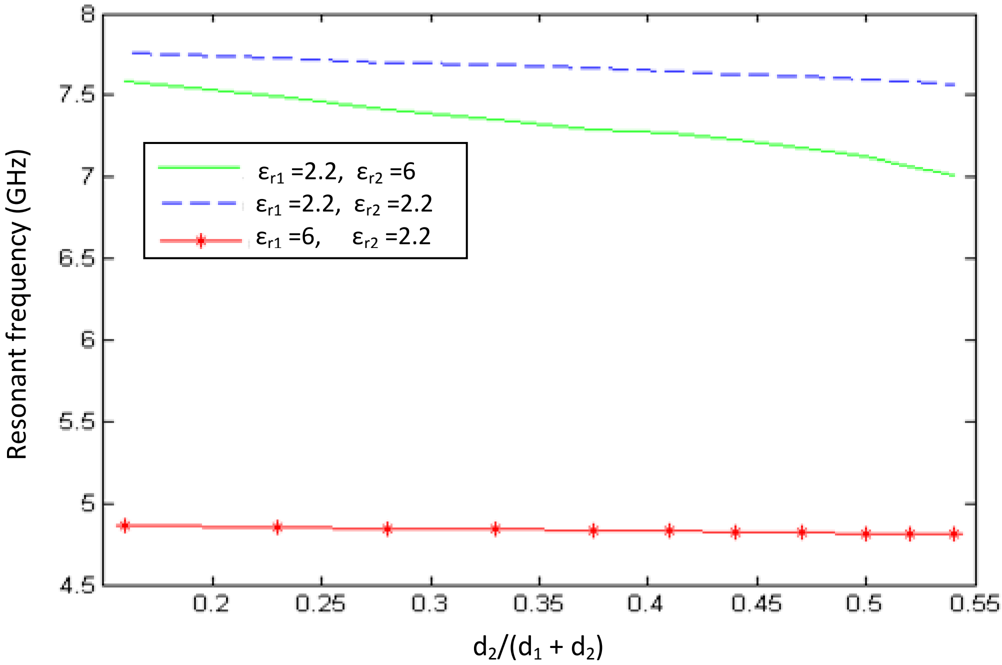

(a)

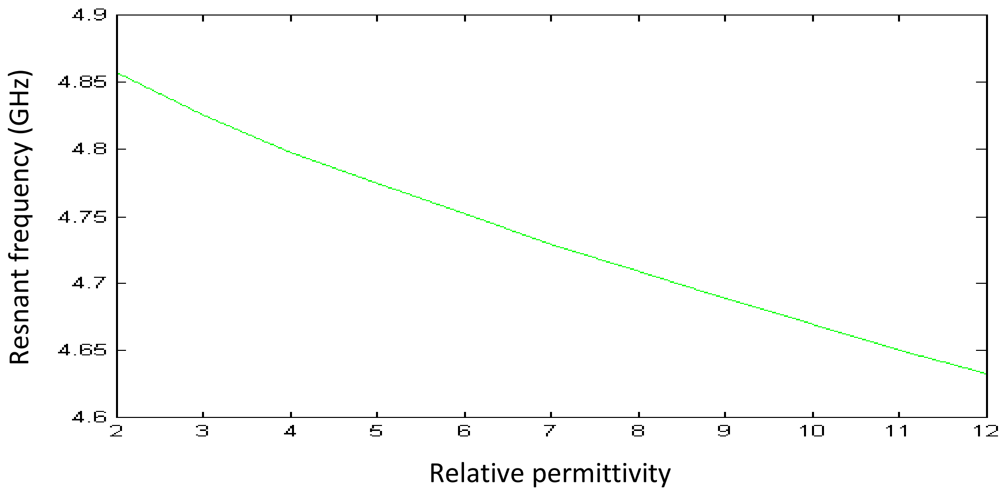

(b)

Fig. 7 Impact of Cover layer **(a)** thickness for d_1 = 0.6 mm **(b)** permittivity for d_1 = d_2 = 0.5 cm, ε_{r1} = 6, on the resonant frequency of substrate-superstrate structure

c- Effect of permeability

The effect of the permeability is investigated by varying the relative permeability form 1 to 10 for three cases, two layers structures (two layers substrate, substrate-superstrate configurations) with a single patch, and a two layers structure with stacked patches. The effects of the permeability on the resonant frequency and bandwidth of these structures are shown in **Fig. 8** and **9.** The effect of permeability on the radiation pattern is shown in **Fig. 10**.

We notice that the resonant frequency is inversely proportional to the permeability for both single patch and stacked patches structures. The bandwidth of single patch structures is proportional to the permeability. For stacked patches configuration, the same thing applies to the upper resonance bandwidth, but the opposite is noticed for the lower resonance bandwidth.

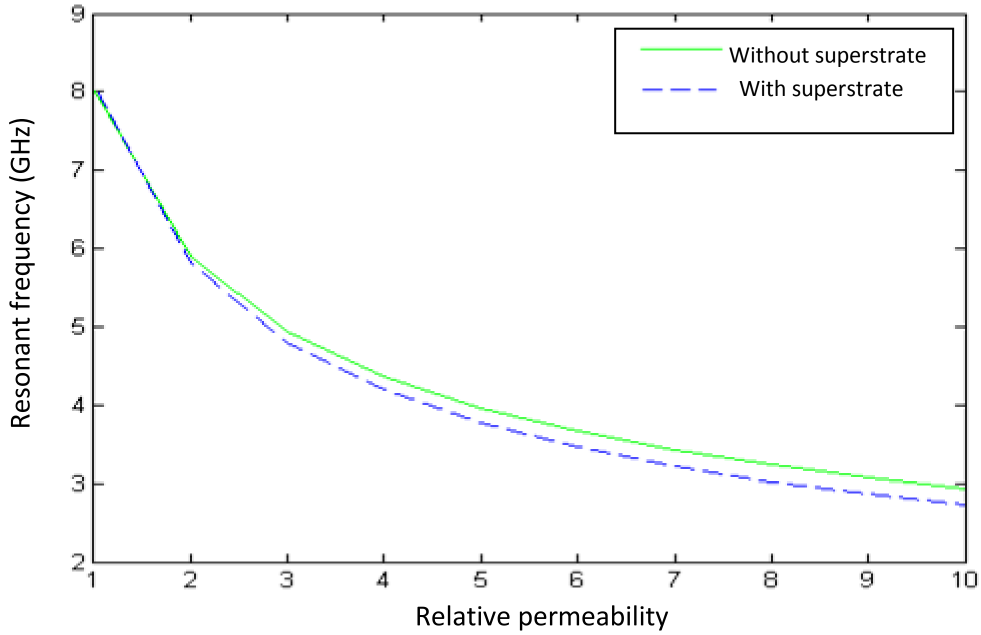

(a)

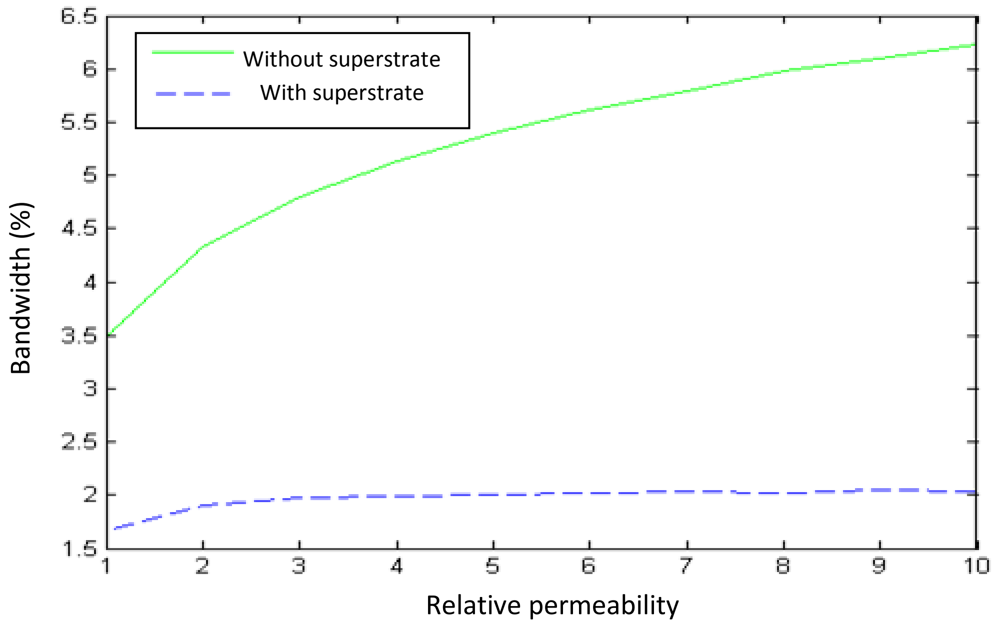

(b)

Fig. 8 The influence of relative permeability on **(a)** resonant frequency and **(b)** bandwidth for the case of a single patch, $d_1 = d_2 = 0.5$ cm, $\varepsilon_{r1} = \varepsilon_{r2} = 2$, a=1 cm, b=1.25 cm

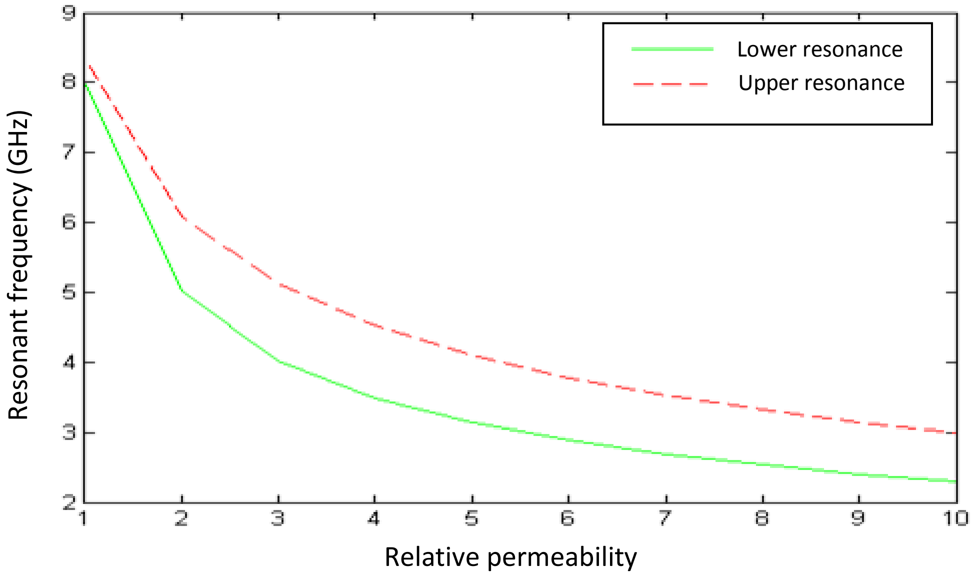

(a)

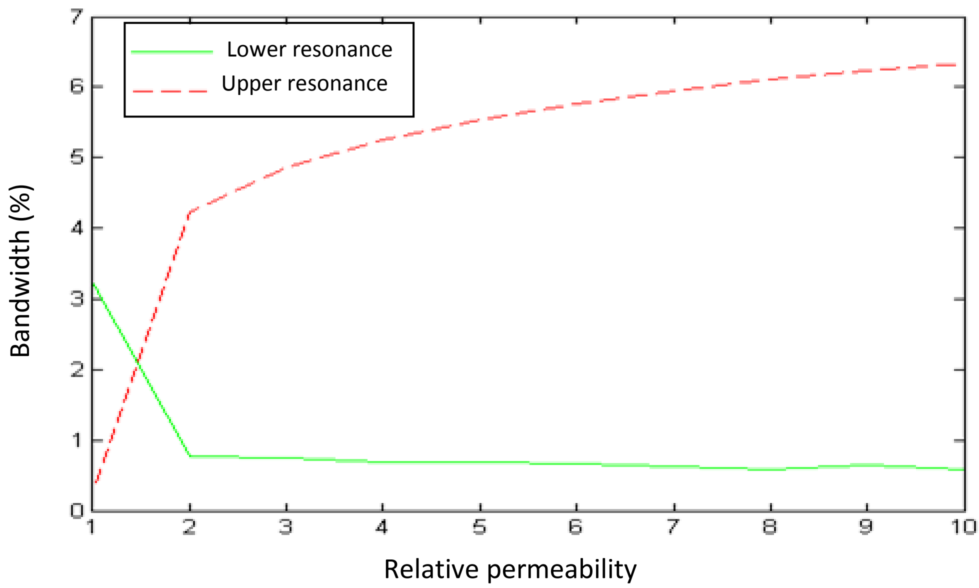

(b)

Fig. 9 Influence of relative permeability on **(a)** resonant frequency and **(b)** bandwidth for the case of stacked patches, $d_1 = d_2 = 0.5$ cm, $\varepsilon_{r1} = \varepsilon_{r2} = 2$, $a_1 = a_2 = 1$ cm, $b_1 = b_2 = 1.25$ cm

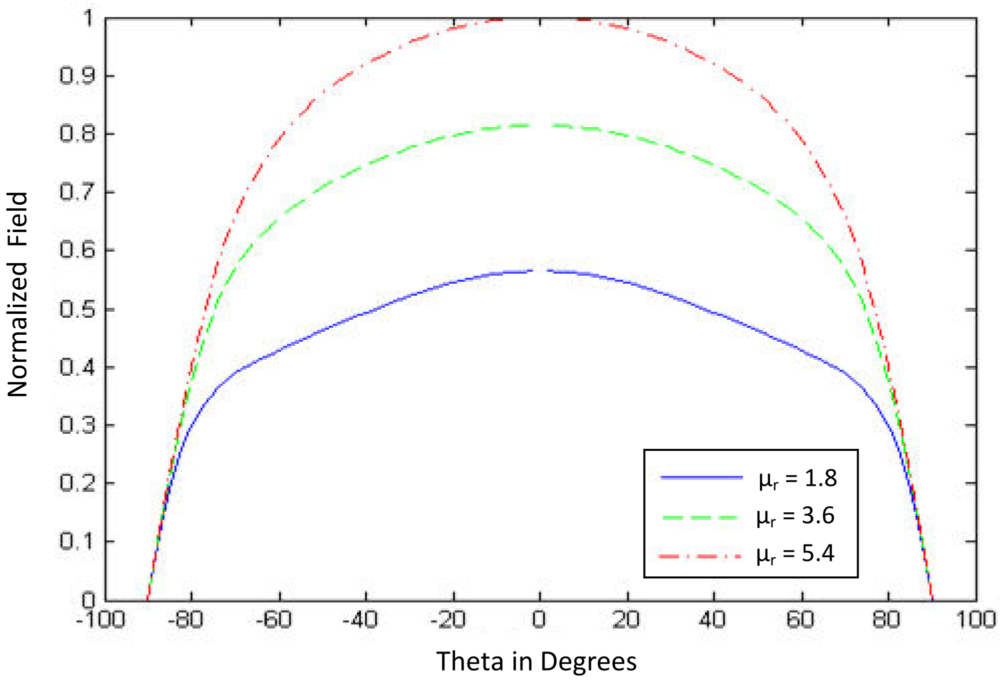

Fig. 10 Effect of permeability on radiation pattern for a=1 cm, b=1.25 cm, d = 1 mm, ε_r = 2.35

The maximum to the minimum resonant frequency ratio in the case of permeability is high which indicates a strong influence of the dielectric permeability on the resonant frequency. Also, we can see that the radiated field is getting stronger as the permeability is increased.

d- Effect of anisotropy

This section will be divided into two parts, first, we will explore the effect of the anisotropy ratio and the elements of permittivity and permeability tensors, and then we will check the effect of the anisotropy on the resonant frequency by comparing the results obtained when the anisotropy is considered to those when it is ignored. The first part is detailed in the **Tables 1** and **2**, where the second part is illustrated by the **Fig. 11** and **Fig. 12.** In this section, the patches have the same size (a=1 cm, b=1.25 cm) and the substrate is homogenous with d = 1, (d_1 = d_2 = 0.5 cm). If we take case 1 (AR =1) in table 1 for example as a reference, when we increase the anisotropy ratio to 2 (cases 2 and 3), we can see that the resonant frequency does not follow a specific direction of variation i.e. the resonant frequency increases as in case 3 and decreases as in case 2 although the anisotropy ratio AR has been increased from 1 to 2 in both cases. This proofs that the consideration of the anisotropy ratio alone does not allow the prediction of the resonant frequency behavior, this conclusion applies on both dielectric and magnetic anisotropy. In order the investigate the effect of elements of the permittivity tensor (ε_x and ε_z), we take case 1 ($\varepsilon_x = 2.32$, $\varepsilon_z = 2.32$) as a reference, and we increase or decrease ε_x (as in cases 2 and 4 respectively) or ε_z (as in cases 5 and 3 respectively), we can see that the rate of change is at most 2.31% for ε_x , but the change reaches 31.85% for ε_z . This means that ε_z has a larger influence than ε_x on the resonant frequency. To investigate the effect of elements of the permeability tensor (μ_x and μ_z), we take case 1 ($\varepsilon_x = 2.4$, $\varepsilon_z = 2.4$) as a reference, and we increase or decrease μ_x (as in cases 2 and 4 respectively), or μ_z (as in cases 5 and 3 respectively), we can see that the maximum rate of change is 0.38% for μ_z , but the rate of change exceeds 35.84% for μ_x . This means that μ_x has a larger influence than μ_z on the resonant frequency.

Table 1 Influence of permittivity tensor elements on resonant frequency, μ_r = 1

Case #	ε_x	ε_z	*AR*	Single patch		Stacked patches			
				f_r (GHz)	Δf_r (%)	f_L (GHz)	Δf_L (%)	f_U (GHz)	Δf_u (%)
1	2.32	2.32	1	7.518	0	7.488	0	7.751	0
2	4.64	2.32	2	7.344	2.31	7.274	2.85	7.692	0.76
3	2.32	1.16	2	9.913	31.85	9.871	31.82	10.812	39.49
4	1.16	2.32	0.5	7.629	1.47	7.62	1.76	7.797	0.59
5	2.32	4.64	0.5	5.555	26.11	5.488	26.71	5.57	28.14

Table 2 Influence of permeability tensor elements on resonant frequency, ε_r = 2.35

Case #	μ_x	μ_z	AR	Single patch		Stacked patches			
				f_r (GHz)	Δf_r (%)	f_L (GHz)	Δf_L (%)	f_U (GHz)	Δf_u (%)
1	2.4	2.4	1	5.482	0	4.632	0	5.657	0
2	4.8	2.4	2	4.068	25.79	3.237	30.11	4.215	25.49
3	2.4	1.2	2	5.503	0.38	4.664	0.69	5.685	0.49
4	1.2	2.4	0.5	7.447	35.84	7.407	59.91	7.686	35.86
5	2.4	4.8	0.5	5.47	0.21	4.611	0.45	5.641	0.28

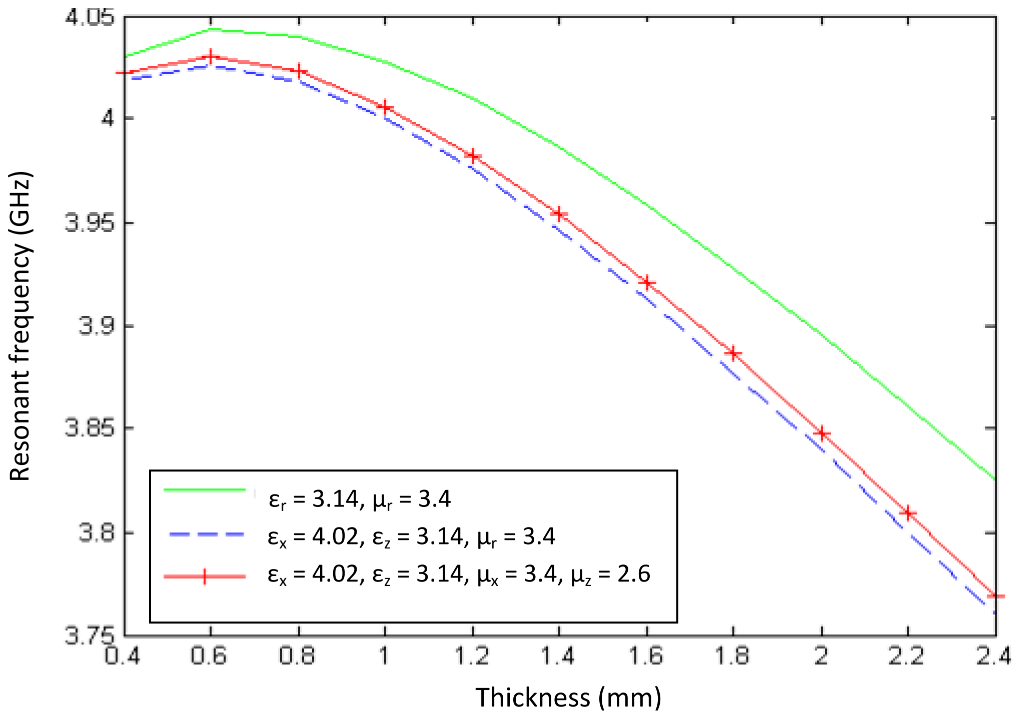

(a)

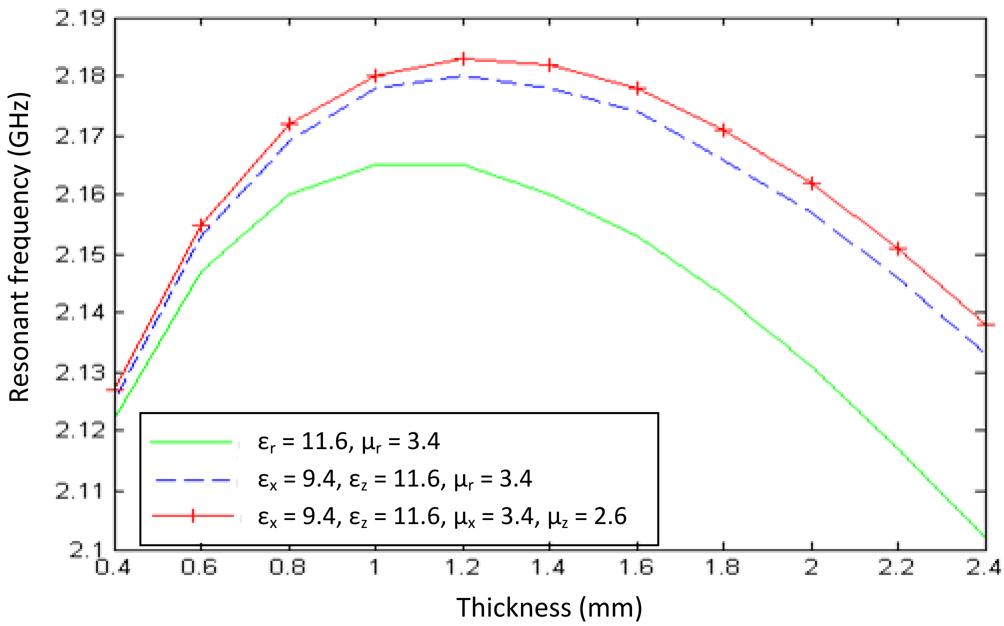

(b)

Fig. 11 Effect of **(a)** negative anisotropy and **(b)** positive anisotropy on the resonant frequency of a single patch configuration

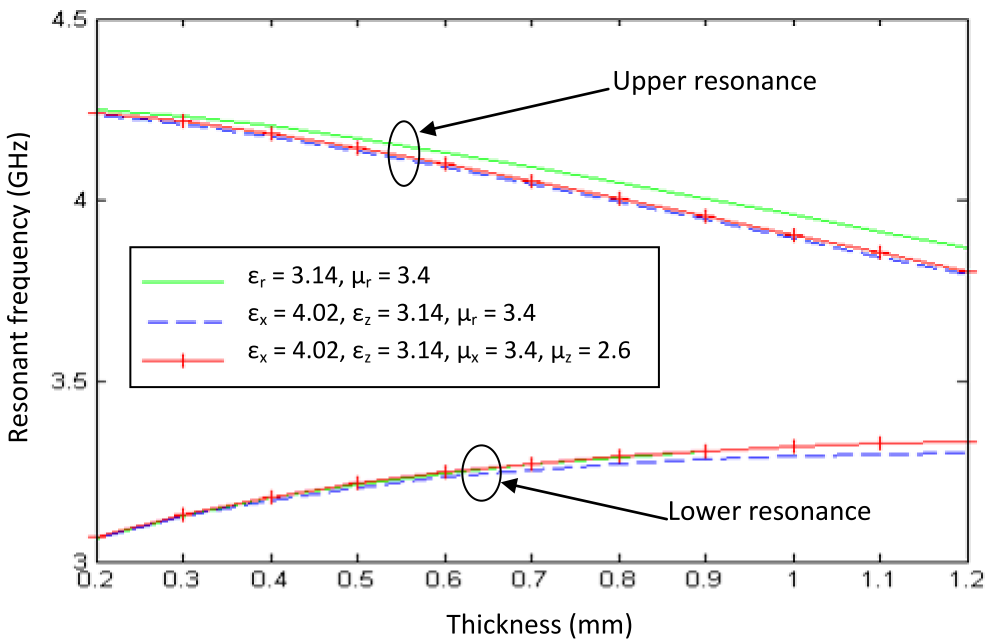

Fig. 12 Effect of anisotropy on the resonant frequency of a stacked patches configuration

When the anisotropy is considered the resonant frequency (for a constant value of the dielectric thickness) increases with respect to isotropic case if the dielectric possess a positive uniaxial anisotropy, and it decreases if the dielectric possess a negative uniaxial anisotropy. The maximum change in the resonant frequency for a single patch is 1.69% (for negative anisotropy), 1.71% (for positive anisotropy) and 2% for stacked patches. The effect of anisotropy becomes significant for thick substrates.

2.3.2. Effect of patch dimensions

Now we will consider that the patch length "*a*" is along the x-axis, and that the patch width "*b*" is along the y-axis, thus the first resonant mode is TM_{10} and the second resonant mode is TM_{01} which they have current density with x and y dependences respectively. We are going to investigate the effect of the patch length when its width is kept constant, and we will see effect of the patch width when its length is kept constant in **Fig. 13** and **14** respectively. After that, we vary both the length and the width while keeping the length to width ratio constant as it is shown in **Table 3**.

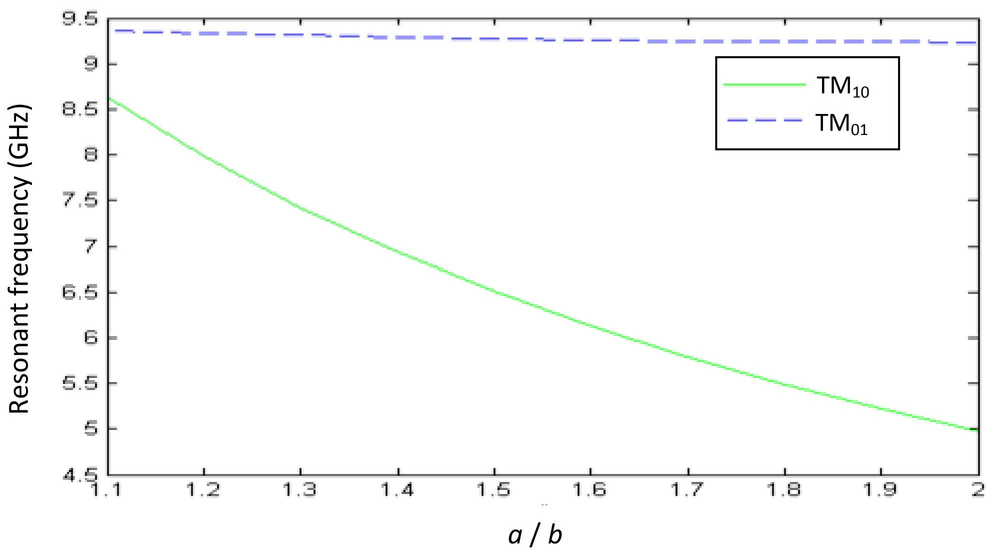

(a)

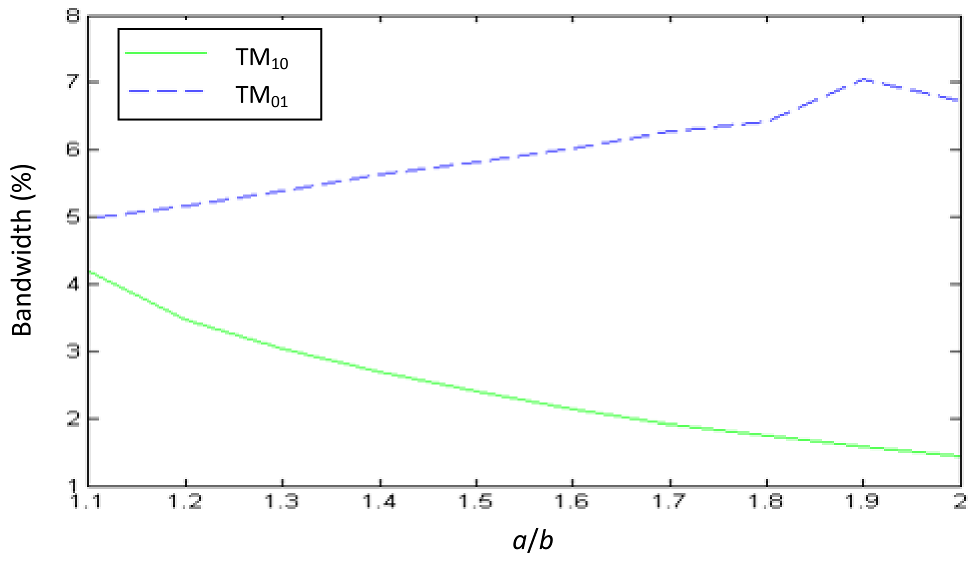

(b)

Fig. 13 Influence of the patch length on **(a)** resonant frequency and **(b)** bandwidth for *b* = 1 cm, *d* = 1 mm, ε_r = 2.2

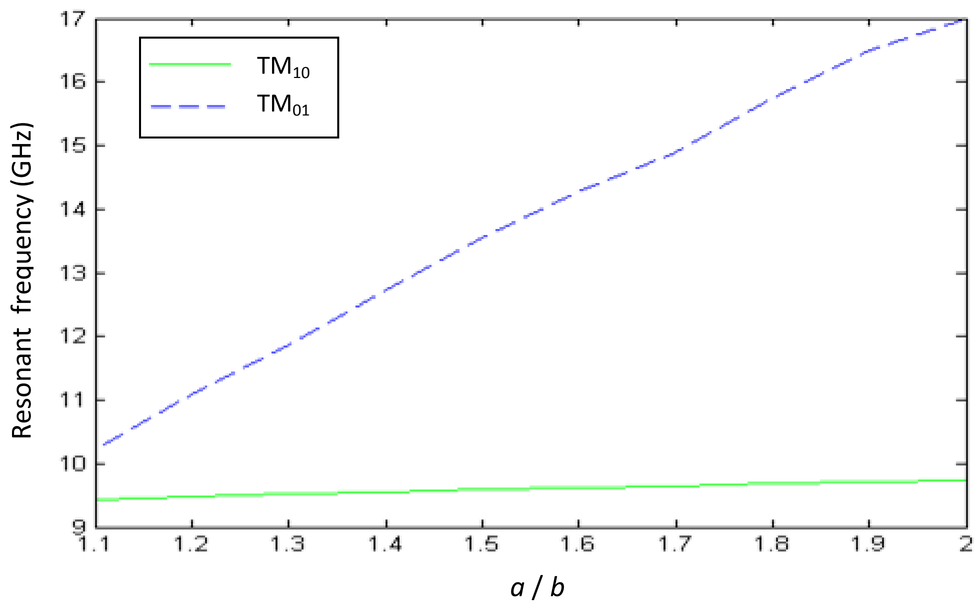

(a)

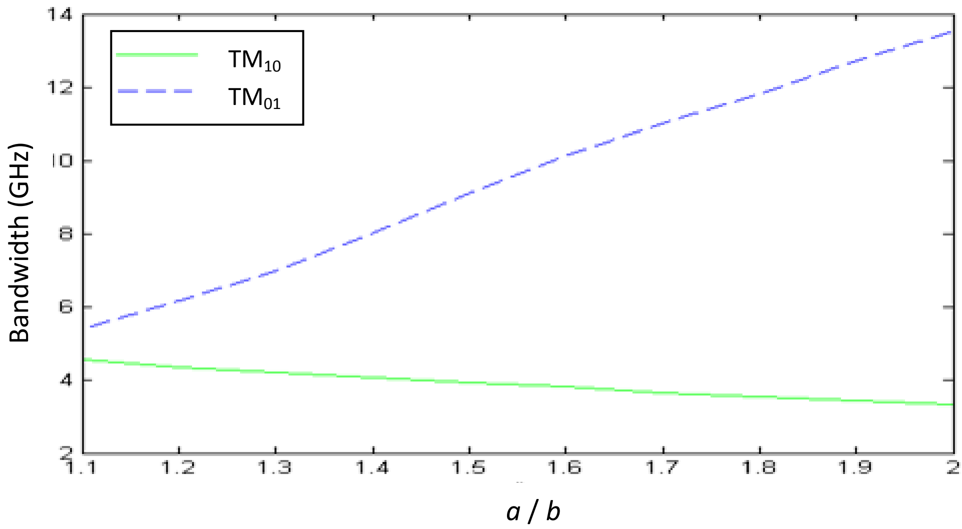

(b)

Fig. 14 Influence of the patch width on **(a)** resonant frequency and **(b)** bandwidth for *a* = 1 cm, *d* = 1 mm, ε_r = 2.2

Table 3 Comparison of the first two resonances (TM_{10} and TM_{01}) for a constant length-to-width ratio (*a*/*b* = 1.25), *d* = 1 mm, ε_r = 2.2

a(cm)	*b*(m)	TM_{10} mode		TM_{01} mode	
		f_r (GHz)	*BW* (%)	f_r (GHz)	*BW* (%)
1	0,8	9,495	4,31	11,465	6,52
1.1	0,88	8,681	3,98	10,501	5,92
1.2	0,96	7,992	3,44	9,687	5,49
1.3	1,04	7,406	3,15	8,99	5,12
1,4	1,12	6,902	2,93	8,398	4,81
1,5	1,2	6,46	2,72	7,873	4,5
1,6	1,28	6,071	2,53	7,408	4,22
1,7	1,36	5,727	2,36	6,996	3,97
1,8	1,44	5,419	2,22	6,627	3,75
1,9	1,52	5,142	2,09	6,296	3,55
2	1,6	4,893	1,98	5,995	3,37

Careful observation of **Fig. 13**, **14** and **Table 3** leads to the following results:

The resonant frequency is inversely proportional to the length and it is proportional to the width (for both modes). The length has a large impact on the TM_{10} mode, where the width has a large impact on the TM_{01} mode. The bandwidth always decreasing for increasing the length or the width for TM_{10} Mode, the opposite is noticed for the TM_{01} mode. When both the length and the width are increased by the same amount (the length to width ratio remains constant), both the resonant frequency and the bandwidth will decrease (for both modes). Furthermore, when we compute the physical bandwidth in GHz, we can find that the TM_{01} mode has a larger physical and fractional bandwidth than the TM_{10} mode. The impact of the patch dimensions on the radiation pattern has been also investigated as shown in **Fig. 15, 16**. The length and the width are chosen so that the fundamental mode is the TM_{01} mode. The radiation pattern of a given microstrip antenna for two resonant modes is also presented **Fig. 17** and **18**. From **Fig. 15** and **16**, we observe that the radiated field intensity increases as the patch becomes larger, however, the impact of the width is larger than the impact of the length on the radiation pattern. Whereas the result concluded from **Fig. 17** and **18** is that the second resonance always has the strongest radiated field regardless of the relative dimensions of the patch.

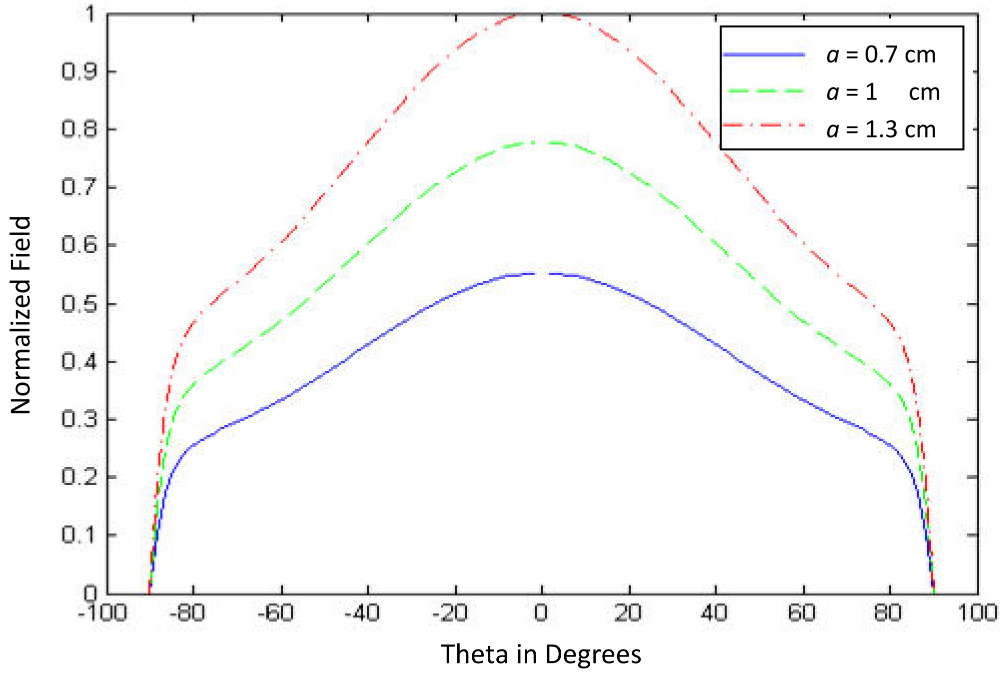

Fig. 15 radiation pattern for *b*=1.5 cm, d = 1 mm, ε_r = 2.2

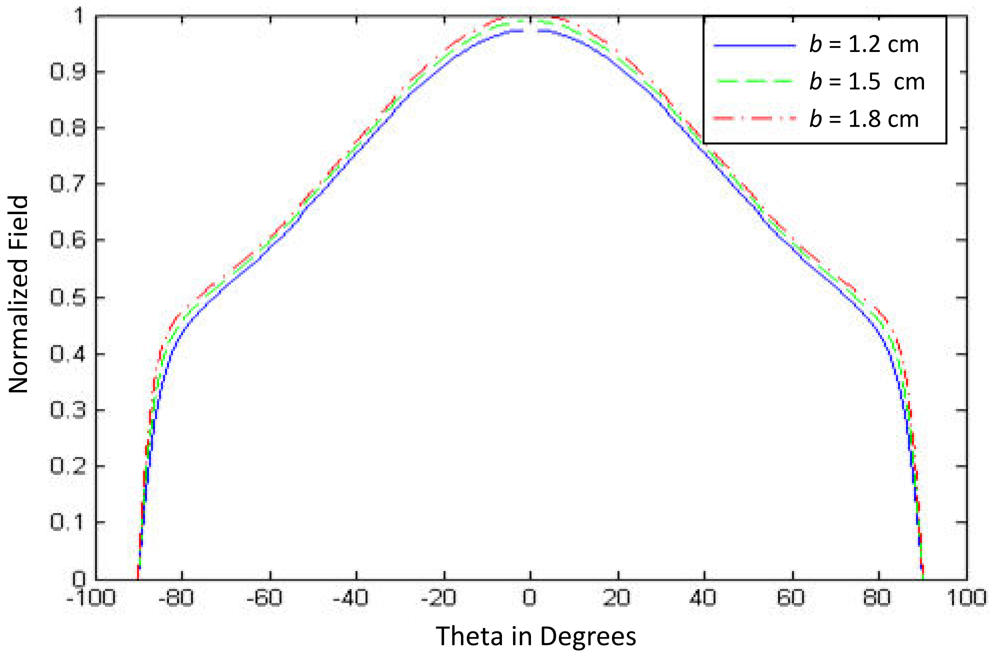

Fig. 16 radiation pattern for *a*=1cm, d = 1 mm, ε_r = 2.2

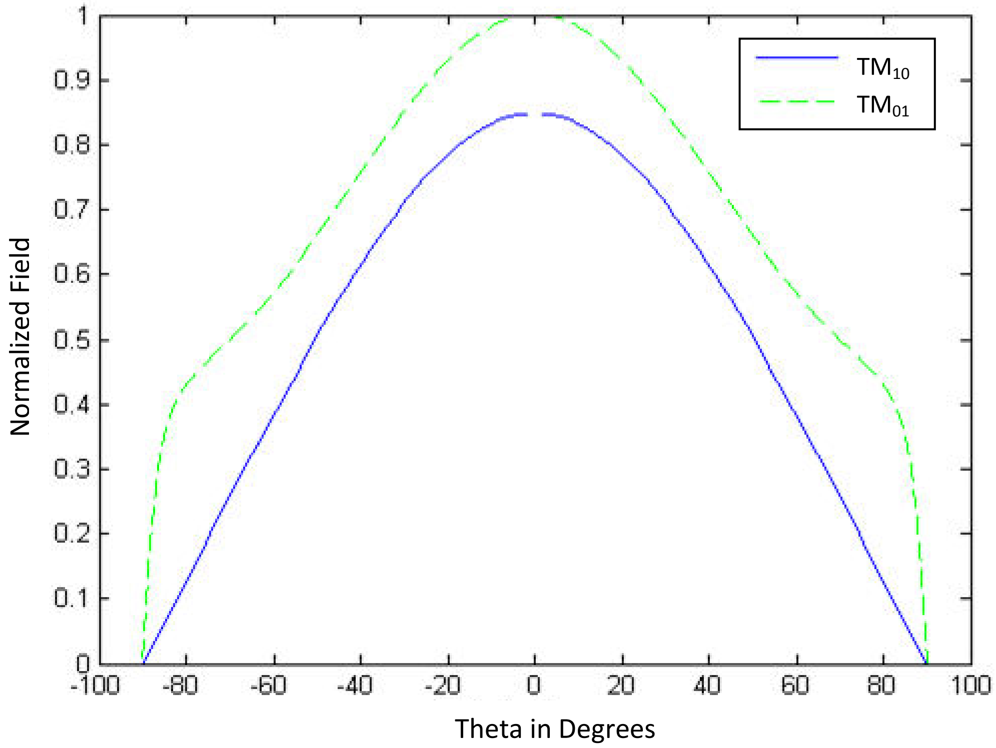

Fig. 17 radiation pattern of TM_{10} and TM_{01} for *a*=1.8 cm, *b*=1.5 cm, d = 1 mm, ε_r = 2

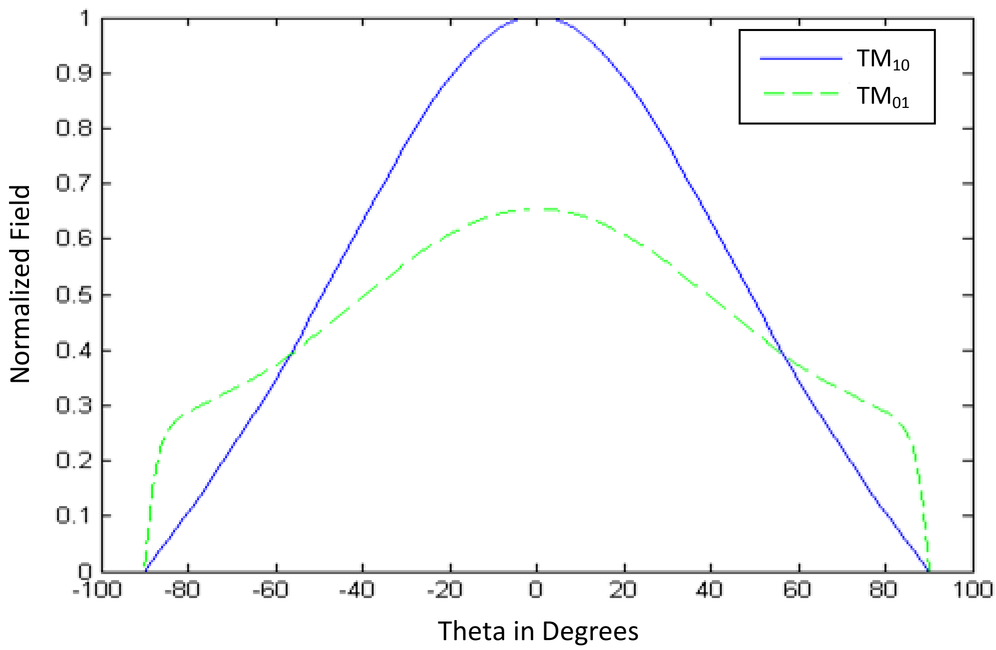

Fig. 18 radiation pattern of TM_{10} and TM_{01} for *a*=1.25 cm, b=2 cm, d = 1 mm, ε_r = 2

2.4. Conclusion

We have presented a full-wave analysis of a multilayered structure microstrip patch antenna. The analysis was based on deriving the dyadic Green's function of the substrate in spectral domain, and on the use of the method of moments to solve the electric field integral equation. The complex resonant frequency, yielding to the determination of the resonant frequency and the bandwidth, is computed by solving the characteristic equation for which the impedance matrix determinant vanishes. Stationary phase theorem allows the computation of the far field and subsequently the antenna radiation pattern. Throughout the accomplished parametric study on the influence of the different parameters of the structure on resonance and radiation characteristics of the microstrip antenna, the following results have been concluded:

- Thicker substrates offer larger bandwidths, but it produces also lower resonant frequencies.
- Permittivity and permeability have similar effects on resonant frequency, but they have opposite effects on bandwidth, where low permittivity values are required for large bandwidth, while for the permeability, high values are required.
- These results mean that choosing thicker substrates with low permittivity and high permeability enhances significantly the antenna bandwidth.
- For the substrate, the impact of the material properties (i.e. permittivity and permeability) on the resonant frequency is larger than the effect of its dimensions (mainly its thickness)

- It was found that in the case of dielectric anisotropy, the element of the permittivity tensor that is along the axis parallel to optical axis is the dominant element. However, in the case of magnetic anisotropy, the element of the permeability tensor that is along the axis perpendicular to optical axis is the dominant element.
- The resonant frequency is directly proportional to the patch width, and it is inversely proportional to the patch length.
- The patch length has a large influence on the first resonance while the width has a large influence on the second resonance (for our case, the first and the second resonances correspond to the modes TM_{10} and TM_{01} respectively).
- The patch width has the greater influence on the radiated field.
- The second resonance has a larger impact on the radiated field than does the first resonance.

Chapter 3

Full-Wave Analysis of Microstrip Patch Embedded in a Multilayered Medium Containing Chiral Materials

3.1. Introduction

Chiral medium is a reciprocal, optically active medium, in which right- and left-circularly polarized waves propagates through it with different phase constants. This property makes it similar to ferrites which are non-reciprocal and anisotropic materials. Physically, a chiral medium consists of an ordinary dielectric containing chiral objects of the same handedness; these objects are randomly oriented and uniformly distributed [11], [71]-[73]. The phenomenon of optical activity was discovered by Arago in 1811. He found that crystals of quartz rotate the plane of polarization of linearly polarized light transmitted in the direction of its optical axis, where the optical activity was found to be a result of chiral molecules in that medium [71]. Chirality or handedness is a purely geometric concept that refers to the lack of bilateral symmetry of an object. A chiral object, by definition, is a body that cannot be brought into congruence with its mirror image by translation and rotation. Such a body has the property of handedness and is either right-handed or left-handed [71], [74]. Optical activity can be explained through the magneto-electric coupling mechanism where, the electric field induces not only an electric polarization but also a magnetic polarization, and conversely, a magnetic field produces both electric and magnetic polarization [75].

Chiral materials are bi-isotropic media, and they are a special case of a wider class referred to as bi-anisotropic media. In a bi-anisotropic medium, the constitutive relations relate ***D*** to both ***E*** and ***B***, and ***H*** to both ***E*** and ***B*** by three-dimensional tensors. When these tensors reduce to scalar quantities, this medium becomes bi-isotropic [9], and sometimes referred to as Tellegan [76]. The prefix “bi” is used to demonstrate the dependence of ***D*** or ***H*** to both ***E*** and ***B*** [9]. Chirality and its effects in optical activity began to attract attention in the

Electromagnetics community with experiments performed by Lindeman [77]-[78] and Pickering [79] in microwave regime where the results were somewhat similar to those in optical frequencies. Since the paper published by Kong [9] in 1972 on the theory of electromagnetic field in bi-anisotropic media, many works have been published on the interaction of the electromagnetic field with both bi-anisotropic and bi-isotropic media. Propagation through chiral media was treated by [10], [76], [80]-[81]. The reflection and transmission through achiral-chiral interface or scattering from a chiral slab have been also considered [10], [82]-[84]. Studies on electromagnetic wave propagation in guided structures such as waveguides have been reported by Eftimiu and Pearson [85], and also by Pelet and Engheta [71]. Microstrip lines on a chiral substrate have been analyzed by Kluskens and Newman [11], and also by Toscano and Vegni [75]. Printed antennas on chiral media have gained similar interest, where the radiation of a straight thin wire embedded in an isotropic chiral media, was investigated by Lakhtakia [85]. A similar work on printed dipoles was accomplished by Lumini and Lacava [86].

Microstrip patch radiators on chiral substrates have been studied by Pelet and Engheta [12]. Pozar [72] has also considered microstrip arrays. Toscano and Vegni [87] presented a formulation for arbitrary shaped patch antennas on a chiral slab. The published studies were not limited only to planar structures. Li et al [88] published a paper on the analysis of a rectangular patch printed on a cylindrical chiral substrate. Furthermore, radiation of dipoles in multilayered chiral media has also been reported for planar [89], spherically- [90] and cylindrically- [91] layered structures. Green's functions associated to the chiral media, was derived by most of the after mentioned references. Specifically, [10], [75], [87] and [92] have derived spectral-domain Green's function for a single layer medium. Ali et al [76] have formulated spectral domain Green's function for layered chiral media. Whereas Li et al [88] have provided spatial domain Green's function.

3.2. Theory

In order to analyze the electromagnetic field in a chiral media, a good starting point is constitutive relations. As described by [11] and [72], constitutive relation s are given by

$$\boldsymbol{D} = \varepsilon\boldsymbol{E} - j\xi\,\boldsymbol{B} \tag{1}$$

$$\boldsymbol{H} = \frac{1}{\mu}\,\boldsymbol{B} - j\xi\,\boldsymbol{E} \tag{2}$$

Where ε, μ, ξ are, respectively, the permittivity, permeability and chiral admittance.

The equations (1) and (2) can be rewritten as

$$\boldsymbol{D} = \varepsilon_c\boldsymbol{E} - j\mu\xi\,\boldsymbol{H} \tag{3}$$

$$\boldsymbol{B} = \mu\boldsymbol{H} + j\mu\xi\,\boldsymbol{E} \tag{4}$$

With

$$\varepsilon_c = \varepsilon + \mu\xi^2 \tag{5}$$

Assuming $e^{j\omega t}$ time-dependence, Maxwell's equations (with current density equal to zero), are defined as

$$\nabla \times \boldsymbol{E} = -j\omega\boldsymbol{B} \tag{6-a}$$

$$\nabla \times \boldsymbol{H} = j\omega\boldsymbol{D} \tag{6-b}$$

$$\nabla . \boldsymbol{D} = \rho \tag{6-c}$$

$$\nabla \, . \, \boldsymbol{B} = 0 \tag{6-d}$$

Using (3) and (4), the equations (6-a) to (6-d) can be rewritten as

$$\nabla \times \boldsymbol{E} = \omega\mu\xi \, \boldsymbol{E} - j\omega\mu \, \boldsymbol{H} \tag{7-a}$$

$$\nabla \times \boldsymbol{H} = j\omega\varepsilon_c \, \boldsymbol{E} + \omega\mu\xi \, \boldsymbol{H} \tag{7-b}$$

$$\nabla \, . \, \boldsymbol{E} = \frac{\rho}{\varepsilon} \tag{7-c}$$

$$\nabla \, . \, \boldsymbol{H} = -j\xi \, \frac{\rho}{\varepsilon} \tag{7-d}$$

Using bi-dimensional Fourier Transform defined by

$$\widetilde{\boldsymbol{A}}\left(k_x \, , k_y \, , z\right) = FT \, \{\boldsymbol{A} \, (x \, , y \, , z)\} = \iint_{-\infty}^{+\infty} \boldsymbol{A} \, (x \, , y \, , z) e^{-j(k_x x \, + \, k_y y)} dx \, dy \tag{8}$$

Then

$$FT\{\nabla \times \boldsymbol{E}\} = \widetilde{\nabla} \times \widetilde{\boldsymbol{E}} \tag{9}$$

With

$$\widetilde{\nabla} = jk_x \, \boldsymbol{e_x} + jk_y \, \boldsymbol{e_y} + \frac{\partial}{\partial z} \, \boldsymbol{e_z} \tag{10}$$

$\boldsymbol{e_x}$, $\boldsymbol{e_y}$, $\boldsymbol{e_z}$ Are the unit vectors of a Cartesian coordinate system.

Thus eq. *(7a) – (7b)* in spectral domain, can be written as

$$\widetilde{\nabla} \times \widetilde{\boldsymbol{E}} = \omega\mu\xi \, \widetilde{\boldsymbol{E}} - j\omega\mu \, \widetilde{\boldsymbol{H}} \tag{11-a}$$

$$\widetilde{\nabla} \times \widetilde{\boldsymbol{H}} = j\omega\varepsilon_c \, \widetilde{\boldsymbol{E}} + \omega\mu\xi \, \widetilde{\boldsymbol{H}} \tag{11-b}$$

We can write eq. *(7-a), (7-b)* in matrix form as

$$\nabla \times \begin{pmatrix} \boldsymbol{E} \\ \boldsymbol{H} \end{pmatrix} = [\boldsymbol{K}] \begin{pmatrix} \boldsymbol{E} \\ \boldsymbol{H} \end{pmatrix} \tag{12}$$

Where

$$[\boldsymbol{K}] = \begin{bmatrix} \omega\mu\xi & -j\omega\mu \\ j\omega\varepsilon_c & \omega\mu\xi \end{bmatrix} \tag{13}$$

Using the properties

$$\nabla \times \nabla \times \boldsymbol{E} = \nabla(\nabla . \boldsymbol{E}) - \nabla^2 \boldsymbol{E} \tag{14}$$

$$\nabla \times \nabla \times \boldsymbol{H} = \nabla(\nabla . \boldsymbol{H}) - \nabla^2 \boldsymbol{H} \tag{15}$$

We find

$$\nabla^2 \boldsymbol{E} + ((\omega\mu\xi)^{\boldsymbol{2}} + \omega^2\mu\varepsilon_c)\, \boldsymbol{E} - j2(\omega\mu)^2\xi\, \boldsymbol{H} = 0 \tag{16}$$

$$\nabla^2 \boldsymbol{H} + ((\omega\mu\xi)^{\boldsymbol{2}} + \omega^2\mu\varepsilon_c)\, \boldsymbol{H} + j2\omega^2\mu\varepsilon_c\xi\, \boldsymbol{E} = 0 \tag{17}$$

In matrix form, equations (16) and (17) can be written as

$$\nabla^2 \begin{pmatrix} \boldsymbol{E} \\ \boldsymbol{H} \end{pmatrix} + [\boldsymbol{M}] \begin{pmatrix} \boldsymbol{E} \\ \boldsymbol{H} \end{pmatrix} = 0 \tag{18}$$

Where

$$[\boldsymbol{M}] = \begin{bmatrix} (\omega\mu\xi)^{\boldsymbol{2}} + \omega^2\mu\varepsilon_c & -j2(\omega\mu)^2\xi \\ j2\omega^2\mu\varepsilon_c\xi & (\omega\mu\xi)^{\boldsymbol{2}} + \omega^2\mu\varepsilon_c \end{bmatrix} \tag{19}$$

With

$$[\boldsymbol{M}] = [\boldsymbol{K}]^2 \tag{20}$$

So we can rewrite eq. (18) as

$$\nabla^2 \begin{pmatrix} \boldsymbol{E} \\ \boldsymbol{H} \end{pmatrix} + [\boldsymbol{K}]^2 \begin{pmatrix} \boldsymbol{E} \\ \boldsymbol{H} \end{pmatrix} = 0 \tag{21}$$

The matrix $[\boldsymbol{K}]$ can be diagonalized as

$$[\boldsymbol{K}] = [\boldsymbol{A}] \begin{bmatrix} k_+ & 0 \\ 0 & k_- \end{bmatrix} [\boldsymbol{A}]^{-1} \tag{22}$$

Where

$$[\boldsymbol{A}] = \begin{bmatrix} 1 & 1 \\ \frac{j}{\eta_c} & -\frac{j}{\eta_c} \end{bmatrix} \tag{23}$$

$$[\boldsymbol{A}]^{-1} = \frac{1}{2} \begin{bmatrix} 1 & -j\eta_c \\ 1 & j\eta_c \end{bmatrix} \tag{24}$$

And

$$\eta_c = \sqrt{\frac{\mu}{\varepsilon_c}} \tag{25}$$

$$k_\pm = \omega\sqrt{\mu\varepsilon_c} \pm \omega\mu\xi \tag{26}$$

In eq. (26), k_+ is related to right-hand circularly polarized (RHCP) wave, whereas k_- is related to left-hand circularly polarized (LHCP) wave. Substituting $[\boldsymbol{K}]$ by its expression given in eq. (22) in eq. (21) will lead to

$$[\boldsymbol{A}]^{-1}\nabla^2 \begin{pmatrix} \mathbf{E} \\ \mathbf{H} \end{pmatrix} + \begin{bmatrix} k_+ & 0 \\ 0 & k_- \end{bmatrix}^2 [\boldsymbol{A}]^{-1} \begin{pmatrix} \mathbf{E} \\ \mathbf{H} \end{pmatrix} = 0 \tag{27}$$

If we put

$$[\boldsymbol{A}]^{-1} \begin{pmatrix} \mathbf{E} \\ \mathbf{H} \end{pmatrix} = \begin{pmatrix} \mathbf{E}_+ \\ \mathbf{E}_- \end{pmatrix} \tag{28}$$

Then eq. (27) becomes

$$\nabla^2 \begin{pmatrix} \mathbf{E}_+ \\ \mathbf{E}_- \end{pmatrix} + \begin{bmatrix} k_+ & 0 \\ 0 & k_- \end{bmatrix}^2 \begin{pmatrix} \mathbf{E}_+ \\ \mathbf{E}_- \end{pmatrix} = 0 \tag{29}$$

Or more simply by

$$\nabla^2 \begin{pmatrix} \mathbf{E}_+ \\ \mathbf{E}_- \end{pmatrix} + \begin{pmatrix} \mathrm{k}_+^2 \mathbf{E}_+ \\ \mathrm{k}_-^2 \mathbf{E}_- \end{pmatrix} = 0 \tag{30}$$

$\boldsymbol{E}$, $\boldsymbol{H}$ are related to $\boldsymbol{E}_+$ and $\boldsymbol{E}_-$ by

$$\begin{pmatrix} \boldsymbol{E} \\ \boldsymbol{H} \end{pmatrix} = \begin{bmatrix} 1 & 1 \\ \frac{j}{\eta_c} & -\frac{j}{\eta_c} \end{bmatrix} \begin{pmatrix} \mathbf{E}_+ \\ \mathbf{E}_- \end{pmatrix} \tag{31}$$

This yield to

$$\boldsymbol{E} = \mathbf{E}_+ + \mathbf{E}_- \tag{32}$$

$$\boldsymbol{H} = \frac{j}{\eta_c} \mathbf{E}_+ - \frac{j}{\eta_c} \mathbf{E}_- = \mathbf{H}_+ + \mathbf{H}_- \tag{33}$$

With

$$\begin{pmatrix} \boldsymbol{H}_+ \\ \boldsymbol{H}_- \end{pmatrix} = \frac{j}{\eta_c} \begin{pmatrix} \boldsymbol{E}_+ \\ -\boldsymbol{E}_- \end{pmatrix} \tag{34}$$

By replacing eq. (31) in (12) we can rewrite Maxwell's equations in terms of $\boldsymbol{E}_+$ and $\boldsymbol{E}_-$

$$\nabla \times \boldsymbol{E}_+ = k_+ \boldsymbol{E}_+ \tag{35-a}$$

$$\nabla \times \boldsymbol{E}_- = -k_- \boldsymbol{E}_- \tag{35-b}$$

Consequently, the wave equations in terms of $\boldsymbol{E}_+$ and $\boldsymbol{E}_-$ can be defined as

$$\nabla^2 \boldsymbol{E}_+ + k_+^2 \boldsymbol{E}_+ = 0 \tag{36-a}$$

$$\nabla^2 \boldsymbol{E}_- + k_-^2 \boldsymbol{E}_- = 0 \tag{36-b}$$

In spectral domain equations (36-a), (36-b) can be written as

$$\tilde{\nabla}^2 \tilde{\boldsymbol{E}}_+ + k_+^2 \tilde{\boldsymbol{E}}_+ = 0 \tag{37-a}$$

$$\tilde{\nabla}^2 \tilde{\boldsymbol{E}}_- + k_-^2 \tilde{\boldsymbol{E}}_- = 0 \tag{37-b}$$

Using the expression of $\tilde{\nabla}$ given in eq. (10), $\tilde{\nabla}^2$ can be defined as

$$\tilde{\nabla}^2 = \tilde{\nabla} . \tilde{\nabla} = -k_s^2 + \frac{\partial^2}{\partial z^2} \tag{38}$$

Substituting $\tilde{\nabla}^2$ as defined by (38), in equations (37-a), (37-b) gives

$$\frac{\partial^2 \tilde{E}_+}{\partial z^2} + k_{z+}^2 \tilde{E}_+ = 0 \tag{39-a}$$

$$\frac{\partial^2 \tilde{E}_-}{\partial z^2} + k_{z-}^2 \tilde{E}_- = 0 \tag{39-b}$$

Where

$$k_{z+} = \sqrt{k_+^2 - k_s^2} \tag{40-a}$$

$$k_{z-} = \sqrt{k_-^2 - k_s^2} \tag{40-b}$$

For z-component**,** the general solution for $\tilde{E}_+$ and $\tilde{E}_-$ are given by

$$\tilde{E}_{z+} = A_1 e^{-jk_{z+}z} + B_1 e^{jk_{z+}z} \tag{41-a}$$

$$\tilde{E}_{z-} = A_2 e^{-jk_{z-}z} + B_2 e^{jk_{z-}z} \tag{41-b}$$

We point out that both $\tilde{E}_+$ and $\tilde{E}_-$ have x-, y- and z-components. By using eq. (10), (39-a) and (39-b), the x- and y-components of $\tilde{E}_+$ and $\tilde{E}_-$ (Transverse components) can be expressed in terms of z-components of $\tilde{E}_+$ and $\tilde{E}_-$ (longitudinal components) as

$$\tilde{E}_{x+} = \frac{jk_x}{k_s^2}\frac{\partial \tilde{E}_{z+}}{\partial z} + \frac{jk_y}{k_s^2}\, k_+\, \tilde{E}_{z+} \tag{42-a}$$

$$\tilde{E}_{y+} = \frac{jk_y}{k_s^2}\frac{\partial \tilde{E}_{z+}}{\partial z} - \frac{jk_x}{k_s^2}\, k_+\, \tilde{E}_{z+} \tag{42-b}$$

$$\tilde{E}_{x-} = \frac{jk_y}{k_s^2}\, k_-\tilde{E}_{z-} - \frac{jk_x}{k_s^2}\,\frac{\partial \tilde{E}_{z-}}{\partial z} \tag{43-a}$$

$$\tilde{E}_{y-} = \frac{jk_x}{k_s^2}\, k_-\tilde{E}_{z-} + \frac{jk_y}{k_s^2}\,\frac{\partial \tilde{E}_{z-}}{\partial z} \tag{43-b}$$

By substituting eq. (41-a), (41-b) in eq. (42-a) – (43-b), and applying boundary conditions at the interface ground plane-dielectric, and at the interface patch/dielectric- air, dyadic Green’s function in closed-form, can determined. The detailed expressions of Green’s function elements are given in [72]. We note that the symmetry in the dyadic Green’s tensor that usually exists for an ordinary dielectric substrate does not exist for the case of chiral substrate, which increase the computational effort by a factor of four. Moreover, extending the solution for a patch antenna on an ordinary dielectric substrate to chiral substrate, involves only the use of the new Green’s function components.

3.3. Results and Discussions

In this section we will investigate the effect of chirality, represented by chiral admittance ξ, on the resonant frequency, bandwidth and radiated field. The numerical results illustrated in **Fig**. **1-6**, are computed for two different patch sizes and for each case the impact of chirality is shown for different substrate thicknesses. From **Fig. 1** and **2** it can be noticed that increasing chiral admittance, which measures the degree of chirality, increases the resonant frequency. However, this seems to be thickness- and patch size-dependent, in another word, this result is valid only for thick substrates. How a substrate looks thick, depends to the patch size as depicted by **Fig. 1** and **2**. In term of the bandwidth, **Fig. 3, 4** show that increasing chiral admittance increases the bandwidth regardless to dielectric thickness. However, this enhancement in the bandwidth does not exceed 1.42% and it looks also dependent to the patch size, where smaller patches offer better bandwidths. Radiated field intensity increases by about 10% with the increase of the substrate chirality as shown in **Fig. 5** and **6**. Again, this increase is patch-size dependent where it is significant for small size patches.

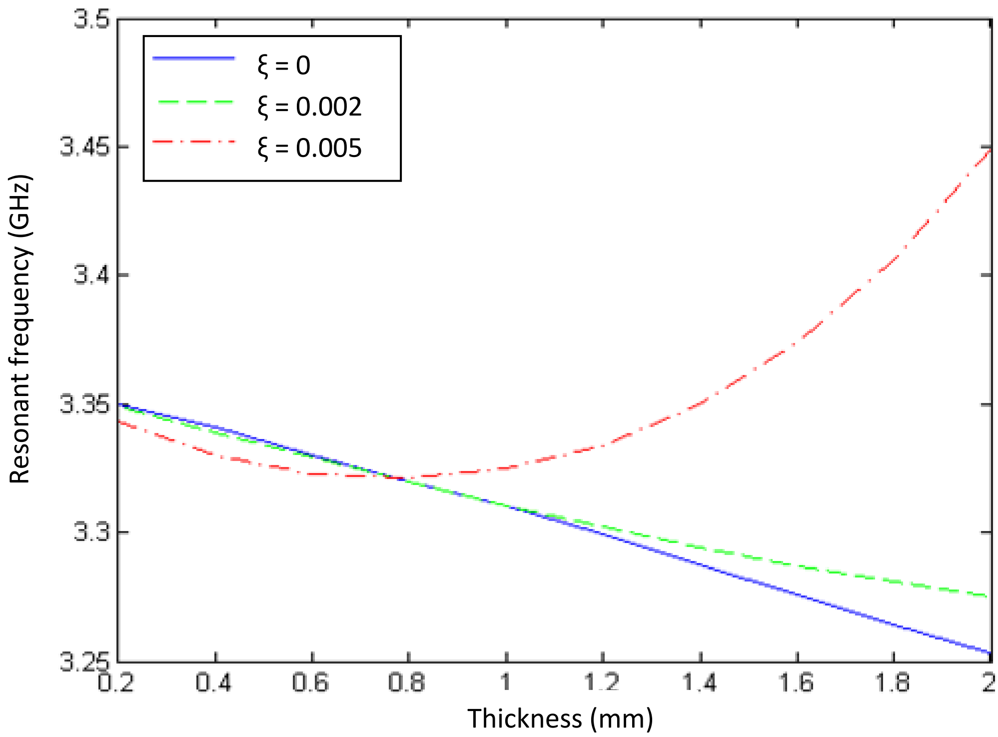

Fig. 1 Influence of Chirality on the resonant frequency for *a* x *b* = 2 x 3 cm, ε_r = 2.2

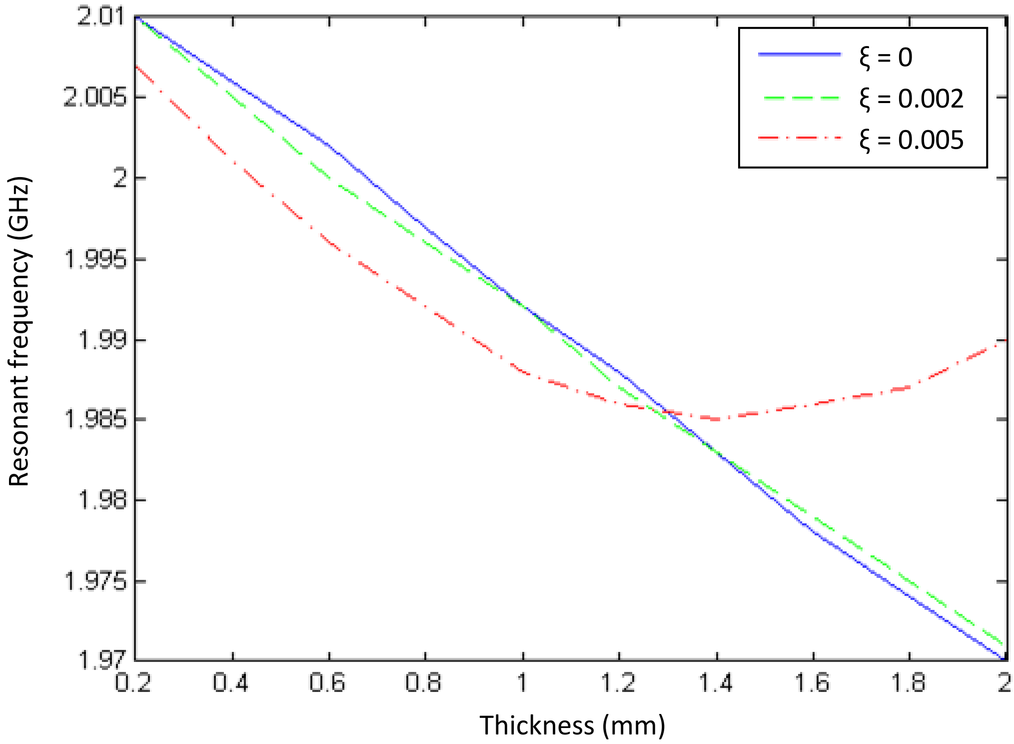

Fig. 2 Influence of Chirality on the resonant frequency for a x b = 4 x 5 cm, ε_r = 2.2

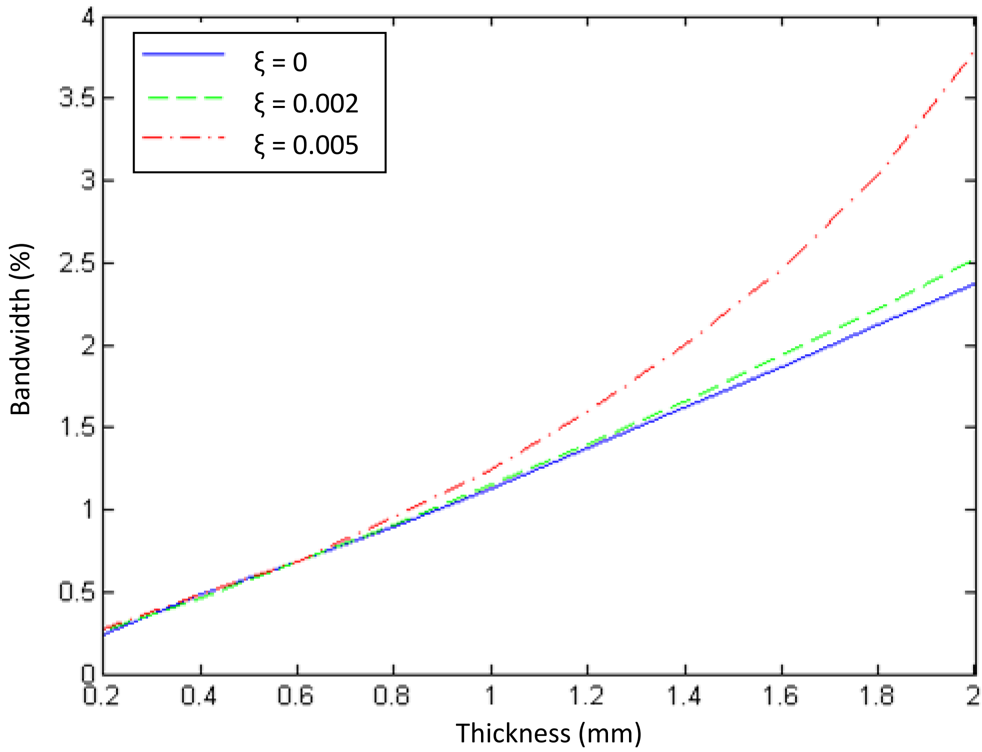

Fig. 3 Influence of Chirality on the bandwidth for a x b = 2 x 3 cm, ε_r = 2.2

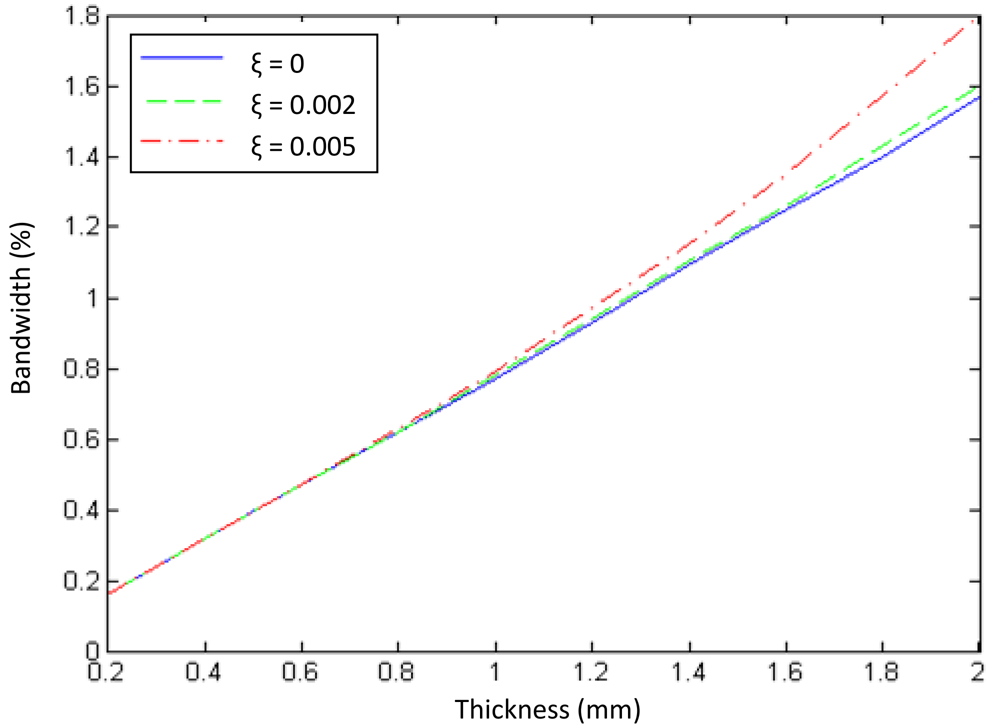

Fig. 4 Influence of Chirality on the bandwidth for *a* x *b* = 4 x 5 cm, ε_r = 2.2

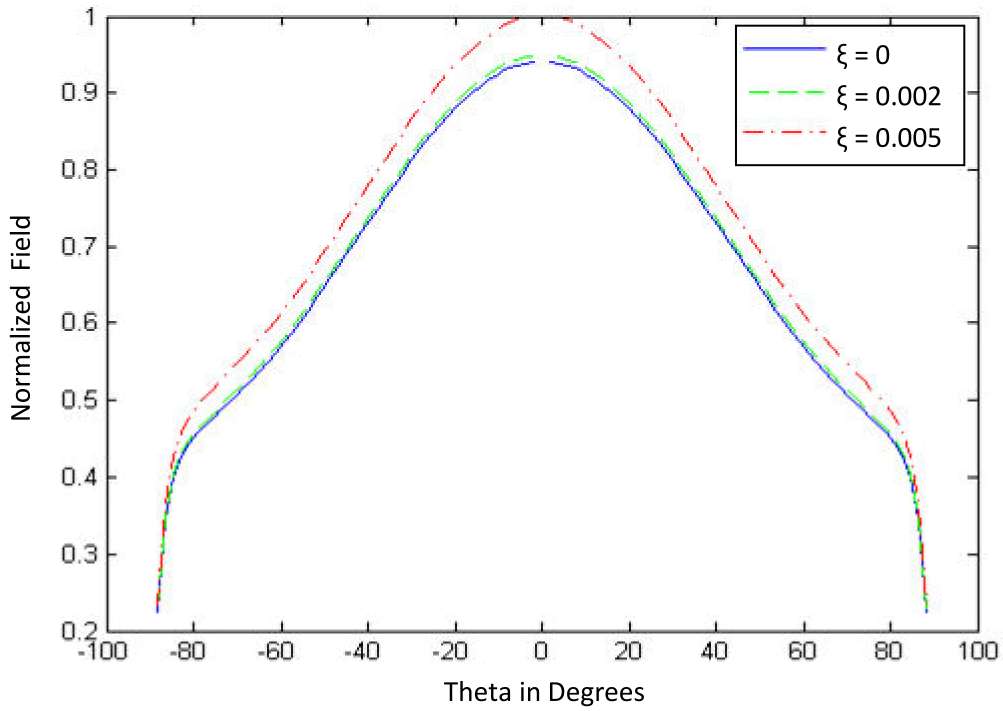

Fig. 5 Effect of chirality on the far field for *a* x *b* = 2 x 3 cm, ε_r = 2.2, *d* = 1.5 mm and φ = 90˚

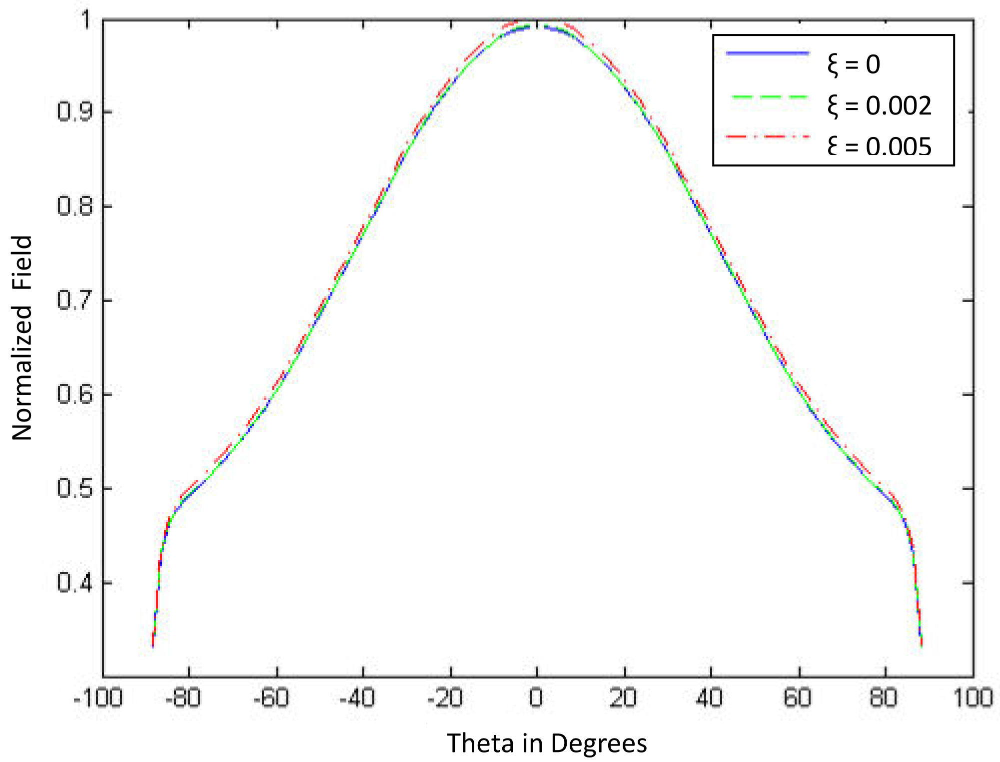

Fig. 6 Effect of chirality on the far field for *a* x *b* = 4 x 5 cm, ε_r = 2.2, *d* = 1.5 mm and φ = 90˚

3.4. Conclusion

The theory of electromagnetic waves propagation in chiral media is presented. It was shown the chirality is basically a purely geometric concept, and it has been studied extensively in different fields, prior electromagnetics. The interest in chiral materials, by the electromagnetics community, date back to the early seventies. The chiral materials are referred to as bi-isotropic materials, and they are a sub-class of the more general class called bi-anisotropic materials. The background of this subject has been sufficiently described. The interest in chiral materials in the field of microstrip antennas and wave guiding structures was motivated by the similarities shared with the ferrites, where the phenomenon of optical activity is present in both materials. Since ferrites have proven novel characteristics for microwave applications in general and microstrip antennas in particular, chiral materials have been studied to check whether they can provide similar operational characteristics. It was also shown that modeling chiral medium starts with the use of constitutive relations to derive the associated Maxwell's equation. Then matrix algebra is used to decouple the wave equation yielding to right and left circularly polarized waves for the electric and magnetic fields. After that, Maxwell's equations in terms of the new components are derived. The rest of the process to derive Green's function associate to the structure, is similar to that of ordinary substrate. It has been shown that the influence of chirality on resonant frequency in particular, is dependent to substrate thickness and patch size. It has been shown also that increasing the substrate chirality increases, although to a small degree, the bandwidth and the radiated field of a microstrip antenna. The positive impact of chirality, on bandwidth and the radiated field, becomes significant for small size patches.

Chapter 4

Feeding Techniques

4.1. Introduction

When a microstrip antenna is operating in transmitting/receiving mode, RF signals are usually carried to/from the antenna using a transmission line called a feed. Different feeding methods have been suggested and many theoretical models have been proposed for microstrip antenna structures where these feeding methods are including in the formulation. The availability of theoretical models for the feed, allows quantifying its possible effects on the characteristics of the microstrip antenna. Early microstrip antennas used either a microstrip line feed or a coaxial probe feed. Pozar published a paper [93], on the calculation of the input impedance of microstrip line fed and coaxial probe fed rectangular patch antenna. Few years later, he participated in developing a more elaborate study on the modeling of microstrip line fed and proximity coupling fed patch antenna [94]. Similar works [95], [96] were published later. The published theoretical models were not limited to a single layer structures, but they were also extended to multilayered structures [52]. In addition to full-wave analysis based works treating stacked circular [97] and rectangular [98] patches, as well coaxial probe fed- [99] and microstrip line fed- [100] arrays of rectangular patches. Most of the numerical studies on such structures were based on the use of Green's functions and the method of moments. However, formulations based on finite difference time domain (FDTD) method, were also reported [101]-[102].Experimental studies were also reported [62], [103]. These studies provide a set of measured data to examine the accuracy of the theoretical models, and to determine their range of validity. Microstrip line and coaxial probe feeds belong to direct contacting feeding methods. Such feeding methods have the advantage of simplicity, but they have several disadvantages such as the bandwidth/feed radiation trade off. Where, an increase of the substrate thickness for the purpose of increasing the bandwidth leads to an increase of spurious feed radiation. Practically, such antennas are limited in bandwidth to about 2 - 5 % [4].

Another type of non-contacting feeds, have been developed for microstrip antennas, namely, the proximity coupling and the aperture coupling feeds. For proximity coupling, the patch can be placed on a relatively thick substrate for improved bandwidth, while the feed line is placed on a thinner substrate to reduce spurious radiation. In 1987, Pozar and Kaufman [104] have published a work on increasing the bandwidth of a microstrip antenna by proximity coupling. In the same year, another paper has been published by Pozar and Voda [94], in which a modeling of proximity coupling feed has been presented. Splitt et al [105] have provided a similar study for both circular and rectangular patch antennas. Other works have been published in this regard for arrays [106] and single-element rectangular patch antennas [96], [107]. Aperture coupling is another type of non-contacting feeds. This type is proposed by Pozar in 1985 [108]. A microstrip feed line on the bottom substrate is coupled through a small aperture in the ground plane to a microstrip patch on the top substrate. This arrangement allows a thin, high dielectric constant substrate for the feed, and a thick, low dielectric constant substrate for the antenna element. In addition, the ground plane eliminates spurious radiation from the feed from interfering with the antenna pattern [4]. Aperture coupled-fed stacked rectangular patch antenna has been studied in a paper published by Croq et al [95]. Aperture-fed circular patch also has been analyzed [109]. Circular [47] and rectangular [110] microstrip patches in layered medium have been also studied. Aperture coupling feed technique has been applied on an array of circular patches [111]. Aperture shape is usually, although it is not limited to, rectangular or circular. H-shaped aperture, with a microstrip line feed, has been used in feeding a dual-band square patch [103].

4.2. Theory

4.2.1. Microstrip line feed

Two possible configurations of a microstrip line fed patch antenna **Fig. 1 (b)** ordinary microstrip, **(c)** feed line and inset feed line.

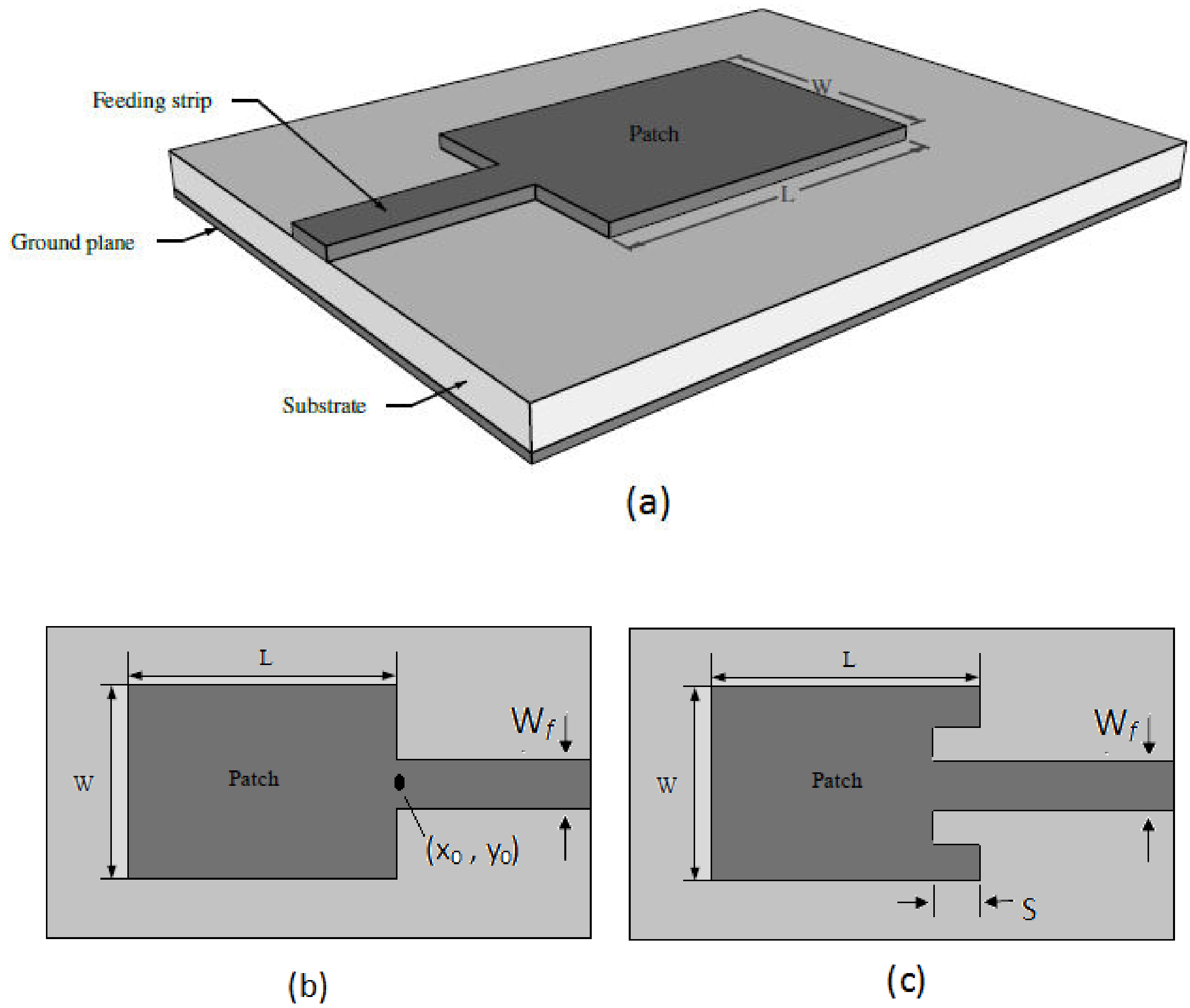

Fig.1 Structures of microstrip line fed patch antenna

Where

W: the patch width

L: the patch length

W_f : the feed line width

S: the inset length

(x_0 , y_0): the feed position

The equivalent circuit of the both configurations of microstrip line fed patch antenna is shown in **Fig. 2.** Where the RLC circuit represents the resonant patch and the feed is represented by the series inductance [4].

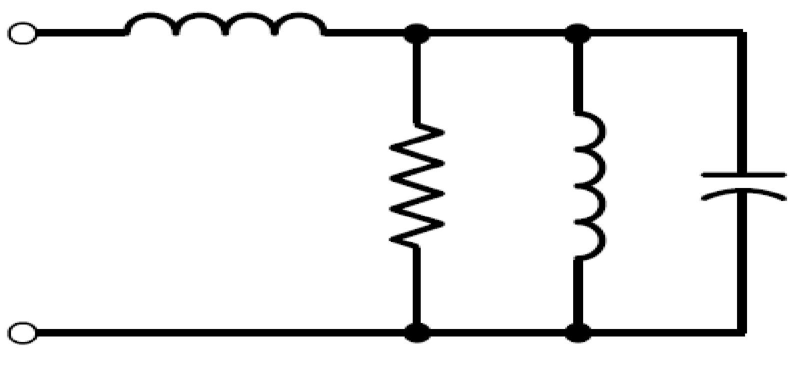

Fig. 2 Equivalent circuit of microstrip line fed patch antenna

The method of moments transforms the integral equation of the electric field into matrix equation of the form [Z]. [I] = [V], where the voltage vector [V] represents the excitation. In [94], the impressed (source) current is modeled as

$$J_i = \delta(x - x_0)\,.\,\delta(y - y_0) \tag{1}$$

Where (x_0 , y_0) are the coordinates of the feed position. The feed is incorporated in the computation of the elements of the voltage vector which is expressed as

$$V_m = 4j \int_0^{\pi/2} \int_0^{\infty} Q_v \, Im \left[F_x^*(J_m) e^{jk_x x_0}\right] Re \left[F_y^*(J_m) e^{jk_y y_0}\right] \beta d\beta d\alpha \qquad (2)$$

F_x and F_y are the Fourier transforms of x and y dependences of the current density. The expressions of F_x, F_y and Q_v are given in [93]. The feed width can be included in the formulation by modifying the voltage term in eq. (2) by the factor $\sqrt{\frac{W_e}{d}}$ to account for the edge effect of the microstrip line. W_e is the effect width of the feed line and *d* is the substrate thickness [93]. In the study presented in [94], Pozar and Voda have presented a theoretical model which is suitable for both microstrip line fed and proximity coupling fed patch antennas. In this model, the currents on the feed line and on the patch are expanded in term of three types of modes:

1/ Traveling wave current on the feed line

2/Patch current (expanded in terms of entire domain modes)

3/ Overlap current (expanded in terms of piecewise sinusoidal (PWS) modes)

Overlap currents enforce continuity of current from the feed line to the patch.

The inset length is included in the modeling of the current density in the feed line.

Feeding along the radiating edge is the most common in feeding patch antennas, where the feed line is usually placed at the center of this edge. One of the reasons why the feed line-patch contact point is on the resonant edge is that the feed currents are co-polarized with the currents of the patch which minimizes cross-polarization radiation. In addition, there is a little change in the input impedance as the feed point is moved along this edge [94].

The formulation provided by [94] has been used in [96] to derive a MoM formulation of microstrip line fed patch antenna. PWS basis functions have been used to approximate both the feed line and the patch currents. The final matrix equation has the form

$$\begin{bmatrix} Z & C \\ T & Y \end{bmatrix} \begin{bmatrix} I^a \\ I^b \end{bmatrix} = \begin{bmatrix} V_1 \\ V_2 \end{bmatrix} \tag{3}$$

The matrix Z and the vector V_1 are associated to the feed line, and the matrix Y and the vector V_2 are associated to the patch. Whereas the matrices T and C represent the coupling between the feed line and the patch basis functions [96].

4.2.2. Coaxial probe feed

The structure of coaxial probe fed patch antenna is illustrated in **Fig. 3,** its equivalent structure is similar to that of a microstrip line fed patch antenna. Unlike microstrip line feed, the position of a coaxial probe is not restricted to be only on the perimeter of the patch, but rather it can be placed in any point on the patch area. The coaxial probe feed is often modeled as a short, vertical filament of current. If the probe is assumed to be along the z-axis, then the current impressed by the probe has the form

$$\bar{J} = \hat{z}\,\delta(x - x_0).\,\delta(y - y_0) \tag{4}$$

Where (x_0 , y_0) represent the feed position. This formulation of the feed has been adopted before in [93], where the position of the feed probe is included in the calculation of the elements of voltage vector.

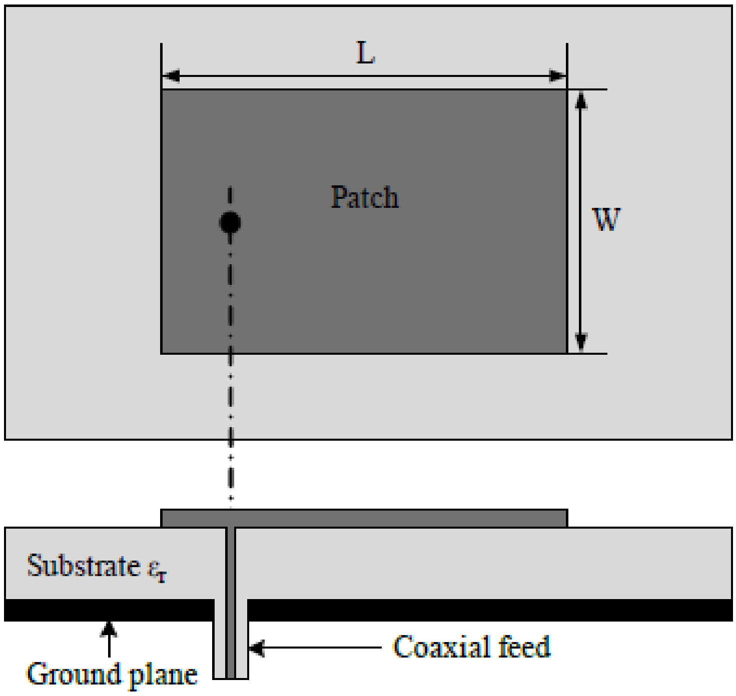

Fig. 3 Structure of coaxial probe fed patch antenna

Also in [93], it has been shown that the probe self inductance can be accounted to by adding jX_p to the input impedance, where

$$X_p = \frac{Z_0}{\sqrt{\varepsilon_r}} \tan(\sqrt{\varepsilon_r}\, k_0\, d) \tag{5}$$

With

Z_0 Is the free space intrinsic impedance ($Z_0 = 120\,\pi \;\; \Omega$)

ε_r Is the dielectric relative permittivity

d Is the dielectric thickness

k_0 Is the free space wave number

In [52], a spectral domain MoM formulation has been presented for a coaxial probe fed patch antenna in a layered medium. The integral equations of such structure are given by

$$\iint_{-\infty}^{+\infty} [\tilde{G}_{xx}\tilde{J}_x + \tilde{G}_{xy}\tilde{J}_y \,]\; e^{-j(k_x x + k_y y)}\, dk_x\, dk_y = \iint_{-\infty}^{+\infty} \tilde{G}_{xz}\tilde{J}_z\; e^{-j(k_x x + k_y y)}\, dk_x\, dk_y \qquad \text{(6-a)}$$

$$\iint_{-\infty}^{+\infty} [\tilde{G}_{yx}\tilde{J}_x + \tilde{G}_{yy}\tilde{J}_y \,]\; e^{-j(k_x x + k_y y)}\, dk_x\, dk_y = \iint_{-\infty}^{+\infty} \tilde{G}_{yz}\tilde{J}_z\; e^{-j(k_x x + k_y y)}\, dk_x\, dk_y \qquad \text{(6-b)}$$

In the above equations, $\tilde{J}_x$ and $\tilde{J}_y$ are the Fourier transforms of the x and y components of

The unknown current on the patch and $\tilde{J}_z$ is the Fourier transform of the known exciting current on the coaxial probe, and it is defined as

$$\tilde{J}_z = I_0\, e^{j(k_x x_0 + k_y y_0)} \qquad (7)$$

Somewhat a similar formulation of coaxial probe feed has been employed by [98], in which a full wave analysis of probe-fed stacked circular patch antenna is provided. A coaxial probe of radius R is placed at a position having the coordinates (ρ_0, φ_0) as depicted by **Fig. 4.**

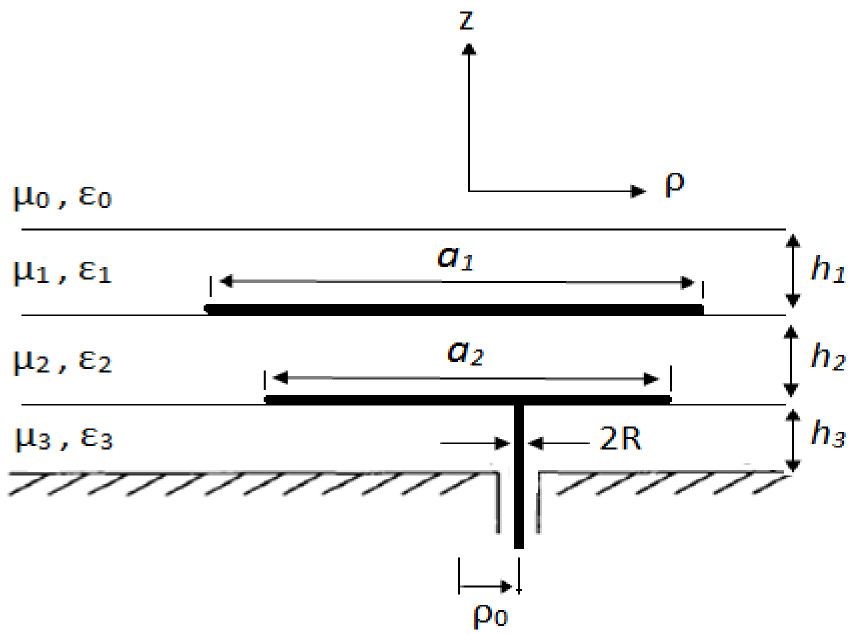

Fig. 4 probe-fed stacked circular patch antenna

The current on the probe has been expressed as

$$\bar{J}_{probe}(\bar{\rho}, z) = \hat{z}\frac{I}{2\pi R}\,\delta(\rho_p - R) \tag{8}$$

With the local coordinates defined as $\bar{\rho}_p = \bar{\rho} - \bar{\rho}_0$ and $\bar{\rho}_0 = (\rho_0, \varphi_0)$

4.2.3. Proximity coupling feed

Proximity coupling is, besides aperture coupling, one of feeding methods in which the signal is transmitted from the feed to the antenna element through electromagnetic coupling, and it is classified among non-contacting feeding methods. The structure of proximity coupling fed patch antenna is illustrated in **Fig. 5.** For this type of feeding, two parameters affect the antenna characteristics, the line-patch overlap, and the patch width to line width ratio [4].Matching the feed line is simply achieved by selecting the appropriate line-patch overlap [105]. The equivalent circuit of proximity coupling fed patch antenna is shown in **Fig. 6**, where the RLC circuit represent always the resonant patch, while the series capacitance represents the feed. The main advantage of using proximity coupling feed is the possibility of placing the feed network on a thin substrate in order to reduce radiation from the transmission feed line, and placing the patch on a thick substrate for an improved bandwidth [105]. Bandwidths of 13% have been achieved using this type of feed [4].

Among the theoretical models that have been proposed for proximity coupling fed patch antenna, a study based on the broadside coupled lines and improved transmission line methods [106]. This model allows the calculation of the input impedance, and can be applied on single element and arrays patch antennas. Method of moments based formulation which valid also for microstrip line fed antennas has been proposed by [94]. Costa et al [107] have

Presented full-wave analysis of proximity coupling fed patch antenna, with anisotropic dielectric. In their study, coaxial-to-microstrip junction has been modeled by a voltage-gap generator. The feed line configuration is illustrated in **Fig. 7**, where

$$V_m = \begin{cases} 1 & at\ (x_0\,, y_0) \\ 0 & \text{elsewehere} \end{cases} \tag{9}$$

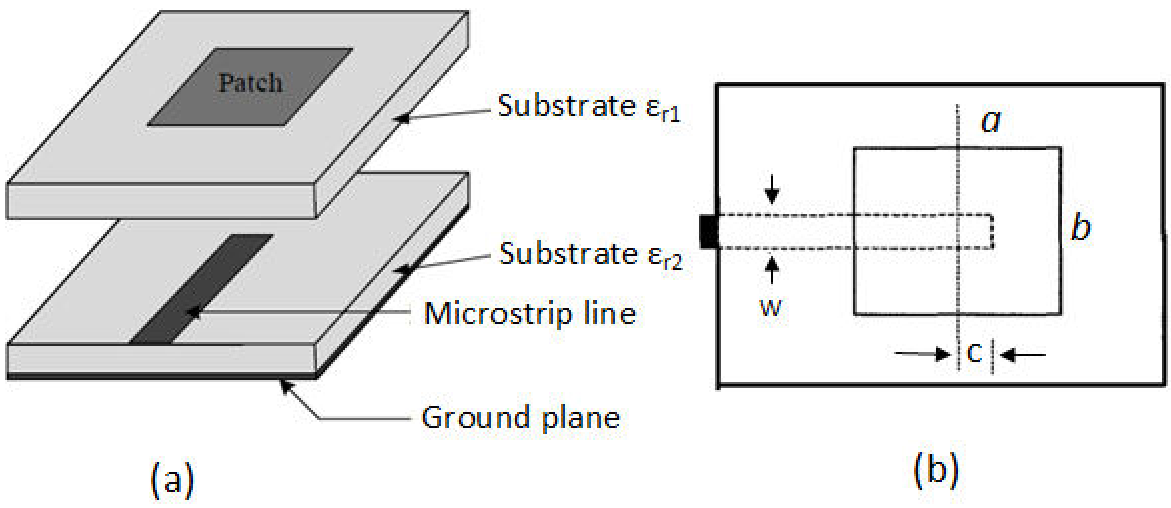

Fig. 5 proximity coupling fed patch antenna **(a)** 3D structure **(b)** Top view

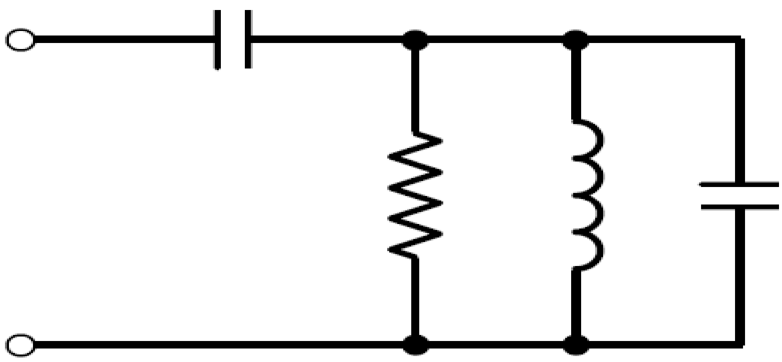

Fig. 6 Equivalent circuit of proximity coupling fed patch antenna

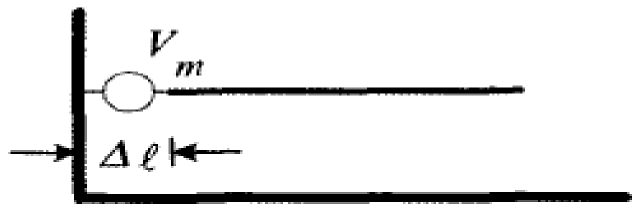

Fig. 7 Voltage-gap model for the feed line

4.2.4. Aperture coupling feed

Another type of non-contacting feed is the aperture coupling feed. This configuration uses two parallel substrates separated by a ground plane, where the patch is excited by the microstrip line etched on the substrate below the ground plane, though a narrow aperture (slot) **Fig. 8**. The equivalent circuit of the structure of **Fig. 8** is illustrated in **Fig. 9**.

The resonant patch now is represented by a series RLC circuit, with a shunt inductance representing the coupling slot. Among the advantages of this type of feeding, the possibility of using thin substrate of a high dielectric constant for the feeding network, and a thick substrate of a low dielectric constant for the antenna element, yielding optimal performance for both the feed and the antenna. Also, the radiation arising from the feeding network cannot interfere with the main radiation pattern generated by the patch antenna since the ground plane separates the two radiating mechanisms. The aperture is usually smaller than the resonant size, so the backlobe radiated by the slot is typically 15-20 dB below the forward main beam [4]. This geometry has at least four degrees of freedom:

- The slot size
- Its position
- The feed substrate parameters
- The feed line width

Impedance matching is performed by adjusting the size of the coupling slot together with the width of the feed line. Coupling can occur via an equivalent electric or magnetic polarizability in the slot, but the magnetic case is the stronger mechanism. The maximum coupling occurs when the aperture is centered below the patch where the magnetic field is at its maximum. The aperture coupled patch with a centered feed, has no cross-polarization in the principle planes [4]. For a slot-coupled patch antenna, the slot becomes the feed element to be modeled. A system of two integral equations is generated where the various unknowns, the patch current density and the transverse electric field over the aperture, are expanded into a series of basis functions covering the entire domain.

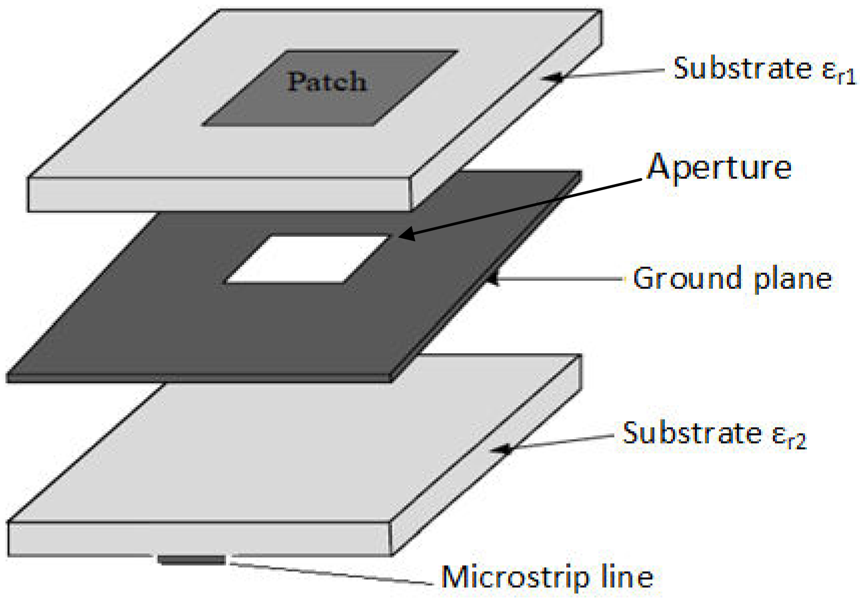

Fig. 8 Aperture coupled fed microstrip patch

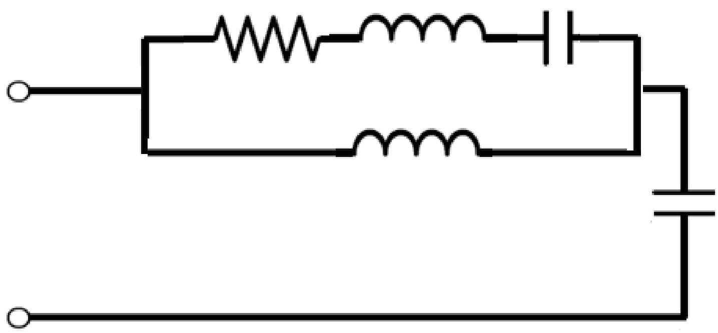

Fig. 9 Equivalent circuit of aperture coupling fed patch antenna

Method of moments is used to compute the surface current on the patch and reflection coefficient on the microstrip line. The input impedance and radiation pattern are then easily obtained [95]. One of the methods developed to model aperture coupling fed patch antenna, is that adopted by Losada et al [47], where dyadic Green's functions in Hankel transform domain (HTD), have been derived for the structure illustrated in **Fig. 10**.

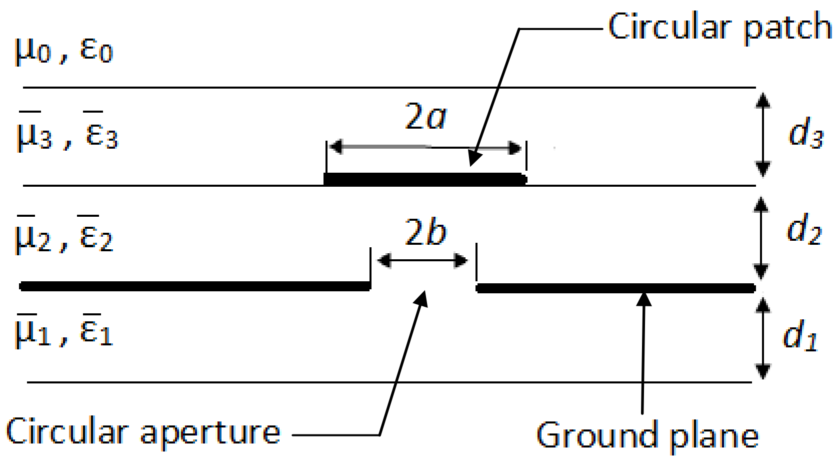

Fig. 10 Circular patch fed by circular aperture

For such structures, regardless the numbers of the dielectric layers, the unknown quantities are the surface current density on the patch and the transverse electric field on the aperture. Considering the structure of **Fig. 10**, let $j_1(\rho,\varphi)$ be the current density on the ground plane with a circular aperture, and $j_2(\rho,\varphi)$ be the current density on the circular patch. And $E_t(\rho,\varphi,z=d_1)$ and $E_t(\rho,\varphi,z=d_2)$ the transverse electric fields on the plane of the aperture and the plane of the patch respectively, these quantities are related by the following equations

$$\tilde{J}_1(k_\rho) = \tilde{H}_{11}(k_\rho)\tilde{E}_1(k_\rho) + \tilde{H}_{12}(k_\rho)\tilde{J}_2(k_\rho) \tag{10-a}$$

$$\tilde{E}_2(k_\rho) = \tilde{H}_{21}(k_\rho)\tilde{E}_1(k_\rho) + \tilde{H}_{22}(k_\rho)\tilde{J}_2(k_\rho) \tag{10-b}$$

Where

$\tilde{J}_1, \tilde{J}_2, \tilde{E}_1$ and $\tilde{E}_2$ are the Hankel transforms of $j_1(\rho,\varphi)$, $j_2(\rho,\varphi)$, $E_t(\rho,\varphi,z=d_1)$ and $E_t(\rho,\varphi,z=d_2)$ respectively, and $\tilde{H}_{11}, \tilde{H}_{12}, \tilde{H}_{21}$ and $\tilde{H}_{22}$ are 2 x 2 matrices that stands for dyadic Green's functions in the HTD. Chebychev polynomials have been used as expansion functions. By starting from equations (10-*a*), (10-*b*) the hybrid integral equations could be formulated and then solved using the method of moments. Instead of the transverse electric field on the aperture, the equivalent magnetic current density could be expanded using the same set of basis functions where [47]

$$M_1(\rho\,,\varphi) = -\,\hat{z}\;x\;E_t(\rho\,,\varphi,z=\,d_1) \tag{11}$$

A similar study has been reported in [113], where the patch and the aperture now have a rectangular shape and Green's functions are formulated in Fourier transform domain instead of Hankel transform domain. Unlike [47], expansion functions derived from the cavity model are employed instead of Chebychev polynomials. A quiet different formulation is used in

[109] where the authors have presented a mathematical formulation for a circular patch fed by a rectangular aperture. Green's functions are formulated in spectral domain. The chosen basis functions are based on the TM_z modes of a circular cavity. Reciprocity theorem is used along the analysis. Similar to the analysis of a slot on a waveguide wall, the effect of a slot discontinuity on the microstrip transmission line can be considered as a series impedance Z. Thus the equivalent circuit for the aperture coupled patch antenna is shown in **Fig. 11**. In this circuit, the series impedance Z is found by applying the reciprocity theorem to the fields of the microstrip line and considering the reflected and the transmitted waves on the line, the impedance Z is given by

$$Z = Z_c \frac{\Delta v^2}{Y^e + Y^a} \tag{12}$$

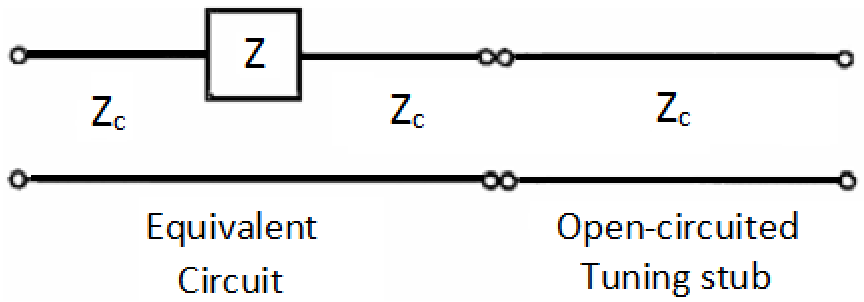

Fig. 11 equivalent circuit for the aperture coupled patch antenna as seen by the feed line

The expressions of Δv and Y^e can be computed directly, whereas Y^a has to be computed using the method of moments. Finally the input impedance is given by

$$Z_{in} = Z - jZ_c \cot(\beta L_s) \tag{13}$$

Where

L_s Is the stub length

4.3. Results and Discussions

In this part, a parametric study is provided on two different structures, namely microstrip line fed- and coaxial probe fed-patch antennas. The influence of the feed characteristics on the resonant frequency and radiated fields is shown. The reported results are generated using HFSS software. The structures data are synthesized using ADK tool so that the patch operates around 4 GHz and 5 GHz for microstrip line fed- and coaxial probe fed-patch respectively.

4.3.1. Microstrip line feed

The patch dimensions are *a* x *b* = 2.96 x 2.53 cm, the substrate is characterized by a dielectric constant equal to 2.2, a tangent loss of 0.0005 and a thickness of 3 mm. The feed line width, Inset distance and inset gap are varied and their impact on the resonant frequency **Tables 1-3**, and the far-field **Fig. 12-14**, is observed.

Table 1 Effect of feed line width on resonant frequency and return loss with Inset distance=0.771 cm and Inset gap = 0.012 cm

Feed width (cm)	Resonant frequency (GHz)	Return loss (dB)
0.012	No resonance	-
0.023	3.818	-16.86
0.046	3.939	-1.15
0.092	3.899	-2.24
0.115	3.818	-1.53

Table 2 Effect of Inset distance on resonant frequency and return loss with feed width = 0.023 cm and Inset gap = 0.012 cm

Inset distance (cm)	Resonant frequency (GHz)	Return loss (dB)
0	3.939	-2.93
0.385	3.939	-4.93
0.771	3.818	-16.86
1.265	No resonance	-

Table 3 Effect of inset gap on resonant frequency and return loss with feed width = 0.023 cm and Inset distance = 0.771 cm

Inset Gap (cm)	Resonant frequency (GHz)	Return loss (dB)
0	3.939	-2.93
0.006	3.98	-1.30
0.012	3.818	-16.86
0.024	3.98	-4.56
0.048	3.98	-6.30
0.12	4.02	-0.66

The initial feed line width set by the ADK tool is 0.023 cm and the corresponding resonant frequency (equal to 3.818 GHz) is considered as a reference resonant frequency. Frequency shift is computed with respect to this frequency. The initial values set by the ADK tool for the inset distance and the inset gap are 0.771 cm and 0.012 cm respectively. Therefore, the corresponding resonant frequencies are also considered as reference frequencies.

When the feed width is varied with integer multiples of the initial value the maximum frequency shift is about 3%. Return loss levels are highly affected when the feed line width shifts from its initial value, resulting in poor impedance matching. This is result natural because the characteristic impedance, which is a function of the feed width, of the microstrip line is substantially changed. Similar results are observed for the case of the inset distance and the inset gap. In terms of return loss, the best result is offered by using the feed parameters generated by the ADK tool, where the return loss at the resonant frequency 3.818 GHz is about -16 dB.

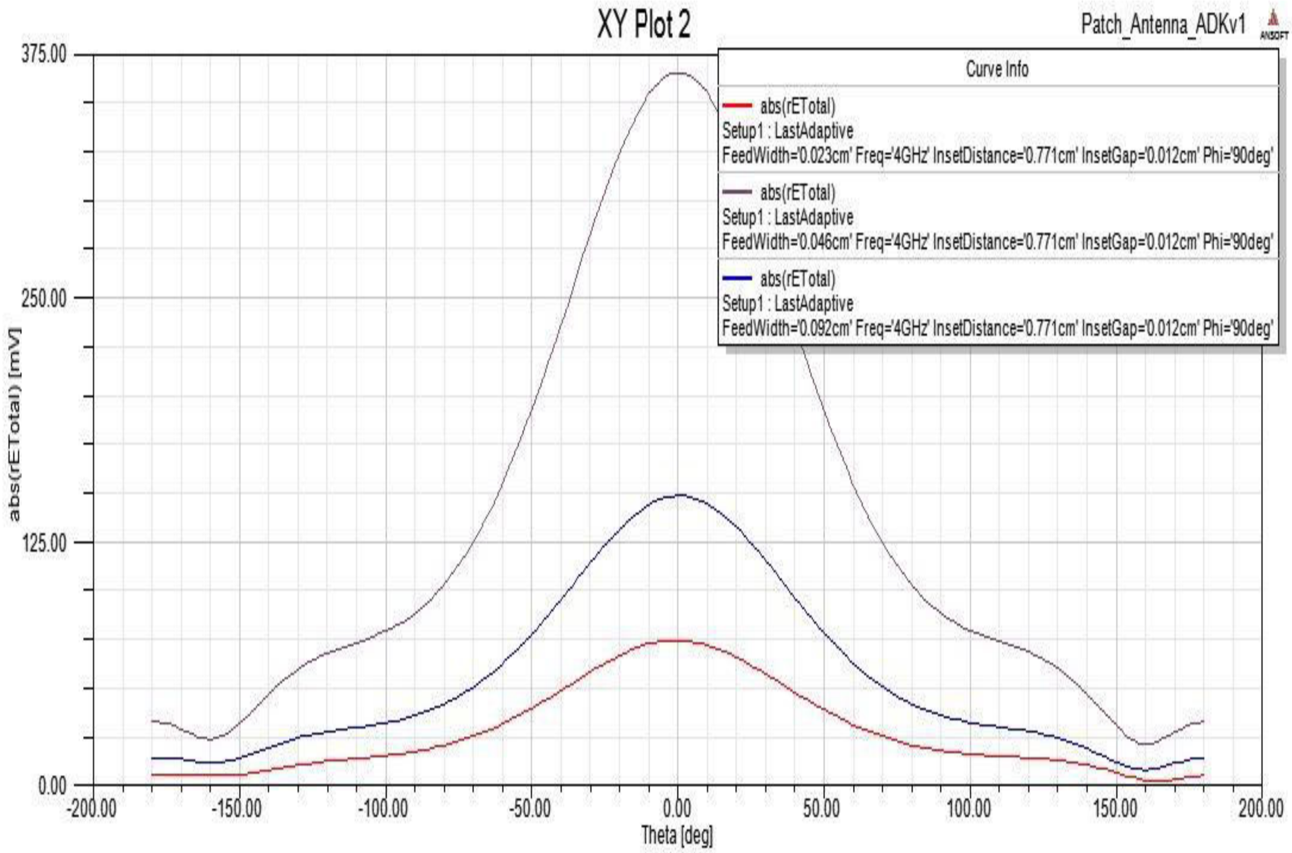

Fig. 12 Impact of feed line width on the radiated field

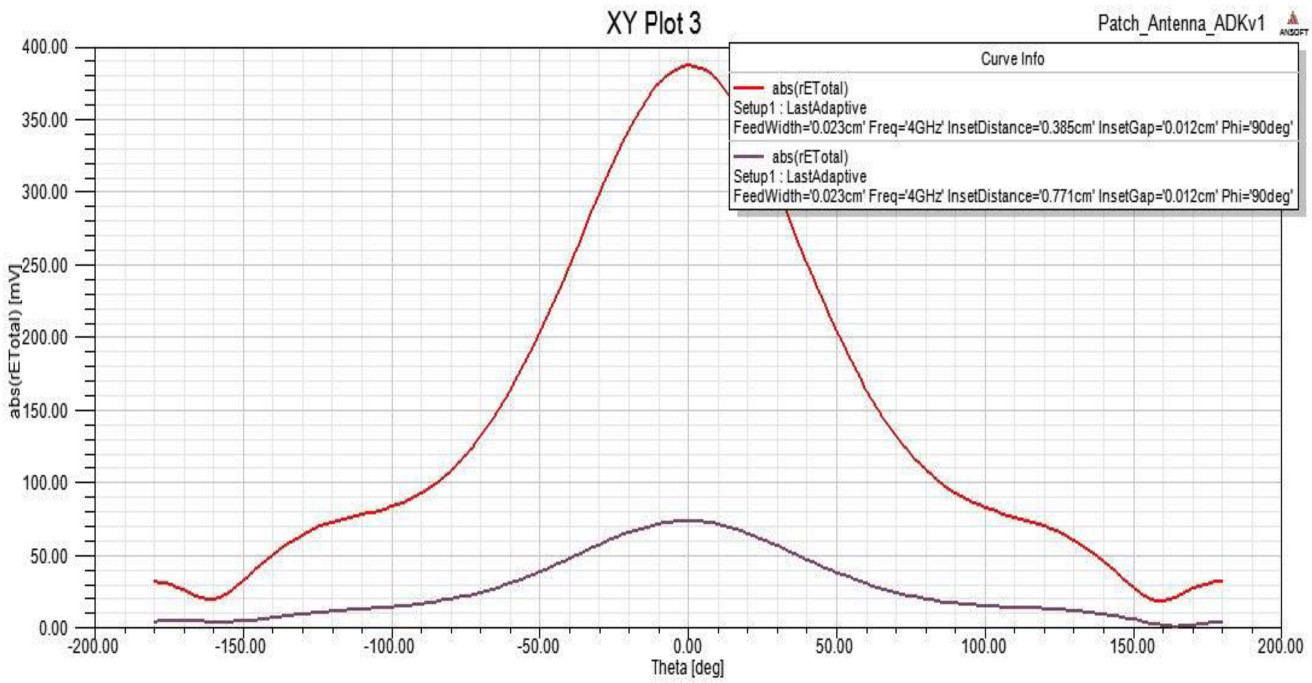

Fig. 13 Impact of Inset distance on the radiated field

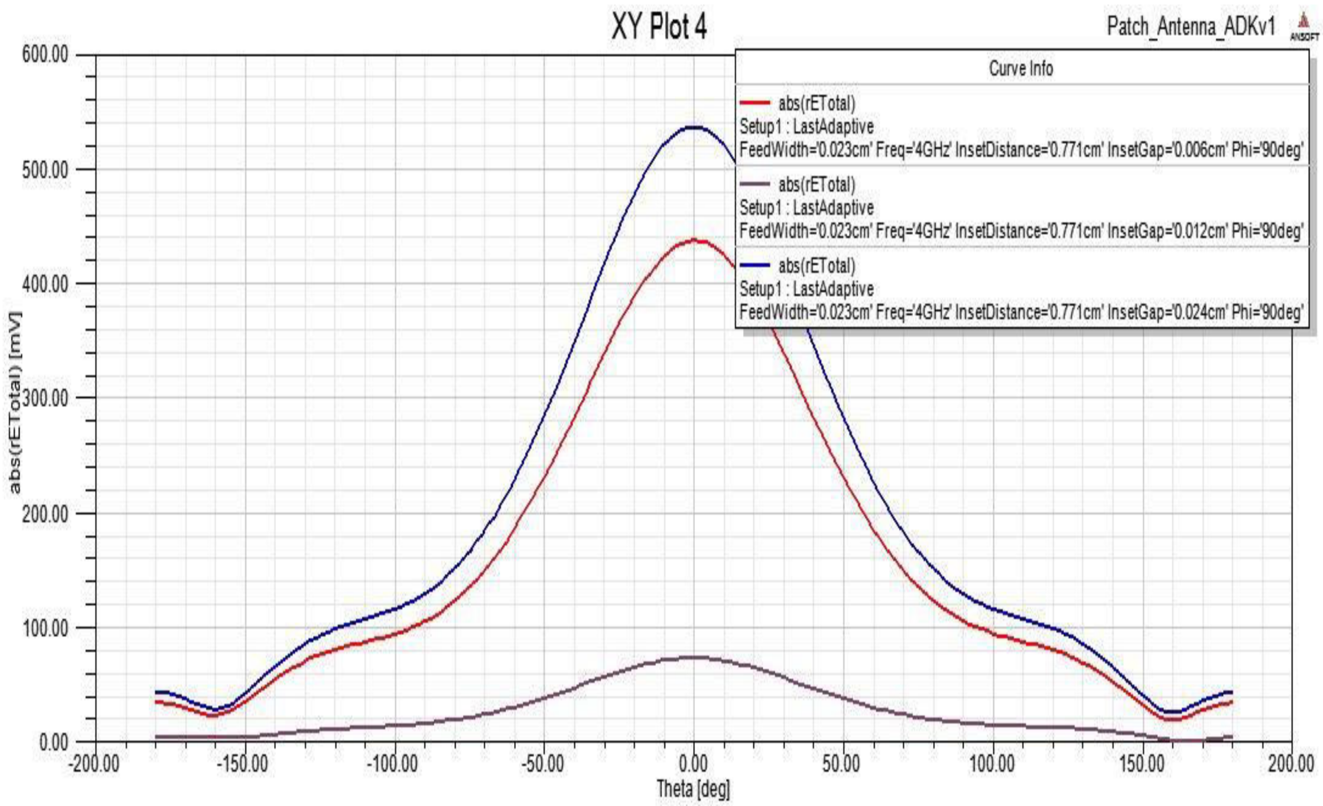

Fig. 14 Impact of Inset gap on the radiated field

Careful observation of influence of feed parameters on the radiated field leads to the conclusion that the radiated field variation does not follow any clear behavior. However when particular cases are compared to each other, we find that feed characteristics offering good results in terms of impedance matching do not necessarily offer the best result in terms of the radiated field.

4.3.2. Coaxial probe feed

The patch dimensions are *a* x *b* = 2.37 x 2.02 cm, the substrate is characterized by a dielectric constant equal to 2.2, a tangent loss of 0.0005 and a thickness of 3 mm. The resonant frequency **Table 4**, and the radiation pattern **Fig. 16-17**, variations in terms of the probe location (x_0 , y_0) are reported. We note that patch is centered at the coordinate system as shown in **Fig. 15.** The initial feed location set by ADK software is (0, 0.39 cm). The results reported in **Table 4** show that when the feed location is near the center of the patch gives the lowest resonant frequency. Unlike the case of microstrip line feed, the coaxial probe location set by ADK did not gave the best results in term of return loss, although is acceptable, but rather when the feed probe is at (-0.4 cm, -0.39 cm) where the return loss is -14 dB. The radiation pattern of a coaxial probe fed-patch antenna shows that the main lobe slightly deviates from the direction normal to the patch plane (i.e. theta = 0). Moving the feed probe along the y-axis also slightly changes the direction of the main lobe as illustrated in **Fig. 17**. Similarly to case of microstrip line fed patch, the probe feed location set by the ADK software give the lowest field magnitude compared to the other locations as shown in **Fig. 17** and **18**. This later result leads to the conclusion that the feed parameters defined by the ADK software as a starting point, puts impedance matching is the primary goal not the radiation characteristics of the patch antenna.

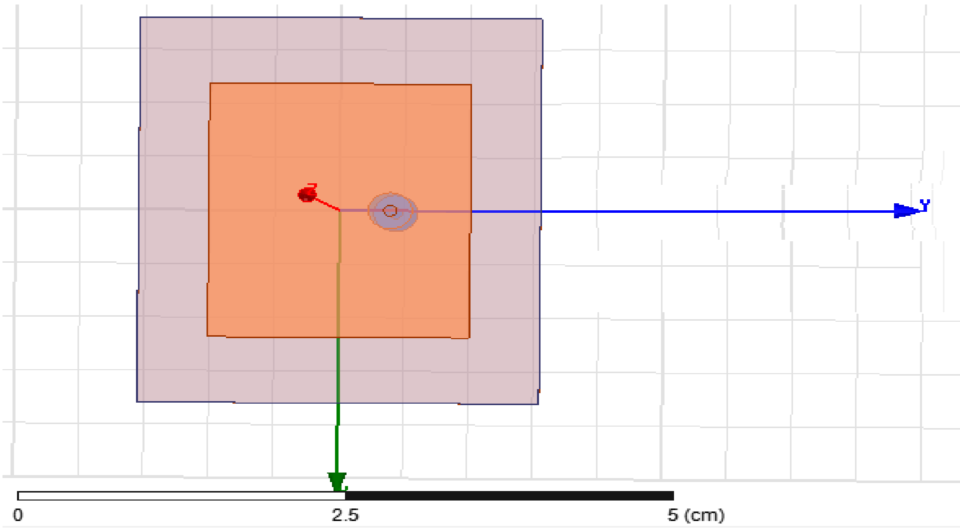

Fig. 15 Coordinates system for coaxial probe fed patch antenna

Table 4 Effect of feed location on resonant frequency and return loss

y_0(cm)	x_0 (cm) = -0.4		x_0 (cm) = 0		x_0 (cm) = 0.9	
	Resonant Frequency (GHz)	Return Loss (dB)	Resonant Frequency (GHz)	Return Loss (dB)	Resonant Frequency (GHz)	Return Loss (dB)
-0.8	4.8	-3	5	-5.41	5	-4.86
-0.6	4.95	-7.19	4.7	-8.02	4.95	-5.94
-0.39	4.6	-14	4.6	-7.14	4.60	-4
-0.18	4.5	-0.48	4.55	-0.27	4.55	-3.14
0	3.9	-1.17	-	-	4.05	-3.5
0.18	3.9	-1.08	4.55	-0.96	4.60	-6.07
0.39	4.6	-2.57	4.55	-9.65	4.65	-3.42
0.6	4.65	-1.78	4.65	-7	4.65	-4.76
0.8	4.7	-4.15	4.7	-2.91	4.70	-4.46

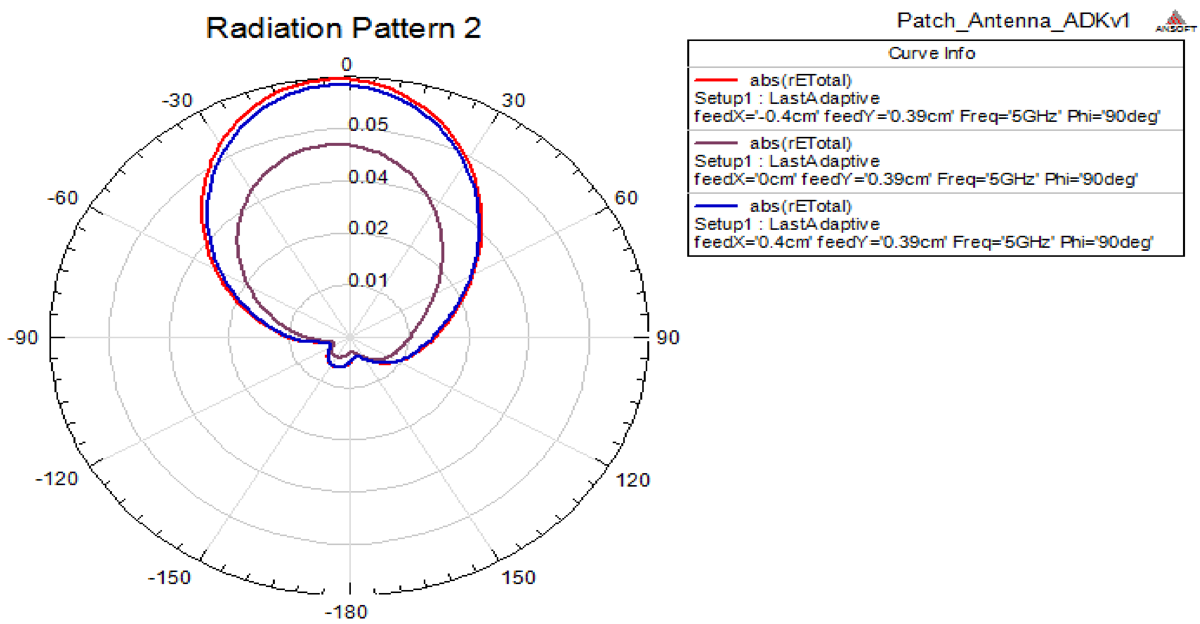

Fig. 16 Effect of probe location along x-axis on the radiation pattern

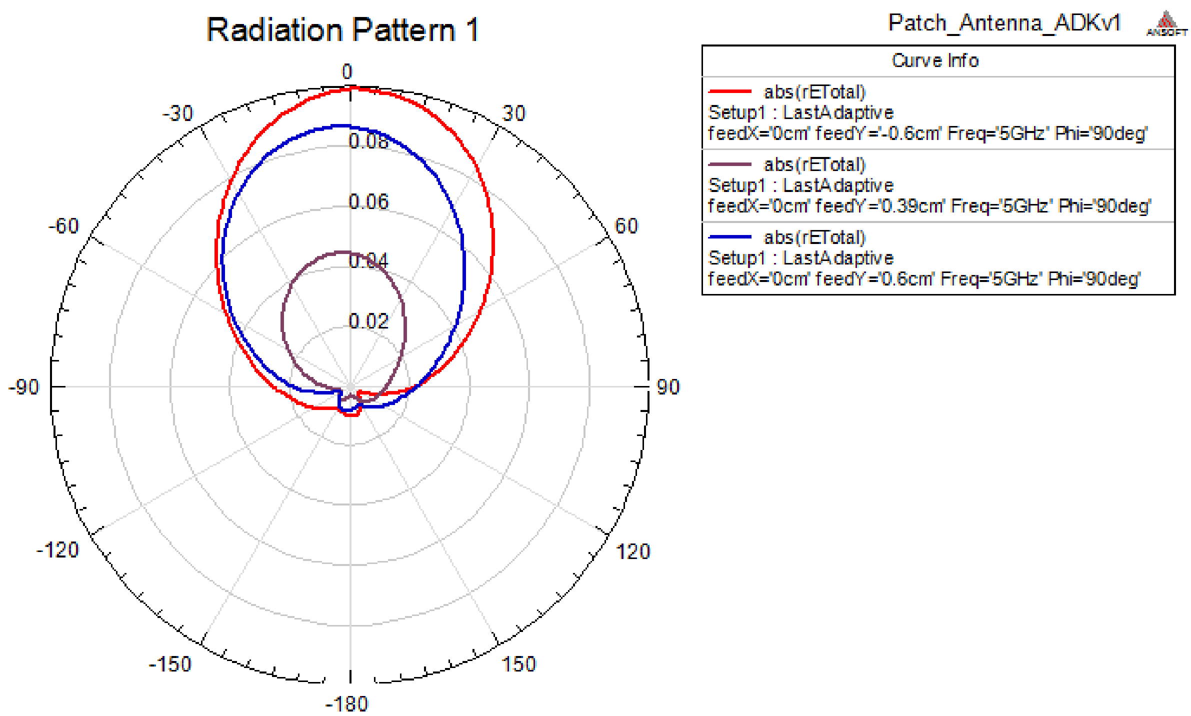

Fig. 17 Effect of probe location along y-axis on the radiation pattern

4.4. Conclusion

The state of art of popular feeding techniques is presented. The operating principles and the parameters of each technique have been described. The features of these methods and their historical development have been also presented. Different mathematical formulations modeling these feeding techniques are mentioned. When the method of moment is employed, the feed model is included in the computation of the elements of the voltage vector which represents the excitation. The different approaches used to compute the input impedance are presented. The influence of the parameters of two feeding techniques on the resonant frequency and the radiation pattern is also reported. Among the concluded results: the feeding technique has an effect, although it is small, on the resonant frequency. Two main criteria are to be met by a given feeding methods, these criteria are the bandwidth, and the radiation pattern, on the basis of these criteria feeding methods are evaluated. Modeling methods are evaluated according to their accuracy in predicting resonant frequency and the input impedance. For a microstrip line feed, the line width is chosen to provide characteristic impedance that is close to the resonant input resistance of the patch antenna. If this is not sufficient, feed inset is used to adjust the input impedance in order to achieve impedance matching. For a coaxial probe feed, the probe location is determined to provide impedance matching between the feed probe and the patch antenna.

Conclusion

Conclusion

We have presented a full wave analysis of microstrip patch embedded in a multilayered medium containing isotropic or anisotropic dielectrics and chiral substances. The analysis is based on the derivation of the dyadic Green's function in spectral domain. The electric field integral equation is formulated and solved by the method of moments. The complex roots of the impedance matrix determine the resonant frequency and the bandwidth. The general diagram of analytical and numerical methods used electromagnetic modeling is shown. A careful reading of this thesis enables us to draw the following conclusions:

- Analytical methods are based on assimilating the microstrip antenna to a physical device of a known mathematical model such as a transmission line or a cavity.
- Numerical methods share the idea of discretizing some unknown electromagnetic property.
- The differences between popular numerical methods are, basically, in the structure being descretized and solution variables.
- Numerical methods are classified according to different criteria, however, the resulting classes are not completely independent to each other but rather they look like overlapping fields.
- The mathematical foundation of each numerical method makes it more suitable to a particular problem than the other methods.
- Problem complexity and required accuracy versus the computational cost are the factors dictating the choice of the analytical or the numerical method.

- On the effect of dielectric parameters, it has been shown that the impact of material characteristics, permittivity and permeability, is larger than the impact of the dielectric thickness.
- It has been proven that the use of thick substrates with low permittivity and high permeability enhances significantly the antenna performance.
- The patch length has a large influence on the first resonance, whereas the width has a large influence on the second resonance.
- We have shown that for a chiral substrate, the electric and magnetic fields are coupled in the wave equation. Linear algebra is employed to obtain decoupled fields wave equations. Consequently, both the electric and magnetic fields are decomposed into right hand- and left hand-circularly polarized field components.
- Extending the solution from an ordinary dielectric substrate to chiral substrate involves only changing the Green's function.
- It has been found that increasing the substrate chirality enhances the bandwidth and increases the radiated field magnitude. This effect is more prominent for patches with small dimensions.
- Feeding techniques that are based on electromagnetic coupling were proven to be advantageous with respect to direct contacting techniques in terms of antenna performance and the extra degrees of freedom available to designers. However, this advantage is accompanied with increased modeling difficulty.
- It has been found that the feeding technique has a small influence on resonant frequency.

- For a microstrip line fed-patch antenna, the width of the feed line is adjusted to achieve impedance matching with antenna, or alternatively, by adjusting the feed inset.
- For a coaxial probe, the optimal probe location is defined as the location providing impedance matching.

Finally, the parametric study performed throughout this thesis is an attempt to shed some light on the influence of different parameters of the microstrip antenna structure on its performance. This is believed to inspire more elaborate studies which allow exploring the potential possibilities to enhance the microstrip antenna performance.

References

[1] I. J. Bahl, P. Bhartia, S. S. Stuchly, ''Design of microstrip antennas covered with a dielectric layer,'' IEEE Transactions on Antennas and Propagation, Vol. 30, No. 2, pp. 314-318 1982.

[2] N. G. Alexopoulos, D. R. Jackson, ''fundamental superstrate (cover) effects on printed circuit antennas,'' IEEE Transactions on Antennas and Propagation, Vol. 32, No. 8, pp. 807-816, 1984.

[3]V. Losada, R. R. Boix, M. Horno, ''Resonant modes of circular microstrip patches in multilayered substrates," IEEE Transactions on Microwave Theory and Techniques, Vol. 47, No. 4, pp. 488-498, 1999.

[4] D. M. Pozar, "Microstrip antennas," Proceedings of the IEEE, Vol. 80, No. 1, pp. 79-91, 1992.

[5] C. A. Balanis, *Antenna Theory: Analysis and Design*. 3rd edition, John Wiley & Sons INC. 2005

[6] D. M. Pozar, "Radiation and scattering from a microstrip patch on a uniaxial substrate," IEEE Transactions on Antennas and Propagation, Vol. 35, No. 6, pp. 613-621, 1987.

[7] K. L. Wong, J. S. Row, K. C. Huang, "Resonance of a rectangular microstrip patch on a uniaxial substrate," IEEE Transactions on Microwave Theory and Techniques, Vol. 41, No. 4, pp. 698-701, 1993.

[8] J. S. Oliveira, A. G. d'Assunçao, F. J. Sousa, "Microstrip patch antennas on uniaxial anisotropic substrates with several optical axis orientations," Microwave and optoelectronics conference, 1997 SBMO/IEEE MTT- S International, Vol. 1, pp. 297-302.

[9] J. A. Kong, "Theorems of bianisotropic media," Proceedings of the IEEE, Vol. 60, No. 9, pp. 1036-1046, 1972.

[10] S. Bassiri, "Electromagnetic wave propagation and radiation in chiral media," Ph.D. thesis, California Institute of Technology, Pasadena, California 1987.

[11] M. S. Kluskens, E. H. Newman, "A microstrip line on a chiral substrate, " IEEE Transactions on Microwave Theory and Techniques, Vol. 39, No. 11, pp. 1889-1891, 1991.

[12] P. Pelet, N. Engheta, "Chirostrip antenna: line source problem," Journal of Electromagnetic Wave and Applications, Vol. 6, pp. 771-793, 1992.

[13] D. G. Swanson, J. W. Hoefer, *Microwave circuit modeling using electromagnetic field simulation*. ARTECH HOUSE INC. 2003

[14] R. Garg, *Microstrip Antenna Design Handbook*. ARTECH HOUSE INC. 2000

[15]H. Pues, A.Van de Capelle, ''Accurate transmission line model for the rectangular microstrip antenna," IEE Proceedings, vol. 131, No. 6, pp. 334-340, 1984.

[16] A. K. Bhattacharrya, R. Garg, '' Generalized transmission line model for microstrip patches, "IEE Proceedings, vol. 132, No. 2, pp. 93-98, 1985.

[17] A. K. Bhattacharrya, '' Generalized transmission line model for microstrip patch antennas and some applications, '' Ph.D. Thesis, Indian institute of Technology, Kharagpur, India, 1985.

[18] A. K. Bhattacharrya, L. Shafai, R. Garg, "Microstrip antenna – A Generalized transmission line," Progress in Electromagnetics Research, vol. 4, pp. 45-84, 1991.

[19] A. K. Bhattacharrya, R. Garg, "Input impedance of an annular ring microstrip antenna using circuit theory approach," IEEE Transactions on Antennas and Propagation, Vol. 33, pp. 369-374, 1985.

[20] S. A. Long, L. C. Shen, M. D. Walton, M. R. Allerding, "Impedance of a circular-disc printed-circuit antenna," Electronics Letters, vol. 14, pp. 684-686, 1978.

[21] W. F. Richards, Y. Lo, D. Harrison, "An improved theory for microstrip antennas and applications," IEEE Transactions on Antennas and Propagation, vol. 29, pp. 38-46, 1981.

[22] Y. T. Lo, W. F. Richards, "Perturbation approach to design of circularly polarized microstrip antennas," Electronics Letters, Vol. 17, pp. 383 -385, 1981.

[23]V. Palanisamy, "Generalized cavity model microstrip patch antennas and some applications, '' Ph.D. Thesis, Indian institute of Technology, Kharagpur, India, 1985.

[24] V. Palanisamy, R. Garg, ''Analysis of arbitrary shaped microstrip patch antennas using segmentation technique and cavity model, " IEEE Transactions on Antennas and Propagation, Vol. 34, pp. 1208 -1213, 1986.

[25] T. Okoshi, *Planar Circuits for Microwave and Lightwaves.* Springer-Verlag, 1985.

[26] J. R. James, P. S. Hall, *Handbook of Microstrip Antennas*. Peter Peregrinus, London, UK, 1989.

[27] K. Coburn, Computational Electromagnetics, Slides from ATI Professional Development Short course, Applied Technology Institute.

[28]J. Ekman, "Electromagnetic modeling using the partial element equivalent circuit method," EISLAB, Lulea University, Sweden 2003.

[29] Boundary value problem, Dr. Ian Gladwell, department of mathematics, Southern Methodist University, Dallas, Texas, United States, *Scholarpedia.* *http://www.scholarpedia.org/article/Boundary_value_problem*

[30] Boundary value problems, http://homepage.divms.uiowa.edu/~atkinson/m171.dir/sec_6-11.pdf

[31] V. Demir, Simulation of Electromagnetic Fields: The Finite-Difference Time-Domain (FDTD) and its Applications, Northern Illinois University 2006.

[32] The Finite Element Method (FEM). https://www.comsol.com/multiphysics/finite-element-method

[33] L. E. Ping, Computational Electromagnetics for Electromagnetic Compatibility / Signal Integrity Analysis, Advanced Electromagnetics and Electronic Systems Lab. National University of Singapore 2008.

[34]J. N. Reddy, *An Introduction to the Finite Element Method,* 3rd edition, McGraw- Hill 2006

[35]A. A. Salih, *Finite Element method*, Indian Institute of Space Science and Technology.

[36]F. Monsefi, M. Otterskog, S. Silvestrov, "Direct and Inverse Computational Methods for Electromagnetic Scattering in Biological Diagnostics," Mälardalen University, Sweden 2013.

[37] The Finite Difference Method. https://www.ljll.math.upmc.fr/frey/cours/UdC/ma691/ma691_ch6.pdf

[38]Finite Difference Methods, http://www.math.yorku.ca/~hmzhu/Math-6911/lectures/Lecture5/5_BlkSch_FDM.pdf

[39]W. Shin, ''3D Finite-Difference Frequency-Domain Method for Plasmonics and Nanophotonics, " Ph.D. Dissertation, Stanford University, 2013.

[40] P. B. Johns, R. L. Beurle, "Numerical Solution of 2-dimensional scattering problems using a transmission-line matrix," IEE Proceedings, Vol. 118, pp. 1203-1208, 1971.

[41]Z. Rahimi, "The Finite Integration Technique (FIT) and the Application in Lithography Simulations," Ph.D. Thesis, Friedrich-Alexander University, Erlangen, Germany 2011.

[42]M. Thiel, "A General procedure to set up the dyadic Green's function of multilayer conformal structures and its application to microstrip antennas," Applied Computational Electromagnetics Society Journal, 2005.

[43] *Green's function – Optical Physics II,* Photonics Laboratory, ETH Swiss Federal Institute of Technology, Zurich.

https://www.photonics.ethz.ch/fileadmin/user_upload/Courses/PhysicalOpticsII/notes4.pdf

[44] J. K. H. Gamage, "Efficient space domain method of moments for large arbitrary scatterers in planar stratified media, " Ph.D. Thesis, Norwegian University of Science and Technology, Trondheim, Norway 2004.

[45] J. Lee, S. Lee, “General solution of EM wave propagation in anisotropic media,” Journal of the Korean Physical Society, Vol. 57, No. 1, pp. 55-60, 2010.

[46] R. E. Erwert, “Numerical approximations of the Green’s functions for a theoretical model of an aperture fed stacked-patch microstrip antenna,” Master Thesis, Air Force Institute of Technology, Ohio, USA 1990.

[47] V. Losada, R. R. Boix, M. Horno, “Resonant modes of circular microstrip patches over ground planes with circular apertures in multilayered substrates containing anisotropic and ferrite materials,” IEEE Transactions on Microwave Theory and Techniques, vol. 48, No. 10, pp. 1756-1762, 2000.

[48] D. Pingping, “Fast solution of dyadic Green’s functions for planar multilayered media,” Ph.D. Thesis, National University of Singapore, Singapore 2011.

[49]T. Fortaki, A. Benghalia, “An Efficient calculation of surface waves in anisotropic printed antenna structures,” 3rd International conference: Sciences of Electronic, Technologies of Information and Telecommunications, Tunisia, March 27-31, 2005.

[50] H. Y. Yang, A. Nakatani, J. A. Castaneda, “Efficient evaluation of spectral integrals in the moment method solution of microstrip antennas and circuits,” IEEE Transactions on Antennas and Propagation, vol. 38, No. 7, pp. 1127-1130, 1990.

[51] E. H. Newman, D. Forrai, ‘’Scattering from a microstrip patch, “IEEE Transactions on Antennas and Propagation, vol. 35, No. 3, pp. 245-251, 1987.

[52]Y. Chunfei, L. Gang, Z. Shunshi, “Analysis of rectangular microstrip patch antenna covered with N-dielectric layers,” Journal of Electronics, vol. 15, No. 1, pp. 84-89, 1998.

[53]J. T. Bernhard, C. T. Tousignant, “Resonant frequencies rectangular microstrip antennas with flush and spaced dielectric substrates,” IEEE Transactions on Antennas and Propagation, Vol. 47, No. 2, pp. 302-308, 1999.

[54] P. B. Morel, S. A. Long, L. C. Shen, “A Theoretical investigation of the circular disc antenna,” 1976 Region V IEEE Conference Digest, IEEE Catalog No. 76CH1068 REG 5, pp. 286, 1976.

[55] L. C. Shen, S. A. Long, M. R. Allerding, M. D. Walton, “Resonant frequency of circular disk, printed circuit antenna, “ IEEE Transactions on Antennas and Propagation, Vol. 25, No. 4, pp. 595-596, 1977.

[56] A. G. Derneryd, ‘’Analysis of microstrip disk antenna element,” IEEE Transactions on Antennas and Propagation, Vol. 27, No. 5, pp. 660-664, 1979.

[57] K. Araki, T. Itoh, “Hankel transform domain analysis of open circular microstrip radiating structures,” IEEE Transactions on Antennas and Propagation, Vol. 29, No. 1, pp. 84-89, 1981.

[58]Y. T. Lo, D. Solomon, W. F. Richards, "Theory and experiment on microstrip antennas," IEEE Transactions on Antennas and Propagation, Vol. 27, No. 2, pp. 137-145, 1979.

[59] T. Itoh, W. Menzel, "A Full-wave analysis method for open microstrip structures," IEEE Transactions on Antennas and Propagation, Vol. 29, No. 1, pp. 63-68, 1981.

[60] E. Chang, S. A. Long, W. F. Richards, '' An experimental investigation of electrically thick rectangular microstrip patch," Transactions on Antennas and Propagation, Vol. 34, No. 6, pp. 767-772, 1986.

[61] W. C. Chew, Q. Liu, ''Resonance frequency of a rectangular microstrip patch," Transactions on Antennas and Propagation, Vol. 36, No. 8, pp. 1045-1056, 1988.

[62] D. H. Schaubert, D. M. Pozar, A. Adrian, "Effect of microstrip antenna substrate thickness and permittivity: comparison of theories with experiments," IEEE Transactions on Antennas and Propagation, vol. 37, No. 6, pp. 677-682, 1989.

[63]J. S. Row, K. L. Wong, ''Resonance in a superstrate-loaded rectangular microstrip structure," IEEE Transactions on Microwave Theory and Techniques, Vol. 41, No. 8, pp. 1349-1355, 1993.

[64] T. Fortaki, D. Benatia, A. Benghalia, ''Evaluation of the radiation of rectangular microstrip antenna covered with a dielectric layer,'' 4th International conference: sciences of electronic, technologies of information and telecommunications, March 25-29, 2007, Tunisia.

[65]T. Fortaki, L. Djouane, F. Chebara, A. Benghalia, "On the dual-frequency behavior of stacked microstrip patches," IEEE Antennas and Wireless Propagation Letters, Vol. 7, pp. 310-313, 2008.

[66]S. Benkouda, T. Fortaki, "Study of microstrip patch resonator printed on anisotropic substrate characterized by permittivity and permeability tensors," PIERS Proceedings, Marrakesh, Morocco, pp. 578-580, March 20-23, 2011.

[67]H. Mosallaei, K. Sarabandi, "Magneto-dielectrics in electromagnetic: concept and applications," IEEE Transactions on Antennas and Propagation, Vol. 52, No. 6, 1558-1567, 2004.

[68] M. E. Ermutlu, C. R. Simovski, M. K. Kärkäinen, P. Ikonen, A. A. Sochava, S. A. Tretyakov, "Patch antennas with new artificial magnetic layers," https://arxiv.org/abs/physics/0504075

[69]A. Karilainen, "Magnetic materials and responses in antenna applications," Ph.D. dissertation, Aalto University, Espoo, Finland 2012.

[70] F. Namin, T. G. Spence, D. H. Werner, E. Semouchkina, "Broadband, miniaturized stacked-patch antenna based on magneto-dielectric substrates for L-band operation," Antennas and Propagation Society International Symposium, 2009 APSURSI '09

[71] P. Pelet, N. Engheta, "the theory of chirowaveguides," IEEE Transactions on Antennas and Propagation, Vol. 38, No. 1, pp. 90-98, 1990.

[72] D. M. Pozar, "Microstrip antennas and arrays on chiral substrates," IEEE Transactions on Antennas and Propagation, Vol. 40, No. 10, pp. 1260-1263, 1992.

[73] P. Dessai, "Influence of chirality on the electromagnetic wave propagation: unbounded media and chirowaveguides"

[74] D. L. Jaggard, A. R. Mickelson, C. H. Papas, "On electromagnetic waves in chiral media," Applied Physics, Vol. 18, No. 2, pp. 211-216, 1979.

[75] A. Toscano, L. Vegni, "Spectral dyadic Green's function formulation for planar integrated structures with a grounded chiral slab," Journal of Electromagnetic Waves and Applications, Vol. 6, pp. 751-769, 1992.

[76] S. M. Ali, T. M. Habashy, J. A. Kong, "Spectral-domain dyadic Green's function in layered chiral media," Journal of Optics society American A. Vol. 9, No. 3, pp. 413-423, 1992.

[77] K. F. Lindman, Ann. Physics, vol. 63, pp. 621, 1920.

[78] K. F. Lindman, Ann. Physics, vol. 69, pp. 270, 1922.

[79] W. H. Pickering, experiment performed at Caltech, private communication, 1945.

[80] W. S. Weiglhofer, "Electromagnetic field representation in inhomogeneous isotropic chiral media," Electromagnetics, Vol. 10, No. 3, pp. 271-278, 1990.

[81] H. Cory, I. Rosenhouse, "Electromagnetic wave propagation along a chiral slab," IEE Proceedings-H-Microwaves, Antennas and Propagation, Vol. 138, No. 1, pp. 51-54, 1991.

[82]T. Guire, V. V. Varadan, V. K. Varadan, "Influence of chirality on the reflection of EM waves by planar dielectric slabs," IEEE Transactions on Electromagnetic Compatibility, vol. 32, No. 4, pp. 300-303, 1990.

[83] M. S. Kluskens, E. H. Newman, "Method of moments analysis of scattering by chiral media," Technical report 721566-2, The Ohio State University, 1991.

[84] V. A. Neganov, O. V. Osipov, "Scattering of electromagnetic waves from planar chiral structures," Radiophysics and Quantum Electronics, vol. 42, No. 9, pp. 764-772, 1999.

[85] A. Lakhtakia, V. V. Varadan, V. K. Varadan, "Radiation by a straight thin-wire embedded in an isotropic chiral medium," IEEE Transactions on Electromagnetic Compatibility, Vol. 30, No. 1, pp. 84-87, 1988.

[86]F. Lumini, J. C. Lacava, "Radiation properties of Chirostrip antennas," SBMO International Microwave Conference, Vol. 2, pp. 587-592, Brazil 1993.

[87] A. Toscano, L. Vegni, "A new efficient moment method formulation for the design of microstrip antennas over a chiral grounded slab," Journal of Electromagnetic Waves and Applications, vol. 11, pp. 567-592, 1997.

[88]L. W. Li, T. X. Zhao, M. S. Leong, T. S. Yeo, "A spatial-domain method of moments analysis of a cylindrical-rectangular chirostrip," Progress In Electromagnetics Research, PIER, Vol. 35, pp. 165-182, 2002.

[89]W. Ren, "Dyadic Green's functions and dipole radiations in layered chiral media," Journal of Applied Physics, vol. 75, No. 1, pp. 30-35, 1994.

[90] L. W. Li, P. S. Kooi, M. S. Leong, T. S. Yeo, "A general expression of dyadic Green's functions in radially multilayered chiral media," IEEE Transactions on Antennas and Propagation, Vol. 43, No. 3, pp. 232-238, 1995.

[91] L. W. Li, P. S. Kooi, T. S. Yeo, "Analytic representation of scattering dyadic Green's functions coefficients for cylindrically multilayered chiral media," Journal of Electromagnetic Waves and Applications, Vol. 9, No. 9, pp. 1207-1221, 1995.

[92]N. Engheta, S. Bassiri, "One- and Two- dimensional dyadic Green's functions in chiral media," IEEE Transactions on Antennas and Propagation, Vol. 37, No. 4, pp. 512-515, 1989.

[93] D. M. Pozar, "Input impedance and mutual coupling of rectangular microstrip antennas," IEEE Transactions on Antennas and Propagation, Vol. 30, No. 6, pp. 1191-1196, 1982.

[94] D. M. Pozar, S. M. Voda, "A rigorous analysis of a microstrip fed patch antenna," IEEE Transactions on Antennas and Propagation, vol. 35, No. 12, pp. 1343-1350, 1987.

[95] F. Croq, G. Kossiavas, A. Papiernik, "Stacked resonators for bandwidth enhancement: a comparison of two feeding techniques," IEE Proceedings-H-Microwaves, Antennas and Propagation, Vol. 140, No. 4, pp. 303-308, 1993.

[96] E. Ballikaya, "Analysis of slot coupled microstrip patch antennas," M.Sc. Thesis, Middle East Technical University, 2007.

[97] A. N. Tulintseff, S.M. Ali, J. A. Kong, "Input impedance of a probe-fed stacked circular microstrip antenna," IEEE Transactions on Antennas and Propagation, Vol. 39, No. 3, pp. 381-390, 1991.

[98] I. K. Moussa, D. A. E. Mohamed, I. Badran, "Analysis of stacked rectangular microstrip antenna," 24th National radio science conference NRSC 2007, Cairo, March 13-15, 2007.

[99]C. C. Liu, A. Hessel, J. Shmoys, "Performance of probe-fed microstrip-patch element phased arrays," IEEE Transactions on Antennas and Propagation, Vol. 36, No. 11, pp. 1501-1509, 1988.

[100] C. F. Wang, F. Ling, J. M. Jing, "A fast full-wave analysis of scattering and radiation from large finite arrays of microstrip antennas," IEEE Transactions on Antennas and Propagation, Vol. 46, No. 10, pp. 1467-1474, 1998.

[101] Z. Hongxing, Z. Cheng, G. Debiao, "Efficient algorithm for microstrip antennas on a general anisotropic substrate," ICMMT 2000, 2nd International Conference on Microwave and Millimeter Wave Technology Proceedings, 2000.

[102] S. Sandeep, "Broadband analysis of microstrip patch antenna using 3D FDTD – UPML"

[103]P. F. Chuo, T. r. Chen, J. S. Row, "Dual-frequency microstrip antennas," Microwave and optical technology letters, vol. 45, No. 1, pp. 3-5, 2005.

[104] D. M. Pozar, B. Kaufman, "Increasing the bandwidth of a microstrip antenna by proximity coupling," Electronics Letters, vol. 23, No. 8, pp. 368-369, 1987.

[105] G. Splitt, M. Davidovitz, "Guidelines for design of electromagnetically coupled microstrip patch antennas on two-layer substrates," Transactions on Antennas and Propagation, Vol. 38, No. 7, pp. 1136-1140, 1990.

[106]B. Belentepe, "Modeling and design of electromagnetically coupled microstrip patch antennas and antenna arrays," IEEE Antennas and Propagation Magazine, Vol. 37, No. 1, pp. 31-39, 1995.

[107] V. D. Costa, I. Bianchi, J. C. Lacava, L. Cividanes, "Analysis of Modeling and design of electromagnetically coupled antennas printed on anisotropic substrates," International Microwave and Optoelectronics Conference, Vol. 1, pp. 317-322, 2003.

[108] D. M. Pozar, "Microstrip antenna aperture coupled to a microstripline," Electronics Letters, Vol. 21, No. 2, pp. 49-50, 1985.

[109] H. R. Hassani, M. Jahanbakht, "Spectral domain method of moment analysis of aperture coupled circular microstrip patch antenna," Journal of Applied Mathematics Islamic Azad University Lahijan, pp. 14-40, 2005.

[110]T. Fortaki, "Contribution à l'étude des problèmes de caractérisation des antennes microbandes multicouches sans et avec ouverture dans les plans de masse, " Thèse de Doctorat en science, Université de Mentouri, Constantine, 2004.

[111] H. R. Hassani, M. Jahanbakht, "Method of moment analysis of finite phased arrays of aperture coupled circular microstrip patch antenna," Progress In Electromagnetics Research B, Vol. 4, pp. 197-210, 2008.

[112] G. V. Eleftheriades, J. R. Mosig, "On the network characterization of planar passive circuits using the method of moments," IEEE Transactions on Microwave Theory and Techniques, vol. 44, No. 3, pp. 438-455, 1996.

[113]T. Fortaki, A. Benghalia, "Rigorous full-wave analysis of rectangular microstrip patches over ground planes with rectangular aperture in multilayered substrates that contain isotropic and uniaxial anisotropic materials," Microwave and optical technology letters, vol. 41, No. 6, pp. 496-500, 2004.